Mapping Africa's Infrastructure Potential with Geospatial Big Data and Causal ML

Sebastian Krantz*

August 21, 2024

Abstract

Using rich geospatial data and causal machine learning, this paper maps potential economic benefits of incremental investments in all major types of public and economic infrastructure across Africa. These 'infrastructure potential maps' cover all populated areas in Africa, at a spatial resolution of $9.7km$ ($96km^2$ hexagons). They show that the local benefits of additional infrastructure are highly variable and context-specific. The results broadly suggest that 'hard infrastructure' such as paved roads, power, transport, and communications is more beneficial in cities, whereas 'social infrastructure' such as education, health, public services and utilities, is more important in rural areas. Market access and agglomeration effects are important forces governing these returns. Descriptive analysis further reveals that infrastructure in Africa is concentrated in urban areas and often inefficiently allocated. African cities exhibit marked heterogeneity in infrastructure, public services, and economic activities.

Keywords: Africa, infrastructure, investment potential, geospatial big data, causal ML, XAI
JEL Classification: O18; R11; R40; C14

1 Introduction

It is well recognized in economic literature and policy discourse that Africa has great public infrastructure deficits. Estimates by the African Development Bank (ADB) suggest that Africa's infrastructure needs amount to $130-170 billion a year, with a financing gap in the range of $68-108 billion (ADB, 2018). A World Bank report from 2010 states that Sub-Saharan Africa (SSA) has 31 paved roads km per $100km^2$ of land, compared to $134km$ in other low-income countries, estimates the annual infrastructure gap at $93 billion, and urges SSA countries to spend one percent of GDP on roads (Foster & Briceño-Garmendia, 2010). Large gaps also remain in other areas; for example, according to World Bank statistics, by 2022, 51% of Sub-Saharan Africans had access to electricity, 36% were using the internet (although 84% had mobile phones), and 34% were using basic sanitation services. These deficits suggest that public infrastructure investments in Africa may have high returns for economic activity and wealth generation. At least the World Bank spends around a third of its budget on infrastructure projects (Akpandjar & Kitchens, 2017), and much academic research of recent years suggests sizeable economic returns - such as historical railway access increasing real agricultural incomes by 16% (Donaldson, 2018) or land values by 60% (Donaldson & Hornbeck, 2016), power cuts reducing firm revenues and producer surplus by 5-10% (Allcott et al., 2016), internet availability inducing 2% higher growth and structural change (Goldbeck & Lindlacher, 2021), joint roads/power investments yielding an 11% increase in welfare (Moneke, 2020), road network inefficiencies implying a 1.3% welfare loss (Graff, 2024), and changes in transport costs invoking large reshufflings of population, wealth, and economic activity (Storeygard, 2016; Jedwab & Storeygard, 2022; Faber, 2014; Baum-Snow et al., 2020).

This paper contributes to the debate on the returns to infrastructure investments in Africa by utilizing the wealth of granular geospatial data that has become available in recent years to observationally estimate local returns to different types of public and economic infrastructures across Africa. It utilizes recently developed causal machine learning methods (e.g., Chernozhukov, Chetverikov, et al. (2018); Athey et al. (2019); Nie & Wager (2021)), enabling more credible and

*Kiel Institute for the World Economy
Address: Haus Welt-Club, Kiellinie 66, D-24105 Kiel
E-mail: sebastian.krantz@ifw-kiel.de

specific inferences from observational datasets. These methods, also known as 'double' or 'debiased' ML, employ predictive ML models to remove factors confounding the relationship between a treatment (infrastructure), and an outcome (economic activity or wealth). Following this first-stage 'debiasing' step, a second-stage 'causal model' estimates a heterogeneous treatment effect (of infrastructure). With only a large spatial cross-section, the causal model may still suffer from reverse causality, but is plausibly free from confounding, which is a large improvement over single-stage predictive models typically employed in geoAI or other ML contexts.

Causal ML thus does not supersede causal econometrics, which, once a convincing source of quasi-random variation has been identified, estimates the causal effect of a specific infrastructure. However, convincing quasi-random variation is hard to find, particularly with infrastructure, and causal studies of infrastructure seldom extend beyond a single country or region. Few econometric studies are also able to provide local heterogeneity in treatment effects. In other words, limited external validity and differences in data and methodology complicate drawing broad inferences from such studies for policy purposes. Conflicting studies of the same intervention in different settings also produce conundrums in academic knowledge, as exemplified by the academic literature on returns to household electrification (Lee et al., 2020; Bayer et al., 2020).

In contrast, granular geospatial data has recently become increasingly rich and uniform and is available at high resolution for vast geographic areas. By analyzing this data with causal ML, I am able to make a contribution that is quite different from most causal econometric research on infrastructure. In particular, I provide localized (1) marginal effects and counterfactual predictions for (2) 14 different types of public and economic infrastructure as well as local and overseas market access, at (3) $9.7km$ ($96km^2$) spatial resolution,[1] for (4) >100,000 populated locations across the entire African continent. My results thus exhibit comparability between different types of infrastructure and across space, and suggest that heterogeneity in returns to infrastructure is indeed eminent. The high-resolution 'infrastructure potential maps' produced in this paper thus present an advance toward policymakers asking about the returns to an additional road, generator, school, or hospital in a specific city, village, or suburb. These maps are necessarily limited by the quality of open geospatial data for Africa, ground-truth measures for wealth and economic activity, and by the identifying assumptions of causal ML.[2] They also only provide partial equilibrium estimates ignoring migration and reshuffling of economic activity following infrastructure investments.

Analyzing granular geospatial data is also useful for gaining insights and uncovering patterns in Africa's spatial economy. Explainable AI (XAI) and other nonparametric methods, such PCA and clustering, can help understand the concentration and the local and global economic significance of different types of infrastructure, as demonstrated in Section 3 of this paper.

The remainder of this paper is structured as follows: Section 2 introduces the detailed geospatial data and describes how it is processed into analyzable form. Section 3 studies the processed data and expounds several stylized facts about Africa's spatial economy. Section 4 introduces the causal ML framework and presents average and heterogeneous partial infrastructure effects. Section 5 does the same for counterfactual predictions. Section 6 summarizes the findings and concludes.

2 Data and Preprocessing

The database of African infrastructure constructed for this project is large and built up from granular data sources. It combines detailed geospatial point and vector data with raster data on population, accessibility, and various economic outcome measures.

2.1 Geospatial Data on Infrastructure

The main source of open geospatial data on infrastructure is Open Street Map (OSM). The Africa OSM has grown rapidly over the past years. As of November 2022, it contains >130 million spatial

[1] Which is roughly the size of a medium-sized city, or of the center of a smaller capital city such as Kigali.

[2] Well known in the literature as the *unconfoundedness assumption*, stipulating the conditional independence of treatment and outcome based on observables. I will present evidence that, in the face of rich geospatial data, this assumption is not easily dismissed via classical arguments such as political favoritism (Dreher et al., 2019).

features covering all areas of public and economic life. More than 50 local OSM groups spawn nearly every African country[3]. The growing reliability of OSM is also reflected in the increased research use of the map. For example, Peng & Chen (2021) use the Zambia OSM in 2019 to train their image segmentation model, and Graff (2024) uses the OSM routing service to generate network connectivity data for his spatial model. As a statistical point of reference, Microsoft Research released a global dataset of segmented roads in 2022 indicating that globally only 2.3% of roads are missing from OSM, and in Africa around 2.6%. To optimally utilize the map, I develop a basic functional classification of OSM features and apply it to the entire Africa OSM, yielding a database of ∼12.6 million points/buildings and ∼3.8 million km of lines of economic interest. An R package *osmclass* (Krantz, 2023) to classify OSM features is released together with this paper.

Apart from OSM, the Overture Maps Foundation aims to create comprehensive open maps data for developers, with steering members Amazon, Meta, Microsoft, and TomTom. In July 2023, the first production-grade maps dataset was released. With all transport-related data taken from OSM and buildings untagged, the biggest addition is a global dataset of 57 million places of interest (POIs) combined from OSM, Meta, and Microsoft. Within Africa, this adds an additional 1.3 million places mostly from Meta, of which 824k have a minimum confidence score above 0.4.

In addition to OSM and Overture, the Alltheplaces open-source project provides web-scraped POI data, adding 114k POIs mostly from established brands like Starbucks or KFC in Africa.

These sources do not reliably map all infrastructures of economic significance, thus I complement them with several curated datasets covering specific infrastructures. In particular, I assemble data on cell towers (OpenCellid), health facilities managed by the public sector (Maina et al., 2019), power plants (Global Integrated Power Tracker and WRI database (Byers et al., 2018)), steel plants (Global Steel Plant Tracker), special economic zones (SEZs) (Open Zone Map), and ports (2015 World Port Index (MSI, 2019) and World Bank). Table 1 summarizes the places dataset by source.

Table 1: Africa Infrastructure Database: Places Dataset by Source

Source	Count	of which Polygons	Categories
Open Street Map (OSM)	12,221,198	9,038,206	45
OpenCellid (Cell Towers)	1,894,356	0	1
Overture Maps Places (confidence > 0.4)	823,786	0	44
All The Places (Open Web-Scraped POIs)	114,382	0	12
Health Facilities in SSA (Nature Scientific Data)	96,290	0	1
Global Integrated Power Tracker	871	0	1
WRI Global Power Plants Database	363	0	1
Global Steel Plant Tracker	41	0	1
Open Zone Map (Special Economic Zones)	387	0	1
World Port Index	235	0	1
WorldBank Global International Ports	9	0	1
SUM	15,151,918	9,038,206	47

Notes: Table shows places of interest (POIs) data collected from different sources. In OSM POIs may be tagged buildings/have geometries.

While the *osmclass* package provides a basic classification of features closely aligned with the OSM tagging system, and curated datasets have a limited number of functionally distinct features, the Overture places (OVP) data follows a different categorization scheme with > 1000 primary place categories. I thus perform a second, more rigorous, classification step to categorize features across sources into 47 specific economic categories and 26 simplified ones. The full classification process is detailed in Appendix A. Table A3 shows the final harmonized classification.

Following harmonization, I also deduplicate the data across sources by allowing only features of the same category from one source within a 10m radius.[4] Curated datasets thereby take precedence over OSM, which in turn supersedes OVP. Tables 1 and A3 summarize already deduplicated data.

[3] https://medium.com/@kateregga1/the-state-of-openstreetmap-in-africa-223ecadd5556

[4] This is done by shifting a 10m grid over the POI features in steps of 1m and deduplicating features within each 10m × 10m square, thus there is some path dependence in terms of which POIs are compared first.

In addition to POIs, I extract linestring features such as (non-residential) roads, larger waterways, power lines, railways, aeroways, pipelines, and telecommunication lines from OSM. I complement OSM power lines with electricity grid maps from the European Commission (Kakoulaki & Moner-Girona, 2020) and the World Bank. Table 2 provides a breakdown. In Total, I collect $\sim$ 4.4 million km of network infrastructure, of which $\sim$1.6 million km are roads, $\sim$1.5 million km waterways, and 967 thousand km of power lines. The other categories sum to 272 thousand km.

Table 2: Africa Infrastructure Database: Lines Data by Category

Category	Count	Length (Km)
road	763,912	1,621,144
waterway	359,756	1,507,112
power[1]	1,013,150	967,317
railway	84,707	128,408
aeroway	27,360	11,019
pipeline	9,453	55,394
storage	8,551	389
ferry	2,412	48,259
aerialway	171	175
telecom	87	28,682
SUM	2,269,903	4,379,392

[1] OSM power lines were combined with datasets from the EC's Joint Research Centre (JRC) and the World Bank.

Finally, I also obtain 2022 fixed and mobile download and upload speeds from OOKLA via the EU Africa Knowledge Platform - within map tiles at a resolution of around 610m at the equator.

2.2 Spatial Measures of Wealth and Economic Activity

To study the returns to infrastructure, accurate spatial measures of quantities of interest such as economic activity/value-added or household wealth are needed. A popular spatial proxy for economic activity, following the seminal work of V. Henderson et al. (2011, 2012), is remotely sensed nightlight luminosity (Donaldson & Storeygard, 2016). Since 2011, nightlights data is available at high resolution (15 arc second or $\sim$500m at the equator) from the Visible Infrared Imaging Radiometer Suite (VIIRS) onboard the Suomi satellite (Gibson et al., 2020). Recently, NASA released a more processed version of the VIIRS imagery for monitoring human activities across space and time under the label 'NASA Black Marble' (Román et al., 2018). Among the first research users in economics, Peng & Chen (2021) show that this data is substantially more accurate than the conventional VIIRS data in tracking Zambian GDP over time.

Several contributions also spatially distribute GDP (value-added) from national and/or regional accounts via high-resolution data on population, geophysical features, and nightlights. A widely used dataset is the G-Econ database (Nordhaus et al., 2006), providing GDP estimates for 1-degree grid cells from 1990 to 2005. A more recent attempt by Kummu et al. (2018) distributes national GDP estimates from the World Development Indicators and CIA World Factbook in constant 2015 PPP dollars at 5 arc-min (0.0833 degrees or 9.3km at the equator) resolution, using subnational value-added estimates from Gennaioli et al. (2013) and population from the HYDE 3.2 database.

Recent efforts, starting with Jean et al. (2016), use richer data sources to predict wealth/poverty at high spatial resolutions. Due to the requirements of high-resolution ground-truth data, this literature has focused on measures of wealth computed from standardized surveys such as DHS and LSMS, rather than coarse measures such as GDP. A popular contribution by Chi et al. (2022) combines vast and heterogeneous data from satellites, mobile phone networks, topographic maps, as well as aggregated and de-identified connectivity data from Facebook to estimate nationally comparable estimates of wealth - a Relative Wealth Index (RWI) - for all low and middle-income countries at 2.4km resolution. Another recent contribution by Lee & Braithwaite (2022) employs a cross-country prediction methodology that combines day- and nighttime satellite imagery, high-resolution population estimates, and OSM to predict the International Wealth Index (IWI) -

a comparable asset-based wealth index calculated from DHS Surveys for 25 countries in SSA conducted since 2017 - for 929,295 populated places in 44 SSA countries at 1-square mile (1.6km) resolution.[5] They obtain a cross-country R^2 of 91.7% for the IWI, outperforming previous results.

Figure 1 shows four of the latest estimates of wealth/economic activity in Africa discussed above. None of these measures is ideal to study the effects of infrastructure. Nightlights are, by definition, correlated with power infrastructure and also relatively sparse since very low-light areas are set to zero in the Black Marble product. Gridded GDP is, by definition, highly correlated with population and may thus be biased towards residential areas. The RWI is not constructed to be comparable across countries and is not available for (South-)Sudan, whereas the IWI is not available for North Africa and uses parts of OSM and population next to daylight satellite imagery in its construction. In the following, I use all 4 estimates shown in Figure 1 to determine weights applied during the aggregation of granular data, but focus on the IWI for final estimation since it is an accurate high-resolution and cross-country comparable estimate. I also conduct robustness exercises with nightlights and ground truth IWI estimates from DHS surveys conducted since 2010 to ensure that key results are not driven by the ML model of Lee & Braithwaite (2022).

Figure 1: Spatial Measures of Wealth and Economic Activity

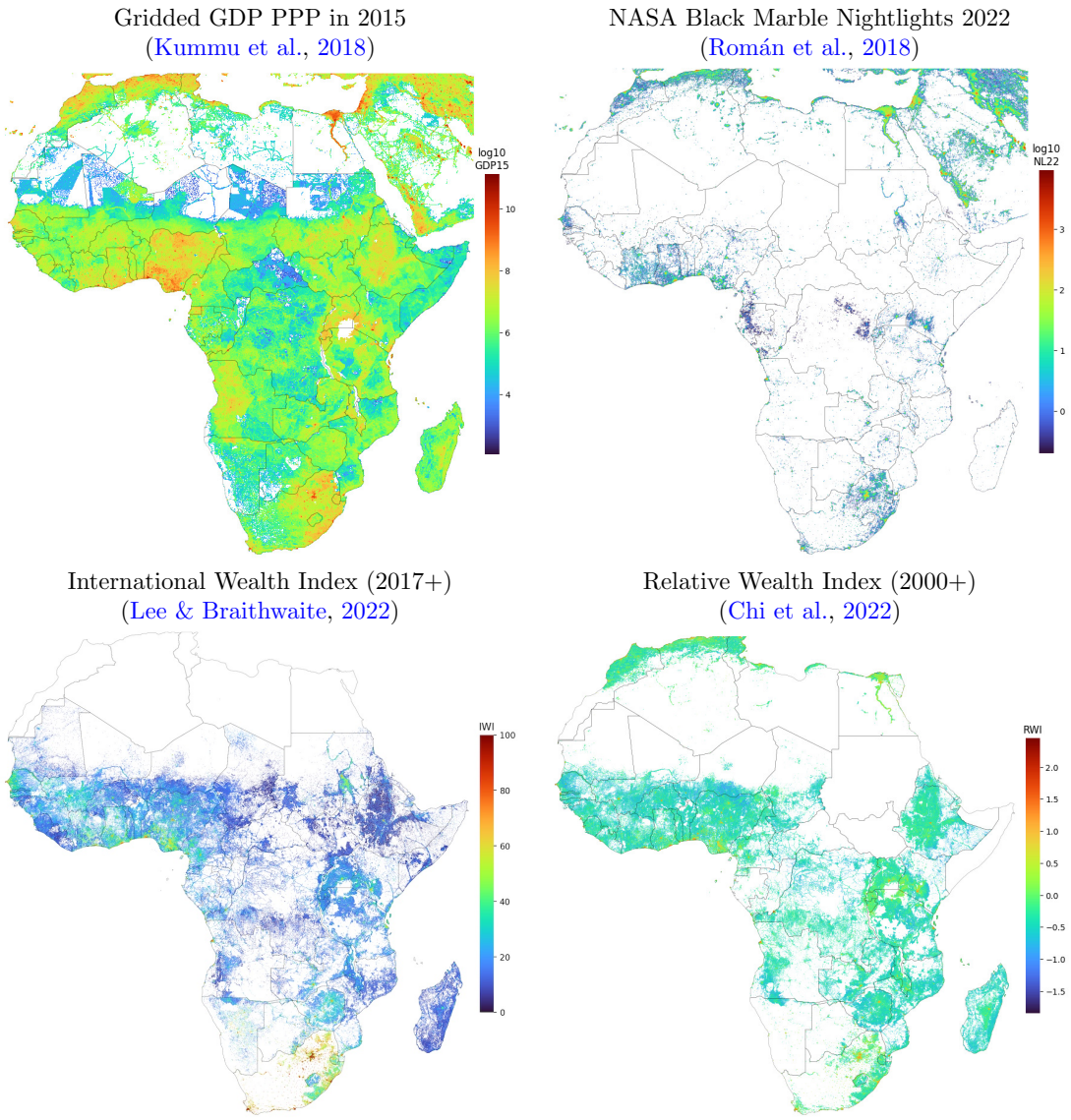

Notes: Figure shows different measures of wealth and economic activity at their original resolution, with blank missing or zero values. The IWI is the main outcome measure, but all measures assist data aggregation (Section 2.5, Table A6).

[5] From OSM, Lee & Braithwaite (2022) employ the total length of roads, distance to the closest road, number of junctions, distance to the closest junction, total building area, and the number of buildings for each 1 square-mile populated area, and the number of and distance to 24 locations of interest such as schools, hospitals, and markets.

2.3 Covariate Raster Layers

Many further sources of high-resolution data layers about geophysical features, agriculture, climate, and conflict could be included as covariates in an analysis of infrastructure and wealth/economic activity. Economic research such as Storeygard (2016), Jedwab & Storeygard (2022), Donaldson (2018) and Peng & Chen (2021) has, however, focussed on two particularly important dimensions of spatial variation affecting economic outcomes: population (urbanization) and market access.

I obtain population estimates for 2020 from the Gridded Population of the World Version 4 (GPW4) project (CIESIN, 2016), which is based on administrative data. I broadly distinguish between the infant (0-14 years) and working-age (15-49 years) population to allow for local variation in demographic characteristics. To approximate market access, I consider global accessibility indicators from Weiss et al. (2018), who developed a global map of travel time (in minutes) to cities with more than 50,000 people in the year 2015 at 1 km^2 resolution. The map is based on a global friction surface constructed from detailed spatial data on transport networks and geophysical features. Nelson et al. (2019) expands this work to settlements of 9 different sizes, from tows of 5000 inhabitants to megacities with more than 5 million inhabitants. Nelson (2022) further computes travel time to ports of 4 different sizes (very small, small, medium, and large) using data from the 2015 (26th) edition of the WPI. From these 12 accessibility maps, I compute 4 which appear most relevant in Africa: (1) travel time to cities >50,000 as in Weiss et al. (2018); (2) travel time to cities >1 million; (3) travel time to the nearest port, and (4) travel time to one of 43 medium or large African ports. Figure 2 shows 3 of these accessibility maps and total GPW4 population.

Figure 2: Raster Covariate Layers: GPW4 Population (2020) and Market Access (2015)

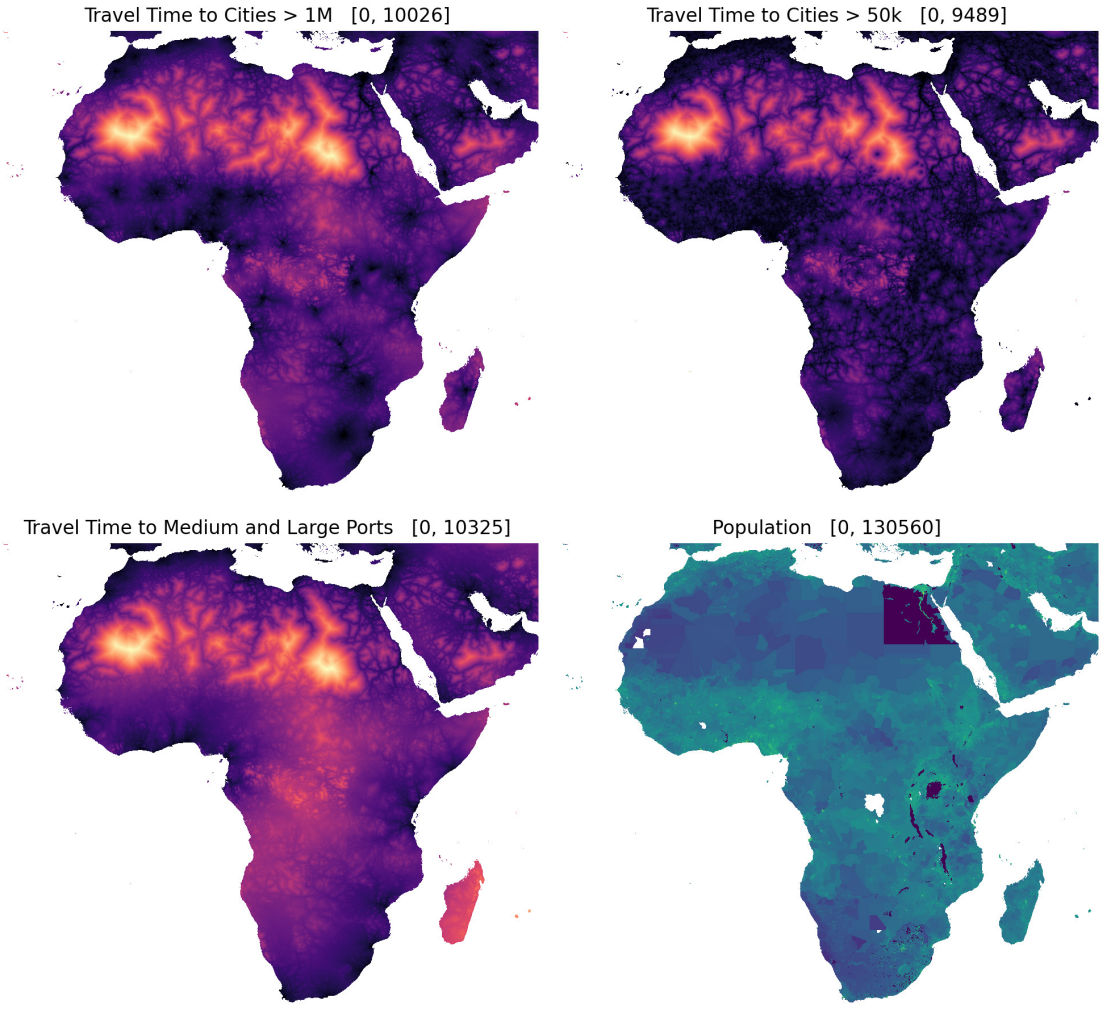

Notes: Figure shows accessibility maps from Nelson et al. (2019); Nelson (2022), and GPW4 population (CIESIN, 2016). The population layer has some missing data. These gaps are imputed in the final dataset following aggregation over a 96kkm^2 grid (in Section 2.4) using the 'missForest' algorithm by Stekhoven & Bühlmann (2012), yielding a 97% OOB-R^2.

This choice of accessibility maps is sensible as diversified economic activity in SSA tends to take place in the largest urban centers, of which most countries have one or two. Towns of 50,000 people often function as important hubs to gather agricultural produce from the region for sale on local markets or transport to larger cities and ports (Jedwab & Storeygard, 2022). The vast majority of exporting or importing in Africa also happens through medium and large-sized ports, with modern container terminals and often intersecting international shipping routes.

2.4 The Ideal Spatial Grid

Jointly analyzing infrastructure and wealth/activity will require some form of spatial binning and data aggregation. For accurate spatial analysis, an equal area grid is desirable. Discrete Global Grid Systems (DGGS) use regular polyhedra for hierarchical tessellation of cells partitioning the globe. Sahr et al. (2003) discuss different DGGS design choices and implementations, and propose the Icosahedral Snyder Equal Area Aperture 3 Hexagon (ISEA3H) as a good general-purpose geodesic DGGS.[6] An aperture of 3 implies that lower-resolution hexagons have an area 3x larger than the next higher-resolution hexagons. The grid is implemented as part of the DGGRID C++ library (Sahr, 2022), and accessed in R through the 'dggridR' package (Barnes, 2020).

ISEA3H is available at 31 different resolutions, from 12 global cells spaced 7054km apart to 2059 trillion cells spaced 0.5m apart. High spatial resolutions are desirable but increase the computational burden and reduce the number of features in each cell, limiting statistical models' ability to learn about the spatial economy. I thus empirically gauge the highest resolution grid that still yields acceptable predictions for wealth/economic activity by counting POIs in each cell and category and computing the average correlation of these counts with the 4 indicators in Figure 1. I also compute the average R^2 of linear models predicting the wealth/activity indicator from all category counts. Table 3 reports the results for ISEA3H grids at 7 different resolutions, ranging from 3,901 cells 87km apart down to resolution 557,766 cells 3.2km apart. Both individual and joint predictions decrease in strength as the grid resolution increases. The largest drop is experienced when moving from a resolution 11 grid (16.8km) to a resolution 12 grid (9.7km). The resolution 12 grid cells have a size comparable to the city center of Kigali (a larger city like Kampala being covered by 3-4 cells) and contain around 94 POIs on average and 10 in the median cell.

Table 3: POIs in ISEA3H Grids of Different Resolutions

Res.	Area (km^2)	Spacing (km)	N. Cells (N)	N. Features Mean	N. Features Median	Mean[Feat./Cat.] Mean	Mean[Feat./Cat.] Median	Corr. (r)	LM R^2
8	7774.21	87.08	4,091	3,703.720	509	116.978	33.235	0.347	0.592
9	2591.40	50.28	11,243	1,347.676	144	58.674	16.200	0.336	0.552
10	863.80	29.03	29,247	518.067	48	33.677	9.250	0.317	0.504
11	287.93	16.76	71,192	212.832	20	21.489	6.000	0.290	0.425
12	**95.98**	**9.68**	**160,719**	**94.276**	**10**	**14.657**	**4.000**	**0.255**	**0.358**
13	31.99	5.59	336,587	45.016	6	10.154	3.000	0.224	0.321
14	10.66	3.23	646,959	23.420	4	7.121	2.000	0.195	0.278

Notes: Res. is the grid resolution, also given in terms of cell area and spacing between the centroids of adjacent cells. N. Cells is the number of grid cells containing any POI in Africa. N. Features is average/median number of POIs in a cell. Mean[Feat./Cat.] is the average number of POIs per detailed category (47) in Table A3, computed for each cell and aggregated across cells using the mean or median. Corr. gives the average Pearson's correlation of the feature count within each category with each of the 4 spatial wealth/activity measures in Figure 1. Thus, it is an average of $47 \times 4 = 188$ correlation coefficients. LM gives the average R^2 of a linear model of the same 4 outcome measures against the features counted in 47 categories, thus it is the average of 4 R^2 estimates. The chosen resolution is highlighted.

To enable high-resolution estimation for city centers and suburban regions, I opt for the

[6] Sahr et al. (2003) summarize the design choices for ISEA3H as: "First, due to its lower distortion characteristics we choose the icosahedron for our base platonic solid. We orient it with the north and south poles lying on edge midpoints such that the resulting DGGS will be symmetrical about the equator. Next, we select a suitable partition. The hexagon partition has numerous advantages, and we choose aperture 3, the smallest possible aligned hexagon aperture. Because equal-area cells are advantageous for many applications, we choose the inverse ISEA projection to transform the hexagon grid to the sphere, and we specify that each DGGS point lies at the center of the corresponding planar cell region". Kmoch et al. (2022) further compare 5 open source DGGS implementations (Uber H3, Google S2, rHEALPix, OpenEAGGR, DGGRID) and constate that DGGRID is excellent for constructing grid cells with desirable properties, i.e., low apertures, convenient shapes, and equal area representation.

resolution 12 grid and mitigate the drop in predictive performance and effects of hard cell borders by allowing spatial spillovers from up to 2nd-order neighbours. The implementation of these spillovers is described below. Figure 3 visualizes the grid with GPW4 2020 total population estimates.

Figure 3: GPW4 2020 Population in 160,719 96km^2 ISEA3H Cells Covering Areas with any POI

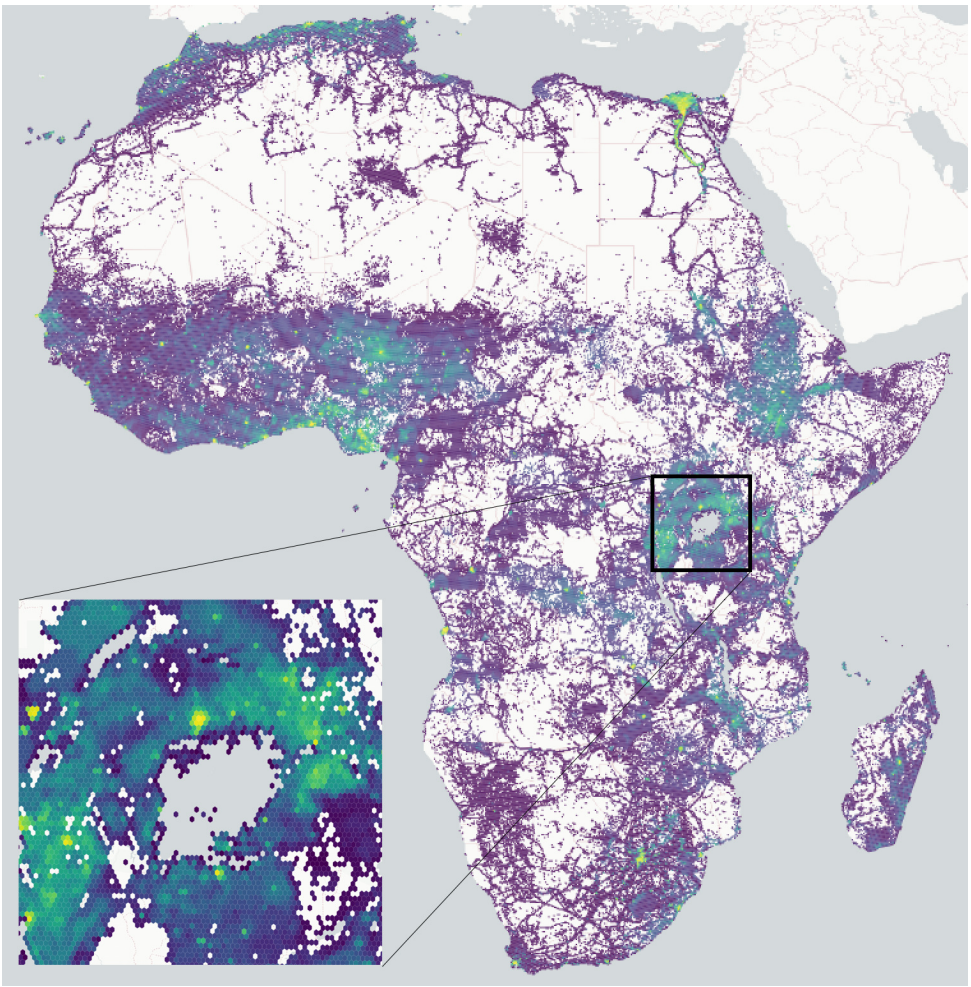

Notes: Figure shows GPW4 population summed over an ISEA3H 96km^2 discrete global grid covering areas with any POI.

2.5 Data Aggregation

I aggregate the raster data over the $96km^2$ equal area ISEA3H grid by taking the mean of wealth indices, travel times, and internet speed, and the sum of GDP, nightlights, and population within each cell. I also compute the total length in m of network features (Table 2) per cell, distinguishing paved from unpaved roads and combining 3 types of waterways using average harmonized coefficients from a Ridge Regression against the outcomes in Figure 1.[7] I count POIs in each cell and category (Table A3), but also consider a weighted approach where I compute quartiles of the building-areas of all OSM features tagged to buildings, and use counts of 2/3/4 if the area is within the 2nd/3rd/4th quartile. In this way, large features such as large school buildings receive up to 4 times the weight of small school buildings or schools that are just points. Similarly, I also apply these quantiles counts to the areas of SEZ's, the capacity of power and steel plants, and the ouflows of ports. The quartile method thus takes into account the intensive margin.

[7]Namely rivers, man-made canals, and man-made waterways relating to utilities or agricultural activities such as drains and ditches, which are initially summed into a variable called 'waterway_other'. I then use Ridge regression to estimate an equation of the form $y = \beta_0 + \beta_1 + \text{river} + \beta_2 + \text{canal} + \beta_3 + \text{waterway\_other} + \epsilon$, where y is the log of GDP, the IWI or the RWI (nightlights is too sparse). The coefficients are restricted to be greater than zero, and the optimal Ridge penalty is chosen by 10-fold cross-validation. I then obtain relative coefficients by dividing through by β_1, and averaging them across the 3 outcomes. The result is $\beta_1 = 1$, $\beta_2 = 9.035$, and $\beta_3 = 6.13$, indicating that man-made features are much more important for spatial activity. Their length is thus increased by a factor β_j.

To aggregated the 47 detailed categories in Table A3 to the 26 simplified ones, which are more independent and thus more useful for analysis, I employ weights derived from penalized regressions on the 4 outcomes from Figure 1. Formally, let there be P_j detailed categories for simplified category j indexed by p. For example the 'communications' category (j) combines $P_j = 3$ detailed categories: 'communications_network' (cell towers, antennas), 'communications_other' (TV or radio station, newspaper, publisher, internet cafe), and 'telecom_len' which is the length (in m) of OSM telecommunications lines in each cell. I combine these detailed categories into a simplified one ($\mathbf{x}_j$) using appropriate linear weights β_{jp} maximizing the correlation with the outcomes ($\mathbf{y}$)

$$\max_{\beta_j} \quad cor(\mathbf{x}_j, \mathbf{y}) \quad \forall\ j \quad \text{s.t.} \quad \beta_{pj} \geq 0 \quad \text{where} \quad \mathbf{x}_j = \sum_{p=1}^{P_j} \beta_{jp} \mathbf{x}_{jp}. \tag{1}$$

To prevent overfitting and negative coefficients β_{jp}, this problem is solved using a Ridge regression, restricting β_{jp} to be positive, and choosing the optimal penalty parameter (λ^*) via 10-fold cross-validation. The resulting coefficients β_{jp}, are normalized by the coefficient of the most populous category ('communications_network'), and surprisingly consistent across outcomes. I thus average them to compute final weights. Appendix Table A6 provides three examples. For 'communications', the coefficient on 'communications_other' is 11.7 and the coefficient on 'telecom_len' is 0.1, which are sensible in relation to a cell tower ('communications_network') having a weight of 1.

Finally, I account for economic geography and mitigate cell-border effects by creating additional 'spillover' variables (a.k.a. spatial lags) as inverse-distance-weighted average of neighbouring cells

$$\mathbf{x}_j^{\text{neigh}} = \sum_i \frac{\mathbf{x}_i}{\delta_{ij}} / \sum_i \frac{1}{\delta_{ij}} \quad \forall i \quad \text{where} \quad \delta_{ij} < \tau. \tag{2}$$

I choose $\tau = 24.2km$, which includes all second-order neighbours. The results are robust to the absence of spillover variables and also to using simple counts instead of quantile counts, but richer processing results in increased predictive power and spatial lags limit confounding influences.

Appendix Table A4 shows summary statistics for the final gridded dataset (simple counts). Appendix Figure A1 additionally shows histograms of the aggregated wealth/activity measures, and Table A5 shows pairwise Pearson's correlations of these measures aggregated over the grid. All measures are moderately correlated but follow slightly different distributions.

3 Africa's Spatial Economy

With rich geospatial data about infrastructure, population, and wealth/activity in Africa at hand, I investigate Africa's spatial economy and the current allocation of infrastructure using a graduated approach. I first analyze the spatial concentration of infrastructure and visualize its allocation. This yields a characterization of locations relatively lacking infrastructure, further illustrated by a case study of 5 African capital cities. I then examine the spatial clustering of different infrastructures and create an index of spatial efficiency measuring the proximity of residential areas, core infrastructure, and economic clusters. I find that this index is correlated with development indicators, logistic performance, and Graff (2024)'s road network inefficiency measure. Finally, I predict the IWI from infrastructure using ML models and interpret them with XAI methods, yielding a global and local characterization of important infrastructure predictors of wealth.

3.1 Infrastructure Concentration

To study infrastructure concentration, I only consider grid cells with more than 960 inhabitants according to both the GPW4 and WorldPop 2020[8] estimates, i.e., cells with more than 10 persons/km^2 and that have any POI. There are 88,960 such cells. I then count the POIs in simplified categories and compute proportions across cells. Sorting these proportions in descending order and cumulatively summing them yields an empirical CDF measuring infrastructure concentration, which I plot against the cell index. Figure 4 shows the result, both for individual feature categories, some of which are highlighted in color, and for averages across categories, computed before or after the CDF calculation. GDP and GPW4 population are also included as a reference.

[8] WorldPop (https://www.worldpop.org/) uses rich geospatial data to estimate population at 1km^2 resolution.

Figure 4 reveals that infrastructure in Africa is highly concentrated - more than population and, for most categories, GDP. The top 1000 cells (1.12% of 88,960) account for 62% of infrastructure in the average feature category, but only 49% of total GDP and 27% of total population. Only education (schools) and power infrastructure (generators) are less concentrated than GDP. The average CDF suggests that close to 100% of any given infrastructure is allocated in $\leq$ 10,000 cells. The only widely mapped feature present in nearly all cells is residential buildings. When infrastructure is pooled across categories, it is less concentrated, and the top 1000 cells only account for 30% of infrastructure. If residential buildings, farmland, power, and construction are excluded, this share rises to 66%. Excluding these four categories also yields 21,891 populated cells (24.6%) that have no other POI. Infrastructure is only moderately correlated with GDP and population, and weakly when aggregated to the country level (see Appendix Table A7), indicating spatial disparities between the allocation of infrastructure, wealth, and economic activities.

Figure 4: POI Feature Concentration - Empirical CDF's

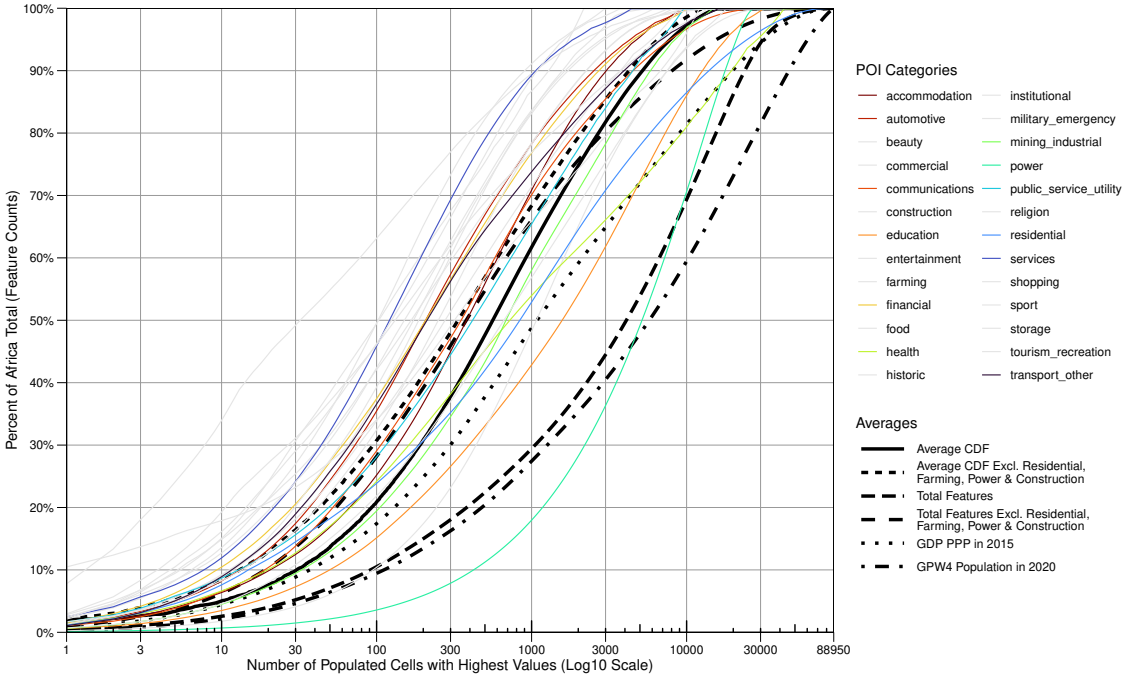

Notes: Figure shows empirical CDF's (with cell-counts on the x-axis) of POIs in different categories.

Figure 5 shows analogous results for line features, indicating that frequent features such as roads, waterways, power, and railways (see Table 2) are less concentrated than GDP, and, in the case of unpaved roads and waterways, also than population.

Figure 5: OSM Line Feature Concentration - Empirical CDF's

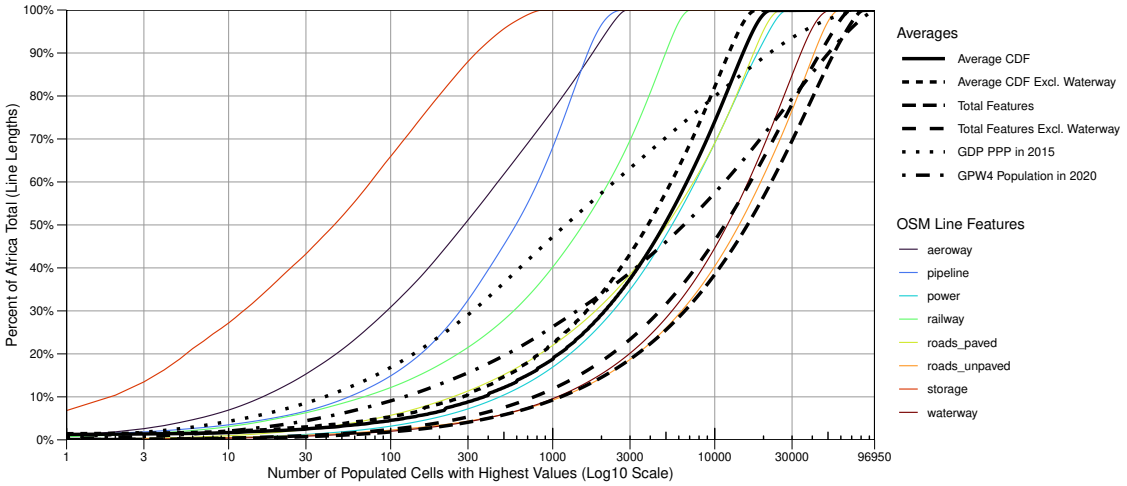

Notes: Figure shows empirical CDF's (with cell-counts on the x-axis) of line lengths in different categories.

With lines, the top 1000 cells only account for 10% of waterways and unpaved roads, 17% of power lines, 23% of paved roads, and 40% of railways. Concentration also proceeds gradually: the top 3000 cells account for 20% of unpaved roads and waterways, 39% of paved roads and 70% of railways, and the top 10,000 cells account for 40% of unpaved roads and 70% of paved roads. At the structurally weak end of the spectrum, excluding waterways yields 27.3% of populated cells that have no other line feature. Appendix Table A7 shows that the total line length in each cell correlates slightly stronger with household wealth than the total POI feature count.

3.2 The Spatial Allocation of Infrastructure

Figure 6 plots the spatial allocation of 9 critical infrastructures. The top panel shows paved roads, power, and communications, indicating absolute quantities in each cell on a log10 scale. Evidently, there are large gaps in central Africa, the Sahel, and the Horn of Africa regions. The great lakes region zoomed in in these plots is well connected in the central populated areas, but still lacks connectivity in sparsely populated peripheries such as eastern Congo, and Northern Kenya.

Figure 6: Spatial Distribution of Selected Infrastructure Features

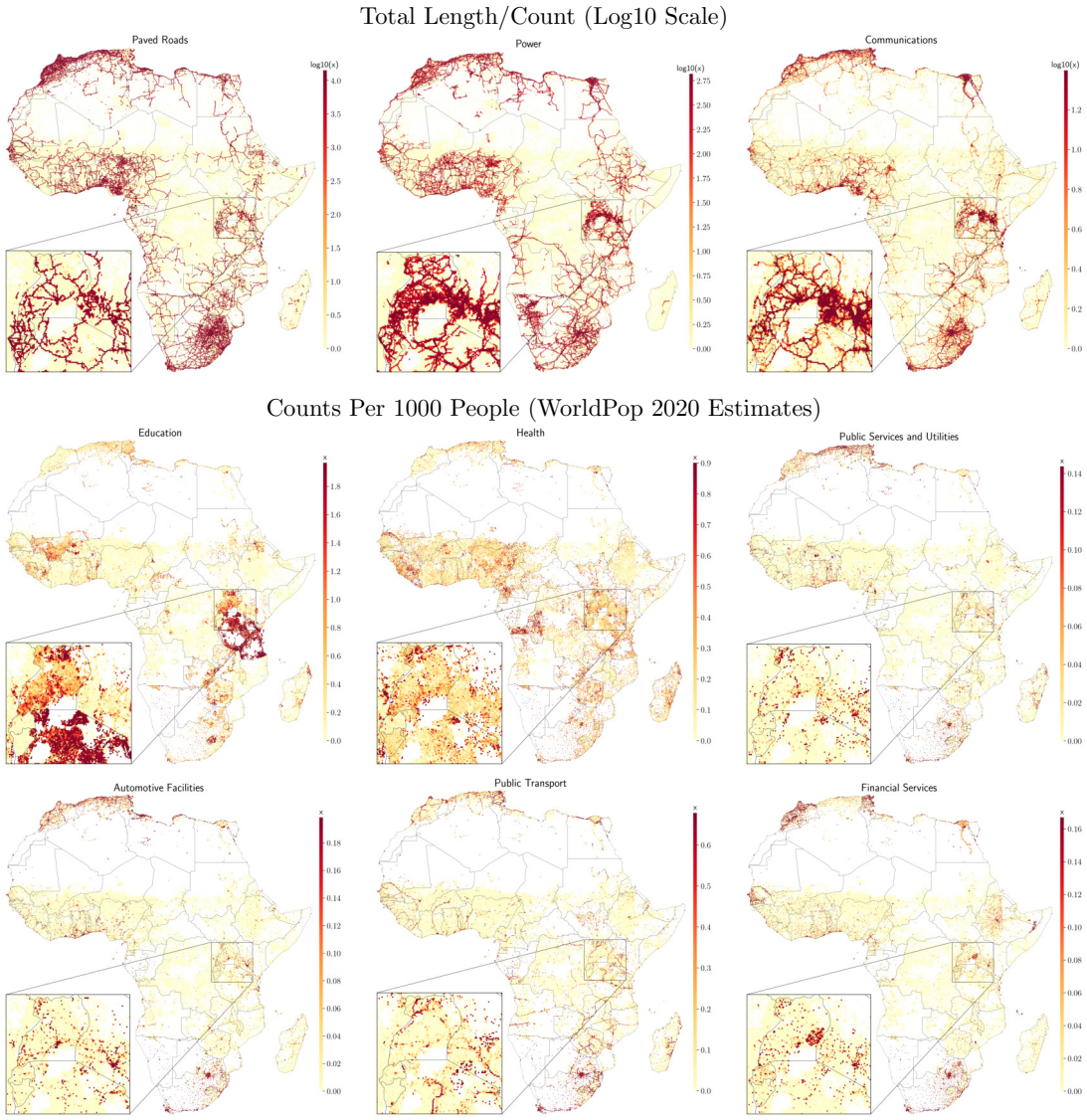

Notes: Figure shows total length/count (top) or count per 1000 people (middle, bottom) per cell for 9 key infrastructures.

The middle and bottom panels of Figure 6 show education and health facilites, public services and utilities (excl. power), automotive facilities, public transport and financial services per 1000 inhabitants - for cells with more than 10 people per km^2. Some of these plots evidence differences in data coverage; for example, Tanzania and Uganda both have a very large amount of educational

facilities, averaging around 1 facility per 1000 people. Health seems more balanced across countries partly due to the data contribution by Maina et al. (2019), but also shows large differences in access across space. Automotive and public transport facilities as well as financial services are more concentrated in towns. Curiously, there appears to be a high concentration of financial services in eastern Uganda, but this is also an administratively very fragmented region. In all three categories, South Africa has significantly higher concentrations per 1000 people than other parts of SSA.

3.3 Comparing Major African Cities

To engage more specifically with the data, I undertake a case study comparing 5 of the largest African cities: Accra, Cairo, Lagos, Nairobi, and Johannesburg. For each city, I consider 7 hexagons covering the central parts of the city, jointly spanning an area of $692km^2$. I then compute the counts of POIs and the length of lines within these areas and divide them by the WorldPop 2020 population estimate. Figure 7 shows the feature intensity per 1000 people in each city.

Figure 7: Feature Density in 5 Major African Capital Cities per 1000 People

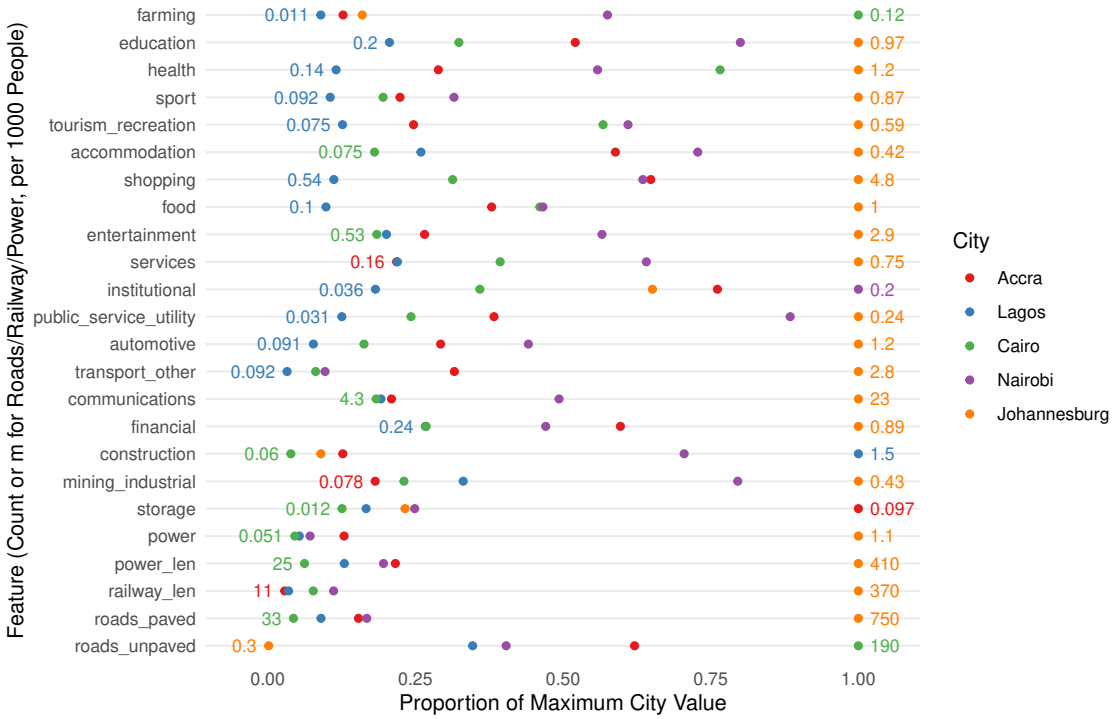

Notes: Figure shows feature counts per 1000 inhabitants (WorldPop 2020 estimates) for 5 significant African cities. For each city, 7 96km^2 hexagons covering essential parts of the city are considered. Features are counted in detailed categories and then combined into simplified categories using the weighted aggregation procedure described in Section 2.5.

It is apparent that the cities are very heterogeneous in terms of spatial features, with Johannesburg topping the ranks for most feature categories. Notably, Johannesburg has 750m of paved transport roads, 370m of railway, and 410m of power lines per 1000 inhabitants, as well as significantly higher automotive, other (public) transport, communications, education, and health infrastructure than other cities. Conversely, Lagos ranks at the bottom in many categories, providing less than a quarter of the services per capita than Johannesburg. Between these two, Nairobi and Accra are doing well, with Nairobi having the most institutions alongside high densities of education, public services, industrial facilities, construction, accommodation (hotels), services, tourism and recreation. Accra also has a high level of institutions, shopping, financial services, accommodation, and education. It is remarkable that, apart from Johannesburg, the level of infrastructure in these cities does not align with their IWI (Accra: 73.5, Lagos: 67.4, Nairobi: 64.2, Cairo: 70.7 [RF prediction], Johannesburg: 81.6) or GDP/Capita[9] (Accra: 3953, Lagos: 7872, Cairo: 9672, Nairobi: 10439, Johannesburg: 14317 in 2015 USD PPP) estimates, with Lagos and Cairo in particular providing less services than their wealth levels would suggest.

[9]These estimates are based on coarse admin. data by Gennaioli et al. (2013), scaled by Kummu et al. (2018).

3.4 Correlations and Clustering

It is also informative to examine the spatial correlations among different features to determine which types of infrastructure often appear together and which are found in populated and/or high-income locations. To study this, I again use the counts of features in the simplified classification. I take the natural log, compute Pearson's correlations among all variables, and use 1 minus the correlations as a distance matrix for hierarchical clustering with complete linkage. Figure 8 shows a dendrogram, and Appendix Figure A2 the corresponding correlation matrix.

Figure 8: Hierarchical Clustering of Variables using Correlation and Complete Linkage

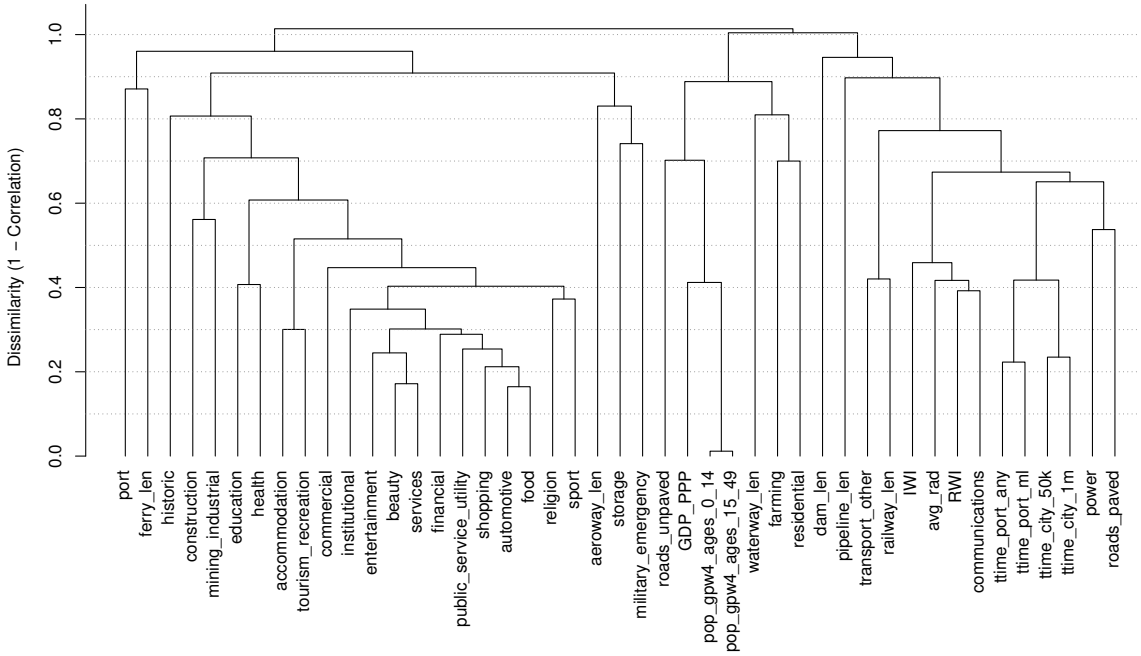

Notes: Figure shows dendrogram from hierachical clustering with complete linkage using a correlation-based distance metric, i.e., 1 minus pairwise Pearson's correlations. Variables in simple counts correspond to Appendix Table A4 and are cast in logs before computing correlations, except for the IWI and RWI which are included in levels. Also, travel time estimates (in minutes) are first logged and then negated to yield positive correlations with other variables.

Figure 8 presents a detailed view of spatial activity in Africa. Different dissimilarity cutoffs reveal distinct groups of correlated variables. Notably, setting the cutoff around $h = 0.98$ reveals three prominent groups in the dendrogram, corroborated by the correlation matrix (Figure A2). The group on the RHS includes travel times, household wealth, nightlights, power infrastructure, paved roads, and communications. These variables seem to be a proxy for physical infrastructure, which in turn correlates highly with nightlights and wealth. The second group, comprising most variables on the LHS of the dendrogram, includes economic activities in the broadest sense. Finally, the middle cluster includes population, residential areas, farming, and GDP, which is interpolated across space using population data. The dendrogram and correlation matrix (Figure A2) thus suggest that there is a disparity in space between where people live, where they work, and where most physical infrastructure is located. Presumably, an efficient spatial organization would imply a stronger spatial correlation among these three constructs/groups.

3.5 An Index of Spatial Efficiency

Informed by these observations, I compute an index of spatial efficiency (ISE) along 3 dimensions: the GPW4 working age (15-49) population, the first principal component (PC1) of paved roads, power, and communications as a compound measure of hard infrastructure, and the PC1 of education, institutional, health, religion, public_service_utility, food, shopping, beauty, services, commercial, mining_industrial, tourism_recreation, sport, construction, farming, entertainment, financial, and accommodation as a compound measure of economic activity. I use simple feature counts without spatial spillovers to keep the index simple. The PC1 of roads, power, and communications accounts for 63% of their joint variance, and the PC1 of the activity variables captures

56% of their joint variance. Table 4 shows Pearson's correlations among these components. The ISE is then obtained simply as the geometric mean of these correlations:

$$\text{ISE} = cor(P,I)^{\frac{1}{3}} cor(P,A)^{\frac{1}{3}} cor(I,A)^{\frac{1}{3}} = 0.642. \tag{3}$$

Table 4: Correlations of ISE Dimensions

N = 160,499	P	I	A
GPW4 POP 15-49 (P)	1.000		
Roads & Power PC1 (I)	0.589	1.000	
Economic Activity PC1 (A)	0.634	0.708	1.000

Notes: Table reports Pearson's correlations among dimension indices (PC1) and population. Their geometric mean is the ISE (Eq. 3).

It is thus an index on the range [0, 1], a value of 1 indicating perfect spatial efficiency with all productive resources concentrated in the same location. Perfect spatial efficiency is unachievable in any real-world setting, but the all-Africa ISE of 0.64 suggests much room for improvement. Table 5 shows ISE estimates at the country level, and Appendix Figure A3 a corresponding map.

Table 5: Country-Level ISE Estimates

#	ISO3	ISE	ISO3	ISE	ISO3	ISE	ISO3	ISE	ISO3	ISE
1	SYC	0.950	TUN	0.788	ZAF	0.719	COD	0.624	BWA	0.508
2	MLI	0.908	MAR	0.783	BFA	0.717	MDG	0.621	LBY	0.486
3	MUS	0.889	TGO	0.779	SWZ	0.715	DJI	0.619	LBR	0.440
4	UGA	0.868	EGY	0.779	GMB	0.712	BDI	0.617	NAM	0.429
5	RWA	0.860	BEN	0.774	GAB	0.694	CAF	0.612	ESH	0.410
6	KEN	0.849	MWI	0.763	NGA	0.693	MOZ	0.593	ERI	0.360
7	GHA	0.830	LSO	0.750	ZWE	0.688	AGO	0.573	SOM	0.284
8	CIV	0.822	TZA	0.745	GIN	0.686	SDN	0.568	CPV	0.252
9	SLE	0.813	ETH	0.744	MRT	0.675	CMR	0.564	COM	0.214
10	STP	0.812	DZA	0.741	COG	0.672	TCD	0.543	GNQ	0.153
11	SEN	0.809	NER	0.729	ZMB	0.651	GNB	0.542	SSD	0.105

Notes: Table reports sorted country-level ISE estimates (Eq. 3) computed from cells within each country.

The average ISE across countries is 0.645. The country-level ISE is mildly correlated with key development indicators in 2020, such as GDP per Capita PPP ($r = 0.159$), Life-Expectancy at Birth ($r = 0.215$), and the Human Development Index ($r = 0.185$). Interestingly, it shows stronger correlations with the 2018 Logistics Performance Index ($r = 0.396$) and the 2020 Doing Business Index ($r = 0.592$). It is also negatively correlated to the hypothetical welfare gains (in percent) from an optimal reallocation of the road network in each country as calculated by Graff (2024)($r = -0.360$). The stronger association of the ISE with these indicators vis-a-vis development outcomes suggests that it indeed measures spatial (in)efficiency. The index is uncorrelated with total land area ($r = -0.033$), although some smaller states like Seychelles score particularly high.

3.6 ML Prediction and Interpretation

Given the rich and diverse nature of Africa's spatial economy, a modern ML approach predicting wealth/activity from infrastructure that is able to capture non-linear associations in the data can yield further insights. The gridded data is in tabular form, and a recent empirical assessment by Borisov et al. (2021) shows that gradient-boosting machines (GBMs) (J. H. Friedman, 2001) still outperform deep learning methods on tabular data. Thus, I employ the competition-winning XGBoost algorithm (Chen & Guestrin, 2016) and tune its hyperparameters with Optuna (Akiba et al., 2019) on a test set containing 25% of the data.[10] The IWI model trained with early stopping

[10]The optimal hyperparameters generally feature a low learning rate ($\eta = 0.01 - 0.02$), deep trees ($max\_depth = 9 - 15$), significant randomization over samples ($subsample = 0.5 - 0.8$) and significant regularization, especially through constraints on the minimal size of final nodes ($min\_child\_weight = 6 - 20$).

achieves a test set R^2 of 78.8%. For comparison, I also train a Random Forest (RF) model with default parameters and 1000 trees, which achieves a test set R^2 of 73.3%. Figure 9 shows empirical CDFs of the absolute values of the residuals, indicating that the XGB model predicts 76% of test-set observations with an error of <5 IWI points. Appendix Figure A4 predicts nightlights.

Figure 9: Empirical CDF's of Residuals from ML Models Predicting the IWI [0, 100]

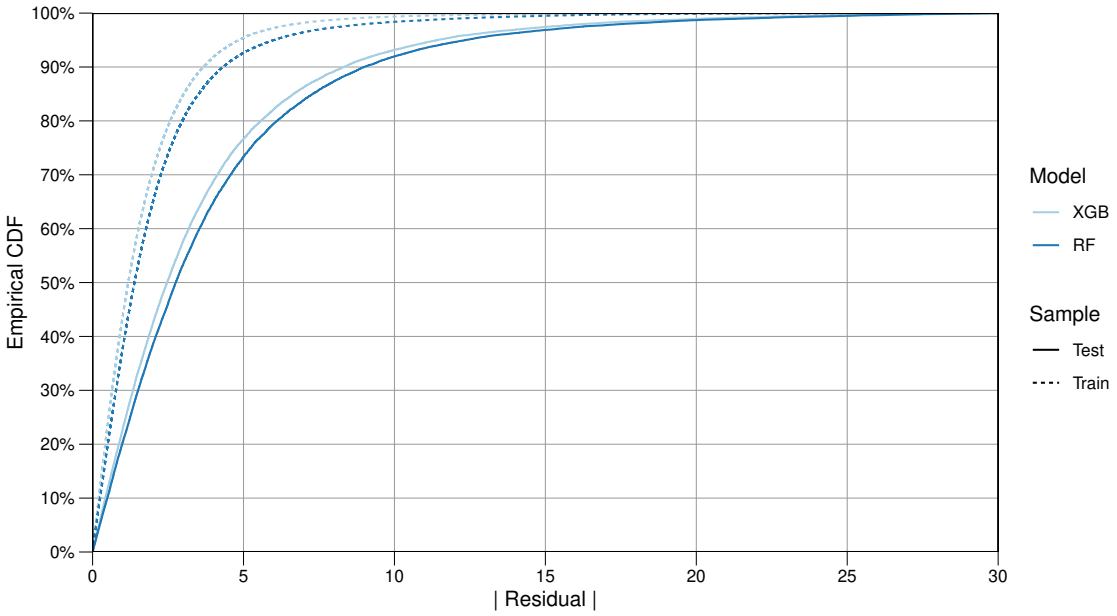

Notes: Dataset has 42 predictors, not including spatial spillover variables. The training set has 86,354 observations, the test set 28,782. Training set R^2 is 96.0% for XGB and 93.9% for RF. Test set R^2 is 78.8% for XGB and 73.3% for RF.

To accurately attribute predictions across the different variables, I compute Shapely Values, a game theoretic approach to fairly attribute the contribution of variables to a single prediction. In particular, SHAP values following Lundberg & Lee (2017); Lundberg et al. (2020) give additive variable contributions for each instance that sum to the difference of the prediction from the average model prediction. To gauge the relative importance of different infrastructure categories, I compute (interventional) SHAP values following Lundberg et al. (2020) for two different XGBoost models: the model trained on the full dataset evaluated above, and a model excluding population and travel time estimates. The latter removes strong correlations of infrastructure with these contextual variables. Figure 10 shows overall variable importance for the IWI based on the average absolute SHAP value across all instances. Appendix Figure A5 does the same for nightlights.

Figure 10: Average SHAP Variable Importance for XGBoost Models Predicting the IWI

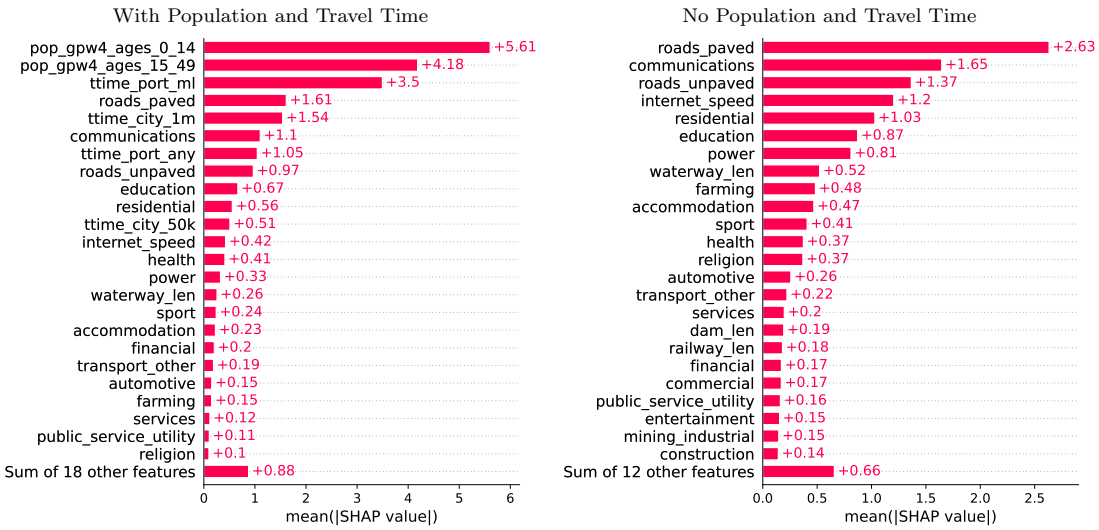

Notes: Figure shows average absolute interventional SHAP values for XGBoost models following Lundberg et al. (2020).

Figure 10 suggests that apart from population and travel time to major cities and ports, roads, communications, education, power infrastructure, and residential areas are the most important predictors of wealth. Many further features such as accommodation (hotels), sport, health, automotive and public transport facilities are also important. With nightlights (Figure A5), population, travel time, communications, roads, and power remain important, but sports, automotive facilities, and industrial areas are also large emitters of light. Appendix Figure A7 shows the same plots using SHAP values derived from feature counts for both IWI and nightlights, with similar results.

To gauge the direction of the effects on the predictions, which may be heterogeneous as SHAP values are computed at the instance level and tree ensembles may be highly non-linear, Figure 11 provides a beeswarm plot of the SHAP values coloured by feature intensity. The plot suggests that most variables have the intended effect, with larger values translating into higher SHAP values. Defying the intuition, residential buildings, education, health, and religion have largely negative effects. This spatial pattern needs to be cautiously interpreted *ceteris paribus*, i.e., in the presence of other correlated features often found in wealthy urban locations (e.g., paved roads, power, communications), more education and health facilities may decrease model predictions. Appendix Figure A6 shows the same plot for nightlights, with similar results. Appendix Figure A8 further provides the same plots derived from feature counts data, with similar outcomes.

Figure 11: SHAP Values for XGBoost Models Predicting the IWI

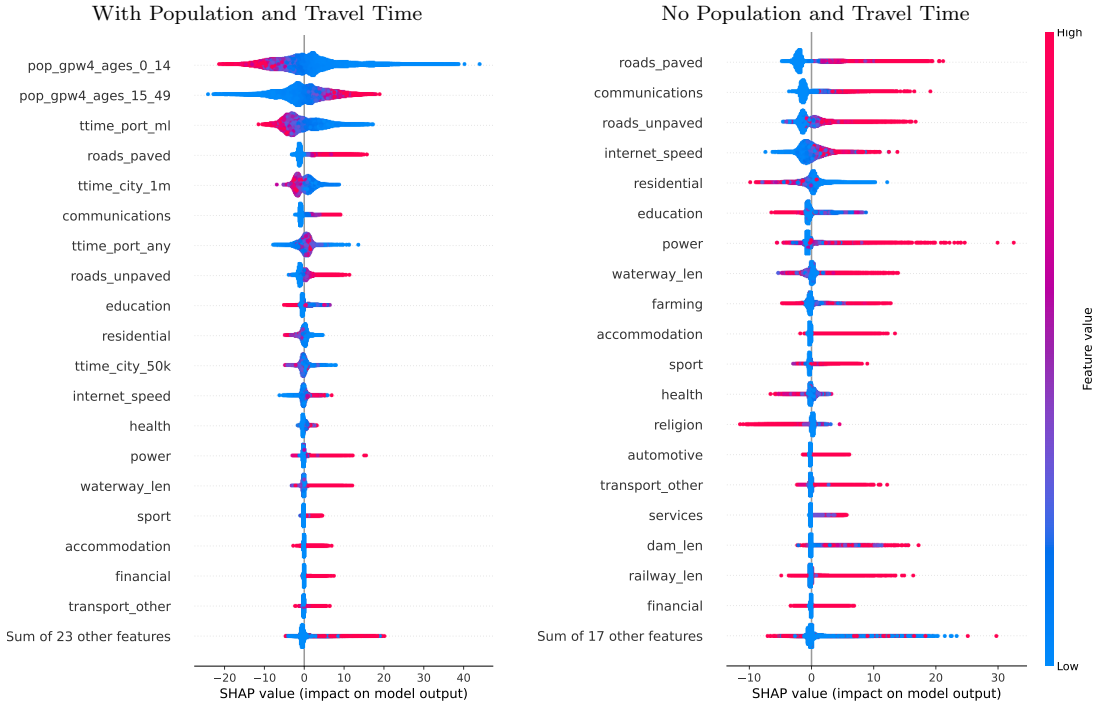

Notes: Figure shows interventional SHAP values for XGBoost models following Lundberg et al. (2020).

The relationship between predictors levels and SHAP values also resembles Accumulated Local Effects (ALE) plots (Apley & Zhu, 2016; Lundberg et al., 2020). Appendix Figures A9 and A10 provide ALE scatterplots corresponding to the beeswarm plots. They are particularly useful for detecting thresholds where a feature's effect on the prediction begins to change. For example, the SHAP value of paved roads strongly increases above $10^4 = 10$km in a cell, suggesting that roads are more important for prediction in urban areas. The same applies to power beyond a threshold of $10^{2.5} \approx 300$ facilities (e.g., transformers, generators) per cell. With education, the opposite is the case: up to 10 facilities per cell, the SHAP value is high, but beyond that, it reduces, indicating that in urban spaces, schools become less critical for wealth prediction. Health and religious facilities exhibit similar but weaker dynamics. In contrast, communications (mainly cell towers) have an almost log-linear positive effect on model predictions. In models with population, the infant (0-14) population has a strong negative effect on predictions, whereas the adult population (15-49) has a strong positive effect, implying Malthusian dynamics in the data.

4 Estimating Marginal Infrastructure Benefits

Having explored the data in some depth, this section advances by asking about the marginal effects of infrastructure on wealth and economic activity. If this were an applied economics paper, I would now present an identification strategy (such as RCT, IV, RDD, DID) to causally identify the effects of infrastructure. However, I consider it impossible to causally identify the effect of every infrastructure in every location in Africa. Thus, I use observational causal inference a.k.a. causal ML.

The traditional econometric view, still held to some extent in other disciplines, is that if one can control for the most important confounding factors in an observational setting, a careful *ceteris paribus* interpretation of the partial effect is possible. So far, this premise has been applied almost exclusively in the context of linear regression, meaning that if all confounders are observed and the population model is linear-additive, a careful *ceteris paribus* interpretation is possible.

However, the *ceteris paribus* statement need not be that strong, as one can relax the assumptions of linearity and additivity. The premise of causal ML (also known as 'double' or 'debiased' ML) is that if one observes all factors that confound or proxy for confounding influences, the relationship between treatment and outcome can be specified conditional on an optimal ML prediction of both from observables. In the setting at hand, this means that if Africa's spatial economy is sufficiently observed through the available granular data on infrastructure, POIs, population, and market access, and if appropriate ML models are deployed, it may be possible to identify marginal partial-equilibrium effects of individual infrastructures on wealth/economic activity. Before examining these identification assumptions in more detail, I introduce this estimation strategy more formally.

I follow Nie & Wager (2021) and Chernozhukov, Chetverikov, et al. (2018); Chernozhukov et al. (2017), and adopt some notation from Hirano & Imbens (2004). Let Y be an outcome of interest, W a continuous treatment of interest with possible values $\omega \in \Omega$, and $\mathbf{X} = [\mathbf{X}'_H, \mathbf{X}'_C]'$ be a vector of observed confounders, where $\mathbf{X}_H$ includes covariates that also affect treatment effect heterogeneity. The *unconfoundedness assumption* is then formally stated as

$$Y(\omega) \perp W \mid \mathbf{X} \quad \forall\, \omega \in \Omega, \tag{4}$$

meaning that the potential outcome $Y(\omega)$ is independent of the treatment realization $W = \omega$ conditional on characteristics $\mathbf{X}$. The quantity of interest is the Conditional Average Partial Effect (CAPE) $\tau(\mathbf{X}_H) = E[\partial Y/\partial W|\mathbf{X}_H]$. I furthermore make the *strong* assumption that the CAPE can be additively separated from the effect of $\mathbf{X}$ on Y, such that the following partial linear specification holds[11]

$$Y = \tau(\mathbf{X}_H) \cdot W + g(\mathbf{X}) + \epsilon \tag{5}$$

$$W = f(\mathbf{X}) + \eta \tag{6}$$

$$E[\epsilon \mid \mathbf{X}] = E[\eta \mid \mathbf{X}] = E[\eta \cdot \epsilon \mid \mathbf{X}] = 0. \tag{7}$$

The *nuisance functions* $g()$ and $f()$, and also the treatment effect function $\tau()$, are assumed to be general functions that can be approximated by appropriate ML estimators. Taking the expectations of Eq. 5 conditional on $\mathbf{X}$ and subtracting it yields

$$Y - E[Y|\mathbf{X}] = \tau(\mathbf{X}_H) \cdot (W - E[W|\mathbf{X}]) + \epsilon. \tag{8}$$

This is the specification of Robinson (1988). Assuming one can estimate $m(\mathbf{X}) = E[Y|\mathbf{X}]$ and $f(\mathbf{X}) = E[W|\mathbf{X}]$, and denoting the 'debiased' variables by $\tilde{Y} = Y - m(\mathbf{X})$ and $\tilde{W} = W - f(\mathbf{X})$, following Nie & Wager (2021), one can then estimate the CAPE $\hat{\tau}(\mathbf{X}_H)$ by minimizing the R-Loss

$$\tau^*() = \text{argmin}_\tau \left\{ E[(\tilde{Y} - \tau(\mathbf{X}_H)\tilde{W})^2] \right\} = \text{argmin}_\tau \left\{ E[\tilde{W}^2(\tilde{Y}/\tilde{W} - \tau(\mathbf{X}_H))^2] \right\}. \tag{9}$$

The RHS of Eq. 9 demonstrates the so-called 'weight trick', i.e., minimizing the R-Loss with a nonparametric (ML) estimator $\tau(\mathbf{X}_H)$ amounts to predicting the target $\tilde{Y}/\tilde{W}$ using sampling weights $\tilde{W}^2$. For the practical implementation of Eq. 9, Chernozhukov, Chetverikov, et al. (2018) show that it is important to estimate the first-stage *nuisance functions* $\hat{m}, \hat{f}$ via cross-fitting.

[11] This assumption will be relaxed in section 5 where I estimate causal dose-response functions.

In that case, a Neyman Orthogonality condition exists to ensure that the estimate $\hat{\tau}(\mathbf{X}_H)$ from minimizing the R-Loss is insensitive to biases (e.g., regularization bias) in $\hat{m}, \hat{f}$.[12] The final stage estimate $\hat{\tau}(\mathbf{X}_H)$ should also be cross-validated to ensure credible out-of-sample CAPE predictions.

Once $\hat{\tau}(\mathbf{X}_H)$ is obtained, further quantities such as the Average Partial Effect (APE) or Group Average Partial Effects (GAPE) can be obtained by doubly-robust methods analogous to Augmented Inverse Probability Weighting (AIPW) (Robins et al., 1994) in the binary treatment case. Following Chernozhukov et al. (2022), Athey & Wager (2021), and *grf* R package (Athey et al., 2019; Tibshirani et al., 2023), the general form of such an AIPW estimator is

$$\bar{\tau} = \frac{1}{n}\sum_{i=1}^{n}\Gamma_i, \qquad \Gamma_i = \tau_i(\mathbf{X}_{Hi}) + h_i(\mathbf{X}_i, W_i)(\tilde{Y}_i - \tau_i(\mathbf{X}_{Hi})\tilde{W}_i). \tag{10}$$

In the binary W case the debiasing weight $h(\mathbf{X}, W)$ amounts to the so-called Horvitz-Thompson transformation.[13] In the continuous W case, Tibshirani et al. (2023) propose $h(\mathbf{X}, W) = \tilde{W}/\hat{\tilde{W}}^2$, where $\hat{\tilde{W}}^2$ denotes a cross-fitted estimate of $\tilde{W}^2$ from $\mathbf{X}$, which Tibshirani et al. (2023) obtain via a honest Random Forest (Athey & Imbens, 2016; Breiman, 2001) OOB predictions. To assess treatment heterogeneity, Athey & Wager (2019) average the doubly robust scores Γ_i in high and low regions of $\hat{\tau}(\mathbf{X}_H)$ and test the difference in means. They also compute the Best Linear Prediction (BLP) of the CATE following Chernozhukov, Demirer, et al. (2018) via Eq. 9 as a calibration test.

To satisfy the unconfoundedness assumption, it is critical to choose appropriate estimators for $m()$, $f()$ and $\tau()$, and a suitable cross-fitting strategy. Because I have no strong prior beliefs on how infrastructure ($\mathbf{X}$) affects wealth/economic activity (Y) and other infrastructure (W), I remain as model-agnostic as possible about these functional forms by employing a *Super Learner* approach (Van der Laan et al., 2007) to create an optimal weighted combination of several candidate learners via cross-validation. The most commonly used functional forms in the heterogeneous treatment effect literature are the LASSO, Random Forests, and Gradient Boosting. Recently, Friedberg et al. (2020) have proposed Local Linear Forests (LLF) as a variant of Generalized Random Forests with greater predictive accuracy for smooth targets. A causal version of LLF is also available in the *grf* package. I thus create a *Super Learner* from the predictions of these 4 algorithms

$$\hat{\text{SL}} = \beta_0 + \beta_1 \hat{\text{LASSO}} + \beta_2 \hat{\text{RF}} + \beta_3 \hat{\text{LLF}} + \beta_4 \hat{\text{GBM}}, \tag{11}$$

where the weights β_i are determined by a relaxed Elastic Net tuned using 10-fold cross-validation. Each algorithm is also cross-validated/fitted: LASSO is tuned with 10-fold cross-validation using the built-in functionality of the *glmnet* R package (J. Friedman et al., 2010). Random forests and LLF are fit using the *grf* package with honest trees and produce OOB predictions. For GBM, I use XGBoost and employ a 3-fold cross-fitting approach, where an XGBoost model is trained on two folds, using the excluded fold as a validation set for early stopping and then predicting the outcome in the excluded fold. The ensemble estimator of the CAPE $[\tau()]$ similarly combines estimates from Causal Forests (Athey et al., 2019) and Local-Linear Causal Forests (Friedberg et al., 2020) obtained via *grf*, with cross-validated/fitted LASSO and XGBoost estimates from minimizing the R-Loss (Eq. 9). A cross-validated relaxed Elastic Net is again used as the final stage estimator and corresponds to the BLP of the CAPE from the 4 constituent estimates. All infrastructure, population, and travel time estimates enter the model in natural logs. This provides a natural interpretation of the CAPE as (semi-)elasticity and improves the fits of the LASSO and LLF models.

The main threat to this DML strategy is the existence of unobserved factors, such as non-physical political, historical, or ethnic contingencies that may affect the local placement of certain infrastructures without affecting the spatial distribution of infrastructure as a whole. Recent

[12] The Neyman Orthogonality Condition states that $\partial_{m,f}(m_0, f_0)E[\epsilon\tilde{W}] = \partial_{m,f}(m_0, f_0)E[(\tilde{Y} - \tau(\mathbf{X}_H)\cdot\tilde{W})\tilde{W}] = 0$, where $\partial_{m,f}(m_0, f_0)$ is the (Gateaux) derivative of the moment condition w.r.t. to the nuisance parameters m, f evaluated at their true values denoted by m_0, f_0. This is zero, such that the moment conditions are not sensitive to small perturbations (biases) in the nuisance parameter estimates $\hat{m}, \hat{f}$. Such moment conditions and the final-stage (GMM) estimators they produce are called Neyman Orthogonal.

[13] The Horvitz-Thompson transformation is given by $h(\mathbf{X}, W) = (W - e(W))/(e(W)(1 - e(W)))$ where $e(W)$ denotes the propensity score.

contributions such as Dreher et al. (2019) and Graff (2024) provide evidence of favouritism and colonial legacy having an impact on activity and infrastructure in Africa, but they do not investigate whether this occurs on a local selective basis. To provide an example in the spirit of Dreher et al. (2019): if an African leader supports his/her birth region by only building additional schools, then this may be problematic because the ML prediction of schools from all other observable characteristics would not be able to capture the favouritism in education. If, however, the support is more broad-based and the region has not only more schools but also more hospitals, roads, and access to power, then these other features increase the ML prediction of schools (and of wealth) in that region and thus favouritism is absorbed by the ML control functions. Even if the first case holds, my nuisance models include a spatial lag (spillover version) of the IWI to eliminate spatial autocorrelation, thus favouritism would have to increase wealth only in the current cell.

To provide empirical evidence, I take data on political and ethnic favouritism and colonial railroad construction from Graff (2024). I aggregate the infrastructure data, debiased at high resolution using the ensemble ML estimatore, into his 0.5° grid. I then run regressions similar to Tables 1 and 2 in Graff (2024) with both raw and debiased infrastructure quantities as outcome variables. Appendix Table A8/A9 reports results for simple/quantile counts. The top half considers raw infrastructure data and provide strong evidence for colonial history and favouritism extended by leaders towards their birth regions in shaping the spatial distribution of infrastructure. With the debiased data in the bottom half, most coefficients become zero and insignificant. A multiple testing adjustment following Clarke et al. (2020) renders all debiased coefficients insignificant. Thus, I argue that favouritism is an aggregate phenomenon and not a threat to high-resolution causal ML estimates controlling for other infrastructure and spatial autocorrelation.

Another caveat is that infrastructure also enters high-resolution outcome measures such as the IWI (through complex ML models learning from OSM and satellite imagery) or nightlights. However, the *Super Learner* can likely recover these 'unobserved nuisance functions', such that the effect of the treatment infrastructure can still be measured, even though the signal-to-noise ratio in the debiased data may be higher than with direct ground-truth measurements.

To test this, I also estimate (C)APEs using IWI estimates from DHS surveys conducted in SSA since 2010. I obtain 17,396 cells with more than 5 households and 10 persons/km^2, for which I compute the average household IWI, vs. 89,044 cells with IWI predictions by Lee & Braithwaite (2022). Both estimates are correlated but not perfectly ($r = 0.814$), reflecting slight methodological differences and Lee & Braithwaite (2022)'s substantially higher resolution and use of DHS surveys only from 2017.[14] Appendix Table A10 shows the Median CAPE prediction (for all 103,922 populated cells) obtained from both IWI measures, and Appendix Table A11 shows APE estimates computed using cells where the respective measure is available. Both tables signify quite similar estimates, especially for important predictors such as roads, communications, travel time, accommodation, health and automotive. Curiously, education has no effect with the DHS data. The DHS-based IWI's median absolute coefficient size is slightly larger than the predicted IWI's. This might be due to noise in the predicted IWI, the reduced cell sample for the DHS-based IWI, or differences in methodology or timing, as elucidated above. Notwithstanding, the estimates are highly correlated across feature categories ($r \geq 0.86$ for the APE). Tables A10 and A11 thus suggest that using a predicted IWI doesn't significantly alter the results.

A final obstacle is reverse causality between infrastructure and wealth/activity. This is impossible to rule out in a pure cross-section. However, controlling for the spatial lags of the IWI and of control infrastructure is likely to mitigate the effects, as similar wealth levels may be present in adjacent cells and wealthy inhabitants of cell i may also build infrastructure in neighbouring cells.

In summary, I argue that the causal ML strategy accounts for most significant spatial planning decisions, and the first stage residuals from the *Super Learners* are likely to represent some noisy local idiosyncracies that can be used to estimate at least a partial equilibrium APE for different types of infrastructure. Notwithstanding, as I cannot formally establish causality or identification, the estimates should be interpreted with caution. I now report the estimates.

[14] I use DHS surveys from 2010 for this exercise to have more data.

4.1 Average Partial Effects

Table 6 reports the APE of the natural log of infrastructure on the IWI. The LHS shows results when features are simply counted in each category and cell, whereas the RHS shows results with quantile counts applied during aggregation, as detailed in Section 2.4. The estimates can be interpreted as the change in IWI points [0, 100] induced by a 100% increase in the corresponding feature intensity. Following Athey & Wager (2019), I also calculate APEs for cells above and below the median CAPE estimate and test for the difference between them as evidence for heterogeneity.[15]

Table 6: Average Partial Effects on IWI

	Simple Counts				Quantile Counts			
Feature	ATE	High	Low	Diff.	ATE	High	Low	Diff.
roads_paved	**0.218*** **	0.283***	0.153***	0.131***	**0.216*** **	0.28***	0.151***	0.128***
power	**0.0683*** **	0.0849***	0.0517***	0.0332	**0.0675*** **	0.0758***	0.0592***	0.0166
education	**0.563*** **	0.958***	0.168***	0.79***	**0.436*** **	0.774***	0.0973***	0.677***
health	**0.803*** **	1.25***	0.359***	0.887***	**0.772*** **	1.15***	0.389***	0.765***
communications	**0.689*** **	0.951***	0.427***	0.525***	**0.689*** **	1.01***	0.371***	0.635***
public_service_utility	**0.327*** **	0.452***	0.203	0.248	**0.331*** **	0.482***	0.179***	0.303*
automotive	**0.873*** **	0.721***	1.02*	-0.299	**0.444** **	0.668**	0.22	0.447
transport_other	**0.332*** **	0.395***	0.27***	0.125	**0.305*** **	0.402***	0.207***	0.194**
financial	**0.626*** **	0.884***	0.369**	0.515**	**0.543*** **	0.791***	0.295	0.496**
services	**1.38**	–	1.38	–	**0.748***	1.27*	0.222	1.05
ttime_city_1m	**-0.513*** **	-0.335***	-0.691***	0.356***	**-0.502*** **	-0.192***	-0.812***	0.62***
ttime_port_any	**-0.293*** **	–	-0.293***	–	**-0.295*** **	-0.141**	-0.448***	0.307***
residential	**-0.0679*** **	0.0271	-0.163***	0.19***	**-0.0519*** **	0.0391**	-0.143***	0.182***
accommodation	**0.807*** **	0.778**	0.835***	-0.0568	**0.771*** **	0.725***	0.817***	-0.0925
tourism_recreation	**0.184** **	0.472***	0.147*	0.325*	**0.309*** **	0.509***	0.108	0.401**
mining_industrial	**0.541*** **	0.878***	0.204***	0.674***	**0.46*** **	0.698***	0.221***	0.477***

*Signif. Codes: ***: 0.01, **: 0.05, *: 0.1. A '–' indicates missing estimates (signifying underidentification).*

Notes: Table shows doubly-robust APE estimates of the log feature intensity (simple counts or quantile counts in each cell, see Section 2.4) on the International Wealth Index [0, 100] by Lee & Braithwaite (2022) (covering 42 SSA countries). The "High" and "Low" estimates report the APE above and below the median CAPE estimate. The "Diff." column indicates their difference to test for heterogeneity. All terms are tested using a two-sided t-test with standard errors derived from the doubly robust scores following Athey & Wager (2019).

Table 6 suggests that, controlling for all other features, including automotive and public transport facilities and travel time to major cities and ports, paved roads have a moderate partial effect on wealth amounting to a 0.22-point IWI increase to a doubling of the paved road quantity. The effect of power is even smaller at only 0.07. On the other hand education, health, communications, automotive facilities, financial services and accommodation (hotels) have rather large effects around 0.56-0.87. Public services and public transport have smaller effects around 0.33. Travel time to major cities and ports, proxying for exogeneous/extra-cell changes in market access, have the expected negative effect of around -0.5 for major cities and -0.3 for ports. Residential areas also have a slight negative effect around -0.07. This must be understood *ceteris paribus*: in the first-stage models I control for GPW4 population, but this is only available at the smallest administrative units. Thus, residential buildings may proxy for the remaining uncontrolled variation in population. The negative coefficient would then suggest that when all other infrastructure is held fixed, adding people does not increase individual wealth ('urbanization without growth' a la Fay & Opal (2000)).

For reference, I have also estimated APEs using the log of nightlights as outcome measures. The results, reported in Table A14, are broadly consistent with Table 6, but emphasize light-generating activities such as automotive facilities (presumably correlated with traffic at night), industrial facilities, and financial services (CBDs), and yield smaller effects of roads, communications, and health/education. Surprisingly, power infrastructure does not have very large effects either.

4.2 Effect Heterogeneity

The cell-level CAPE estimates are arguably more interesting than an all-Africa infrastructure APE. This subsection investigates their distribution and correlates before the next analyzes their spatial patterns. Figure 12 shows kernel density estimates for the IWI CAPEs. The densities indicate that for most infrastructure categories, there is considerable spatial heterogeneity in the partial effect. Only for paved roads and power, there seem to be no negative CAPEs, and the

[15] Since the reported CATE is already a BLP across multiple CATE estimators, the BLP cannot be used as an additional test for effect heterogeneity.

distributions are very narrow. Most other features except for residential buildings and travel time have largely positive but very heterogeneous effects. For education and financial services there are some negative CAPEs. In theory these shouldn't exist, but ML models are unrestricted. Negative values thus indicate that the effects can be zero or close to zero in some locations.

Figure 12: DML CAPE Kernel Density Estimates for IWI

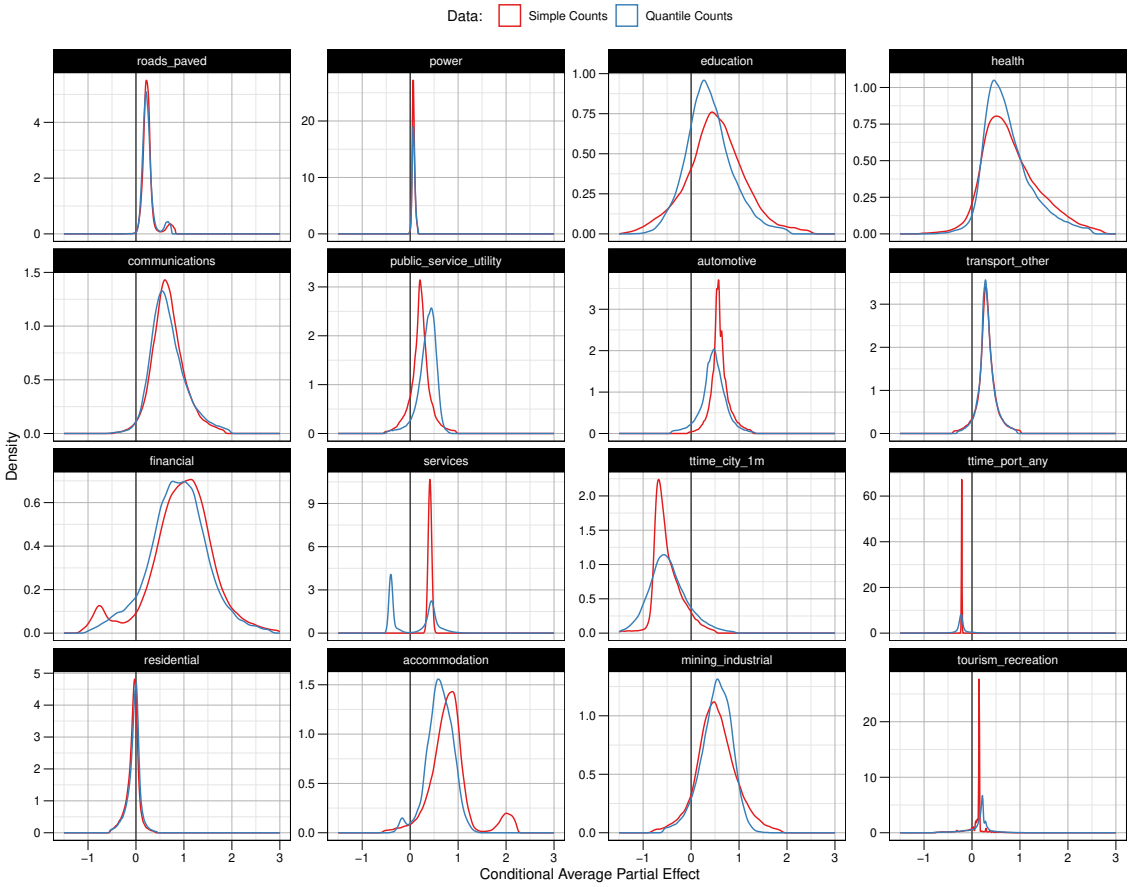

Notes: Figure shows Gaussian kernel density estimates of the Conditional Average Partial Effect (CAPE) of log features' on the International Wealth Index (IWI) [0, 100] by Lee & Braithwaite (2022) (covering 42 SSA countries). Data are aggregated in each cell using either simple counts or quantile counts (see Section 2.4) before taking the natural log.

To compactly summarize important determinants of effect heterogeneity, I compute Pearson's correlations between the CAPEs and all variables in logs. I only report the top heterogeneity variables across infrastructure categories based on their average squared correlation with the CAPEs. Figure 13 reports the results, where the columns are the CAPEs, and the rows are covariates in decreasing order of average squared correlations. The number reported is the average correlation across the simple and quantile counts datasets.

At first sight, Figure 13 exhibits rather simple heterogeneity patterns: most CAPEs are either increasing or decreasing in the level of infrastructure/agglomeration. In particular, the CAPEs of paved roads, travel time to cities (market access), communications, and to a lesser extent, power and financial services, are increasing in the level of agglomeration. For other types of infrastructure the opposite appears to be the case. In particular education, public services and utilities, and mining/industrial facilities have stronger marginal effects on household welfare if found in structurally weak/rural areas. Interestingly, this is also the case for travel time to ports. This suggests some form of infrastructure substitution effects governed by agglomeration forces, e.g., in rural areas, travel time to ports becomes a key determinant of market access, and the presence of a school or a mine/industrial plant as employer has larger wealth effects than in cities with high market access and diverse employment opportunities, even for the uneducated.

As a further robustness exercise, Appendix Figures A12 and A13 show analogous CAPE

estimates from direct DHS wealth estimates, and Tables A12-A13 show correlations among CAPEs from both IWI measures. On average, the CAPEs are similar, particularly for important features with a robust effect, such as paved roads, communications and mining/industrial facilities. The median CAPE correlation is only around 0.13, and 0.25-0.3 if spillover variables are removed.

Figure 13: Correlates of IWI CAPE Estimates ($\mathbf{X}_H$): Average Across Datasets

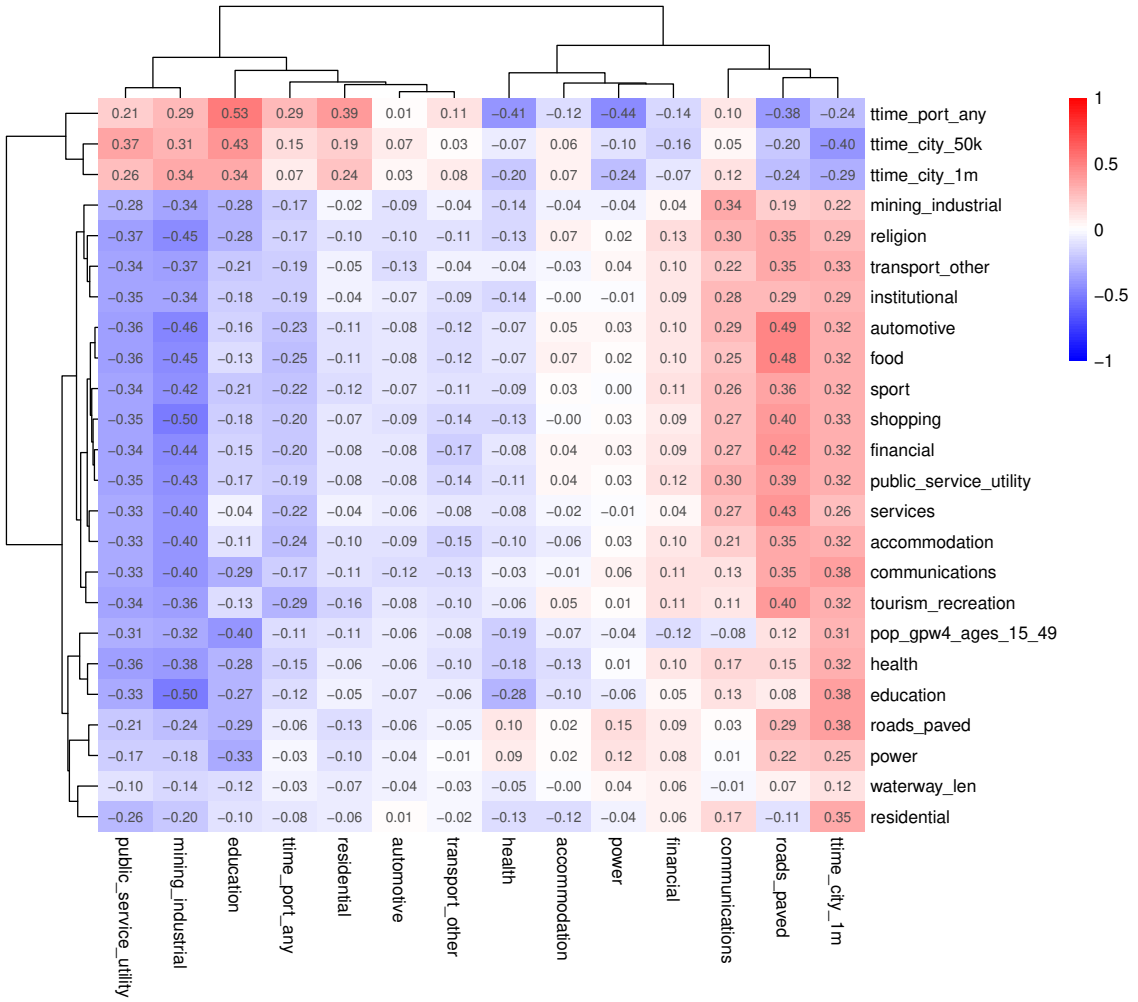

Notes: Figure shows average Pearson's correlations across the simple counts and quantile counts datasets of CAPEs (columns) with the features in logs (rows). A positive correlation implies that the CAPE is increasing in feature intensity.

Appendix Figures A14 and A15 show the densities and main correlates of nightlights CAPEs. While the densities are broadly similar, the correlation are almost all negative. This may be due to the unavailability of data in low-lit areas (zero observations are not considered for training).

There is also a strong spatial dimension to CAPEs not conveyed by correlations with infrastructure variables. Therefore, I now proceed with a visual examination of the IWI CAPE estimates.

4.3 Spatial Examination of Effect Heterogeneity

Figure 14 shows visualizes the geometric mean CAPE across simple and quantile counts-based estimates (to smooth outliers, both estimates are highly correlated at $r > 0.8$) for important features. Overall, there is considerable and complex spatial heterogeneity in the CAPEs. The top panel shows the CAPEs for roads, power, and communications. Exempting power,[16] the effects

[16] In previous versions of this paper, the CAPEs of power was concentrated in cities as well, see Appendix Figure A11. That version only used power infrastructure as reported in OSM. The present version incorporates some higher-resolution grid data from the EU's Joint Research Centre, and yields quite different results. Thus, coverage/definition of infrastructures can significantly affect the outcomes.

are higher in urban areas, particularly for paved roads. Since the IWI is only available for SSA, CAPEs for North Africa are pure predictions from the SSA model. This is problematic for paved roads given their much greater density in North Africa.

Figure 14: Spatial CAPE Estimates: Geometric Mean

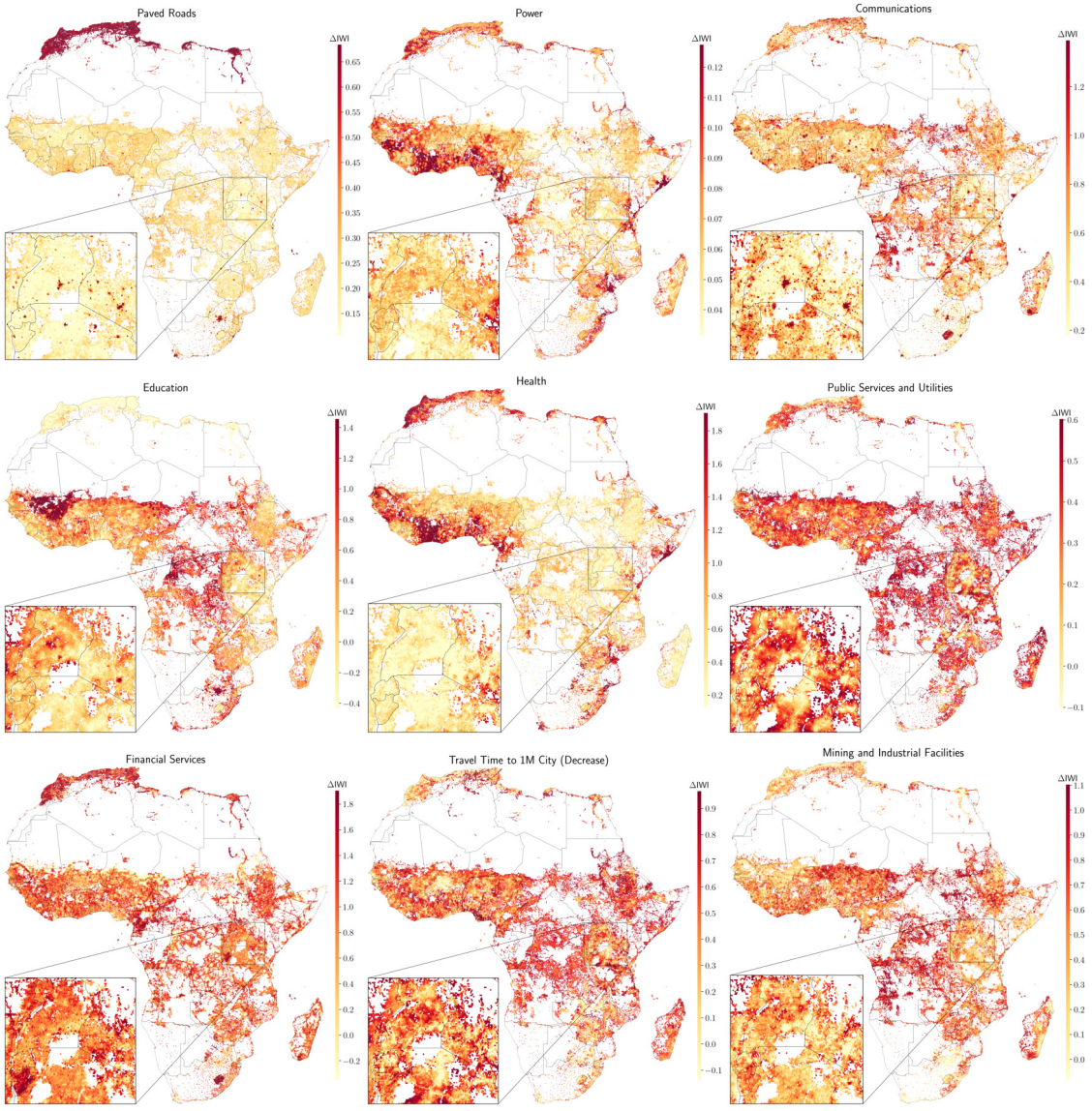

Notes: Figure shows the Conditional Average Partial Effect (CAPE) of log features' on the International Wealth Index (IWI) [0, 100] by Lee & Braithwaite (2022) (covering 42 SSA countries). A geometric mean across estimates derived from simple and quantile counts data (Section 2.5) is reported to limit outliers. Both are correlated ($r > 0.8$ for all features).

The middle panel of Figure 14 shows the CAPEs for education, health, and public services and utilities (excl. power). Excempting health,[17] these broadly follow the opposite spatial pattern, being highest in underdeveloped regions such as the Sahel region, Congo, and rural areas in Ethiopia, (South-)Sudan and Somalia. The bottom panel shows CAPEs for financial services, travel time to large cities, and mining and industrial facilities. The financial services CAPEs suggest that some countries like Burundi or Lesotho are financially underdeveloped. Travel time to cities CAPEs are probably the better estimates for what regional connectivity improvements through new roads could yield in terms of welfare. They are large in many areas outside of urban centers. The mining and industrial facilities CAPEs are also high in many structurally weak areas.

[17] In a previous version of this paper (Version 2), the CAPE of health also very much resembled the one of public services and utilities, see Appendix Figure A11, but this version includes significant data on public health facilities in SSA by Maina et al. (2019), yielding quite different results. Comprehensive and uniform data is needed for robust results.

In summary, CAPE estimates indicate varied associations between distinct infrastructure classes and the spatial distribution of economic activity. The estimates for roads and communications generally suggest stronger marginal effects inside urban spaces, whereas education and public service show stronger effects in semi-urban and rural areas. These findings appear consistent with parts of the literature on urbanization summarized by J. V. Henderson & Turner (2020), suggesting that poor service provision in rural areas is a key driver of rural-to-urban migration.

As pointed out before, there are many limitations to these CAPE estimates, starting from an imperfect classification of features, and non-comprehensive coverage of many infrastructures, especially in less populated regions, over a possibly low signal-to-noise ratio given that IWI estimates partly also depend on infrastructure, to possible reverse causality. They also don't consider general equilibrium effects, such as the relocation of populations and economic activities following infrastructure investments. Their highly partial nature, e.g., the partial effect of roads holding fixed market access and automotive facilities, also complicates policy interpretations.

Notwithstanding all of these caveats, the methodology appears to work well with spatial data and yields interesting spatial heterogeneity that is also broadly sensible and consistent with some of the econometric evidence. This allows for a hopeful outlook that rich and comprehensive spatial datasets (already available in the commercial realm e.g. by Google or Dataplor), and a refined spatial ML methodology, could be developed to generate policy-relevant spatial estimates.

From a policy point of view, another limitation is that marginal effects, and semi-elasticities in particular, are difficult to interpret. Policymakers are more interested in counterfactual predictions, such as the simulated effects of different levels of infrastructure in the same locations. It is possible to generate counterfactual predictions with causal ML, and I attempt to do so in the following section, but the properties of such estimates still need to be established.

5 Counterfactual Predictions

In this section, I explore counterfactual predictions obtained by increasing infrastructure quantities in the data and comparing ML model predictions from this altered dataset to the baseline prediction. This approach is similar to the single-model or 'S-learner' in the context of CATE estimation with binary treatments - applied by Hill (2011) with Bayesian Additive Regression Trees (BART) and discussed in Jacob (2021). I additionally follow Facure & Germano (2021) in using debiased data to avoid confounding influences in the model. Concretely, I estimate

$$\tilde{Y} = \theta(\tilde{W}, \mathbf{X}_H), \tag{12}$$

where $\theta()$ is again an ensemble ML estimator (Eq. 11) and $\tilde{Y}$, $\tilde{W}$ are debiased. In contrast to CAPE estimation, this formulation allows for the effect to be non-linear, i.e., to change with the level of $\tilde{W}$. After estimating $\theta()$ in a cross-fitting manner, I evaluate it at different levels of $\tilde{W}$. Since removing infrastructure is not an interesting policy option, I compute the 10%, 25%, 50%, 75%, and 90% quantiles of the positive (non-missing) distribution of W across cells and alternatingly add them to $\tilde{W}$ and obtain a prediction. Table 7 shows these quantile increases. The 10% increase amounts to one additional facility in most categories, 59 additional power-related items (transformers, generators), or a 2111m increase in the length of paved roads in each cell. Higher quantiles imply much more substantive increases per cell. The increase is only applied to the respective treatment infrastructure $\tilde{W}$; all other infrastructures $\mathbf{X}_H$ are unaltered.

Due to debiasing, the OOB R^2 for the IWI residuals is only 2-5%. The model-based simulation results nevertheless appear meaningful. Figure 15 shows the average predictions with the IWI as outcome measure and Figure A16 with the log of nightlights. Except for residential buildings which have a positive effect with nightlights, the results from both outcomes are very similar. The relative magnitudes are also broadly consistent with the APEs. Appendix Tables A15 and A16-A17 show counterfactual predictions derived from a DHS-based IWI, which are also similar, instilling some confidence in the methodology. Since for many sparse features, both the 10% and 25% treatment levels imply 1 additional feature with count data (see Table 7), the average counterfactual prediction curves in Figure 15 may have some flat segments.

Table 7: Counterfactual Increase in Feature Quantity/Cell for Selected Features

Feature	10%	25%	50%	75%	90%
roads_paved (m)	2111	6295	10371	14493	24119
power	59	168	314	570	980
education	1	1	3	9	24
health	1	1	2	3	8
communications	1	2	6	23	85
public_service_utility	1	1	2	4	10
automotive	1	1	2	7	23
transport_other	1	1	2	7	20
financial	1	1	2	6	21
services	1	1	2	6	24
ttime_city_1m (min)	104	203	363	602	930
ttime_port_any (min)	130	289	564	951	1520
residential	1	3	8	24	84
accommodation	1	1	2	7	24
mining_industrial	1	1	3	8	19
tourism_recreation	1	1	3	8	30

Notes: Table shows sample quantiles on simple-counts data, computed across cells with positive infrastructure for each feature category, respectively. The quantiles are rounded to the full number. They are used for counterfactual predictions, i.e., increasing the infrastructure quantity in all cells by this amount and making a prediction using the causal single-learner (Eq. 12).

Figure 15: Average Counterfactual Predictions for IWI

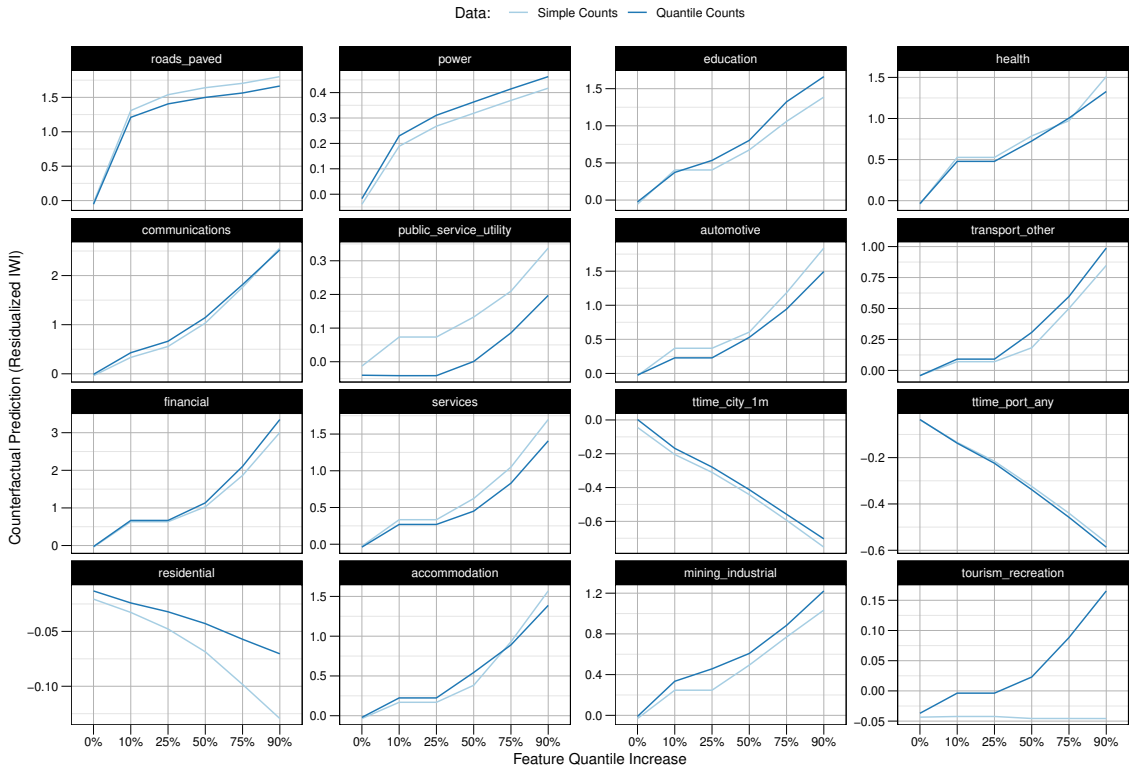

Notes: Figure shows average counterfactual predictions (across all cells) derived from simple and quantile counts data.

Overall, the counterfactual predictions in Figure 15 are very consistent with the CAPE estimates. There is, in general, decreasing returns to scale, i.e., building more of the same infrastructure in each cell does not raise wealth proportionately. For some feature categories such as paved roads and power, the 10% increase has a large initial effect, and further increases add much lower wealth effects. The main reason for this is that, as shown in Section 3.1, most cells are scarcely populated, without paved roads or power supply, and do not have many types of features at all. Thus, the

existence of any paved roads or power suggests to the model that more diverse activity than farming takes place in the cell and implies an increase in average wealth levels. This may be unrealistic, that is, even with debiased data, counterfactual predictions may generate locations that are dissimilar to the ones the model has learned, so further increases in roads/power do not increase wealth much.

Because cells have heterogeneous populations, Appendix Figure A17 also provides the average total wealth effect per cell obtained by multiplying the cell-level predictions with the WorldPop 2020 population measure and computing the average across cells. The relative magnitudes are broadly similar to Figure 15.

5.1 Spatial Examination of 50% Counterfactual Predictions

It remains to examine the spatial distribution of these counterfactual predictions. Since predictions from simple and quantile count data are very similar, I again report a geometric mean across the two which slightly downweights outliers. Since an appraisal of all different treatment levels in the spatial dimension would be overwhelming, I only plot the 50% level in Figure 16.

Figure 16: Spatial 50% Counterfactual Predictions: Geometric Mean

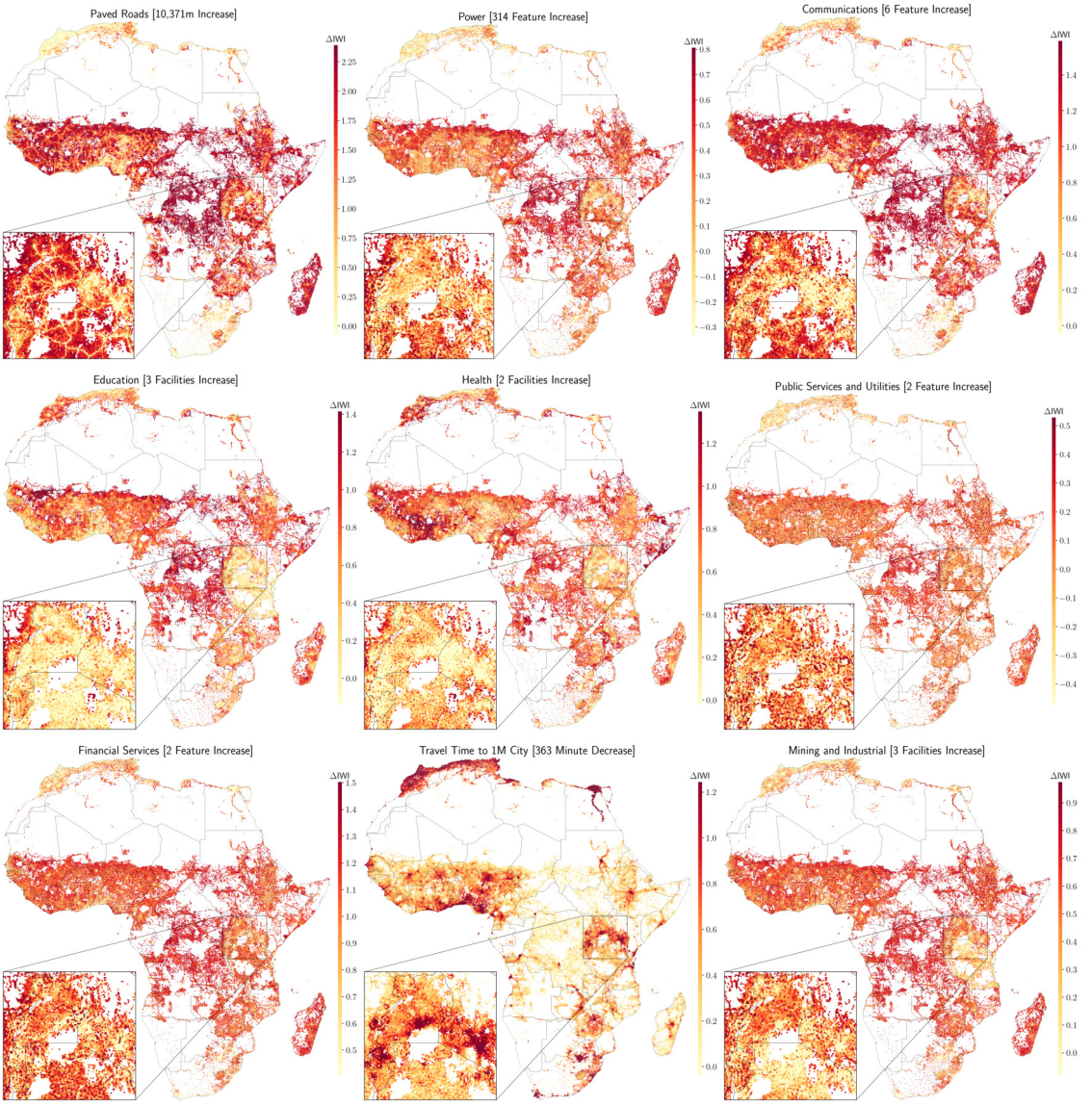

Notes: Figure shows 50% counterfactual predictions of the International Wealth Index (IWI) [0, 100] by Lee & Braithwaite (2022), i.e, the predicted wealth increase (Eq. 12) from an increase in each cell amounting to the median of the non-negative feature density, summarized in Table 7. A geometric mean across estimates derived from simple and quantile counts data (Section 2.5) is reported to limit outliers. Both are correlated ($r > 0.8$ for all features).

Evidently, counterfactual predictions (CFPRs) are more similar across different infrastructure types than CAPEs, indicating that generally the household wealth returns to building a given amount of infrastructure is higher in rural areas than in cities. A notable exception is travel time to major cities, which the CFPRs suggest should be reduced in the vicinity of such cities. Building infrastructure in rural areas as suggested by most of these maps is, however, not aggregate welfare maximizing since most of these areas are scarcely populated. It likely is more sensible to build infrastructure in populated places even though per-household welfare gains are considerably lower.

To provide at least a heuristic, partial equilibrium appraisal of how a social planner seeking to maximize aggregate welfare might allocate investments, I multiply the 50% CFPRs of Figure 16 by the WorldPop 2020 population measure in each cell. Appendix Figure A19 shows the outcome. As expected, investments in populated areas generally yield higher aggregate welfare returns, but there remains considerable heterogeneity across different infrastructures, for example power and education investments are primarily directed to populated rural areas and less to city centers.

Overall, these counterfactual predictions emphasize the benefits of investments in rural areas towards poverty alleviation. The reader should keep in mind that policymakers may consider not only population but also poverty, inequality, and other social and political objectives in determining optimal infrastructure allocations. With more careful efforts at monetizing them (e.g., considering not only the beneficiaries and policy objectives but also the cost of building infrastructure in different locations), counterfactual predictions appear able to provide useful guidance for spatial planning. They are easier to interpret than a semi-elasticity CAPE, allow simulating different 'treatment levels,' and do not require the restrictive additive separability of treatment assumption in CAPE estimation. On the other hand, the single-learner approach needs to be better studied and has significant shortcomings. In particular, the relevance of the 'treatment variable' is not guaranteed in an unrestricted ML model. Estimating a CAPE using multiple estimators and combining them through a BLP model - as done in this paper - has the clear advantage of at least providing well-calibrated estimates. An equivalent estimation and validation strategy for counterfactual predictions remains to be developed.

6 Summary and Conclusion

This paper studies Africa's spatial economy and the interplay of infrastructure with household wealth and economic activity using rich geospatial data compiled from Open Street Map, Overture Maps, and multiple recent research and data contributions. It also maps potential economic benefits from different types of incremental infrastructure investments at high spatial resolutions using causal machine learning methods. The investigation is fruitful in several respects.

It shows that most infrastructure in Africa is highly concentrated in cities - more than population, and, exempting educational facilities, the sum of all features, and network infrastructures such as roads and power, also than GDP. Populated places themselves are very heterogeneous. A case study of 5 African capital cities reveals that some cities, such as Nairobi and Johannesburg, outperform others, such as Lagos, Cairo, and Accra, regarding infrastructure, public services, and amenities per person, even after controlling for wealth, population, and market access. This confirms that other factors, such as city governance and the overall business environment, also shape the distribution of economic activity and infrastructure. Furthermore, in many countries, infrastructure seems inefficiently allocated, with population, roads and, power infrastructure, and economic activities often found in disparate locations. Countries with higher levels of spatial efficiency, characterized by the average proximity of population, infrastructure, and activities, have higher average levels of development, a stronger business environment, and greater logistic performance.

Training tree-based ensemble ML models to predict wealth and economic activity from infrastructure yields that roads, communications, education, power infrastructure, and residential areas are the most important predictors of wealth. Other features such as accommodation (hotels), automotive facilities, sports facilities, commercial buildings, public services and utilities, and health facilities are also important. Models including population and travel time to major cities and ports rank them as top predictors, indicating that market access is similarly essential to physical infrastructure. The relative importance of these variables varies across locations. In cities, the quantity

of paved roads and power infrastructure is very important for wealth prediction. In contrast, education, health, and public service facilities are of greater relevance in structurally weaker areas.

Similar patterns are evident in marginal effects ((semi-)elasticities) of household wealth to infrastructure, computed using causal ML methods. Investments in education, paved roads, power, communications, industrial facilities, health, automotive facilities, transport, public services, and hotels yield high average but spatially very heterogeneous returns. Doubly robust estimates of the Average Partial Effect (APE) of infrastructure on wealth range between 0 and 1 point increases in the International Wealth Index (IWI) in response to the doubling of infrastructure within a specific category. The APE of roads is robustly around 0.22 IWI points, market access held fixed. The Conditional Average Partial Effect (CAPE) for roads is also positive everywhere but highest in urban spaces, implying that more roads are always a good idea, especially in urban agglomerations. Power has a smaller APE of 0.07. Education, on the other hand, has a large APE between 0.44 and 0.56, with the largest CAPEs realized in rural areas lacking schools. Communications also has a large APE of 0.696; the CAPEs are generally higher in urban areas. Public services have an APE of around 0.33, with higher CAPEs in less developed areas. Industrial facilities have an APE around 0.5, with, surprisingly, higher CAPEs in rural areas, presumably because they are not major income generators in African cities. Market access itself also has a sizeable impact, with a doubling of travel time to major cities ($>$ 1 million inhabitants) decreasing the IWI by -0.5 points, and a doubling of travel time to ports having a similar effect of -0.3 IWI points. Residential buildings also have a small negative APE between -0.05 and -0.07, indicating that, all other infrastructure held fixed, individual wealth is an inverse function of the number of people using these infrastructures. These marginal effects are partial equilibrium effects that do not consider the spatial relocation of economic activity and populations following such investments. They may also suffer from reverse causality.

Counterfactual predictions, obtained by applying a spatially uniform increase in infrastructure to the data (e.g., one additional school in all cells) and predicting the outcome (e.g., wealth) using a debiased ML model, yield greater effects in rural areas compared to the CAPEs (which are semi-elasticities). However, the number of beneficiaries in such areas is smaller. Factoring in the different populations of locations generally emphasizes investments in more populated locations, especially those lacking the respective infrastructure. The correct use of counterfactual predictions - even if perfectly causal - thus critically depends on the objective of policymakers: welfare maximization, poverty alleviation, and inequality aversion objectives imply different spatial policies derived from the same set of predictions. Apart from these policy challenges, the less robust estimation methodology and lack of theoretical literature on counterfactual predictions are clear disadvantages despite their more natural interpretation and less restrictive theoretical assumptions.

In conclusion, the findings of this paper need to be digested with caution. They are exploratory and not sufficiently robust or causal to be used for policy advice. However, given the elusiveness of comprehensive causal empirical evidence, they offer a significant advance toward data-driven evidence on the local and global returns of infrastructure and public/private services towards activity and wealth generation/poverty alleviation. Many methodological improvements are conceivable, e.g., using more sophisticated spatial weighting matrices or ML methods explicitly capable of learning spatial dependencies (such as Convolutional Neural Networks). A refined methodology and comprehensive geospatial data may generate infrastructure potential maps that could provide helpful guidance for spatial planning and gauging the returns to small public infrastructure investments. As geospatial data is becoming increasingly rich and the measurement of wealth and activity across space continues to improve, the pioneering results presented in this paper allow for a hopeful outlook on causal machine learning's potential to enhance spatial economic and development planning.

References

ADB. (2018). Africa's infrastructure: great potential but little impact on inclusive growth. *African Economic Outlook*.

Akiba, T., Sano, S., Yanase, T., Ohta, T., & Koyama, M. (2019). Optuna: A next-generation hyperparameter optimization framework. In *Proceedings of the 25th ACM SIGKDD international conference on knowledge discovery and data mining.*

Akpandjar, G., & Kitchens, C. (2017). From darkness to light: The effect of electrification in ghana, 2000–2010. *Economic Development and Cultural Change*, *66*(1), 31–54.

Allcott, H., Collard-Wexler, A., & O'Connell, S. D. (2016, March). How do electricity shortages affect industry? evidence from india. *American Economic Review*, *106*(3), 587-624. Retrieved from https://www.aeaweb.org/articles?id=10.1257/aer.20140389 doi: 10.1257/aer.20140389

Apley, D. W., & Zhu, J. (2016). Visualizing the effects of predictor variables in black box supervised learning models. *arXiv preprint arXiv:1612.08468*.

Athey, S., & Imbens, G. (2016). Recursive partitioning for heterogeneous causal effects. *Proceedings of the National Academy of Sciences*, *113*(27), 7353–7360.

Athey, S., Tibshirani, J., & Wager, S. (2019). Generalized random forests. *The Annals of Statistics*, *47*(2), 1148.

Athey, S., & Wager, S. (2019). Estimating treatment effects with causal forests: An application. *Observational studies*, *5*(2), 37–51.

Athey, S., & Wager, S. (2021). Policy learning with observational data. *Econometrica*, *89*(1), 133–161.

Barnes, R. (2020). dggridr: Discrete global grids [Computer software manual]. Retrieved from https://CRAN.R-project.org/package=dggridR (R package version 2.0.4)

Baum-Snow, N., Henderson, J. V., Turner, M. A., Zhang, Q., & Brandt, L. (2020). Does investment in national highways help or hurt hinterland city growth? *Journal of Urban Economics*, *115*, 103124.

Bayer, P., Kennedy, R., Yang, J., & Urpelainen, J. (2020). The need for impact evaluation in electricity access research. *Energy Policy*, *137*, 111099.

Borisov, V., Leemann, T., Seßler, K., Haug, J., Pawelczyk, M., & Kasneci, G. (2021). Deep neural networks and tabular data: A survey. *arXiv preprint arXiv:2110.01889*.

Breiman, L. (2001). Random forests. *Machine learning*, *45*(1), 5–32.

Byers, L., Friedrich, J., Hennig, R., Kressig, A., Li, X., McCormick, C., & Valeri, L. M. (2018). A global database of power plants. *World Resources Institute*, *18*.

Chen, T., & Guestrin, C. (2016). Xgboost: A scalable tree boosting system. In *Proceedings of the 22nd acm sigkdd international conference on knowledge discovery and data mining* (pp. 785–794).

Chernozhukov, V., Chetverikov, D., Demirer, M., Duflo, E., Hansen, C., & Newey, W. (2017). Double/debiased/neyman machine learning of treatment effects. *American Economic Review*, *107*(5), 261–265.

Chernozhukov, V., Chetverikov, D., Demirer, M., Duflo, E., Hansen, C., Newey, W., & Robins, J. (2018, 01). Double/debiased machine learning for treatment and structural parameters. *The Econometrics Journal*, *21*(1), C1-C68. Retrieved from https://doi.org/10.1111/ectj.12097 doi: 10.1111/ectj.12097

Chernozhukov, V., Demirer, M., Duflo, E., & Fernandez-Val, I. (2018). *Generic machine learning inference on heterogeneous treatment effects in randomized experiments, with an application to immunization in india* (Tech. Rep.). National Bureau of Economic Research.

Chernozhukov, V., Escanciano, J. C., Ichimura, H., Newey, W. K., & Robins, J. M. (2022). Locally robust semiparametric estimation. *Econometrica*, *90*(4), 1501–1535.

Chi, G., Fang, H., Chatterjee, S., & Blumenstock, J. E. (2022). Microestimates of wealth for all low-and middle-income countries. *Proceedings of the National Academy of Sciences*, *119*(3), e2113658119.

CIESIN. (2016). *Gridded population of the world, version 4 (gpwv4): Population count* (Tech. Rep.). NASA Socioeconomic Data and Applications Center (SEDAC). Retrieved from http://dx.doi.org/10.7927/H4X63JVC

Clarke, D., Romano, J. P., & Wolf, M. (2020). The romano–wolf multiple-hypothesis correction in stata. *The Stata Journal*, *20*(4), 812–843.

Donaldson, D. (2018). Railroads of the raj: Estimating the impact of transportation infrastructure. *American Economic Review*, *108*(4-5), 899–934.

Donaldson, D., & Hornbeck, R. (2016). Railroads and american economic growth: A "market access" approach. *The Quarterly Journal of Economics*, *131*(2), 799–858.

Donaldson, D., & Storeygard, A. (2016). The view from above: Applications of satellite data in economics. *Journal of Economic Perspectives*, *30*(4), 171–198.

Dreher, A., Fuchs, A., Hodler, R., Parks, B. C., Raschky, P. A., & Tierney, M. J. (2019). African leaders and the geography of china's foreign assistance. *Journal of Development Economics*, *140*, 44–71.

Faber, B. (2014, 03). Trade Integration, Market Size, and Industrialization: Evidence from China's National Trunk Highway System. *The Review of Economic Studies*, *81*(3), 1046-1070. Retrieved from https://doi.org/10.1093/restud/rdu010 doi: 10.1093/restud/rdu010

Facure, M., & Germano, M. (2021). *Python Causality Handbook: First Edition*. Zenodo. Retrieved from https://doi.org/10.5281/zenodo.4445778 doi: 10.5281/zenodo.4445778

Fay, M., & Opal, C. (2000). *Urbanization without growth: A not so uncommon phenomenon* (Vol. 2412). World Bank Publications.

Foster, V., & Briceño-Garmendia, C. (2010). *Africa's infrastructure: a time for transformation*. World Bank.

Friedberg, R., Tibshirani, J., Athey, S., & Wager, S. (2020). Local linear forests. *Journal of Computational and Graphical Statistics*, *30*(2), 503–517.

Friedman, J., Tibshirani, R., & Hastie, T. (2010). Regularization paths for generalized linear models via coordinate descent. *Journal of Statistical Software*, *33*(1), 1–22. doi: 10.18637/jss.v033.i01

Friedman, J. H. (2001). Greedy function approximation: a gradient boosting machine. *Annals of statistics*, 1189–1232.

Gennaioli, N., La Porta, R., Lopez-de Silanes, F., & Shleifer, A. (2013). Human capital and regional development. *The Quarterly journal of economics*, *128*(1), 105–164.

Gibson, J., Olivia, S., & Boe-Gibson, G. (2020). Night lights in economics: Sources and uses 1. *Journal of Economic Surveys*, *34*(5), 955–980.

Goldbeck, M., & Lindlacher, V. (2021). *Digital infrastructure and local economic growth: Early internet in sub-saharan africa*. ifo Institute for Economic Research, University of Munich.

Graff, T. (2024). Spatial inefficiencies in africa's trade network. *Journal of Development Economics*, 103319.

Henderson, J. V., & Turner, M. A. (2020). Urbanization in the developing world: too early or too slow? *Journal of Economic Perspectives*, *34*(3), 150–173.

Henderson, V., Storeygard, A., & Weil, D. N. (2011). A bright idea for measuring economic growth. *American Economic Review*, *101*(3), 194–199.

Henderson, V., Storeygard, A., & Weil, D. N. (2012). Measuring economic growth from outer space. *American economic review*, *102*(2), 994–1028.

Hill, J. L. (2011). Bayesian nonparametric modeling for causal inference. *Journal of Computational and Graphical Statistics*, *20*(1), 217–240.

Hirano, K., & Imbens, G. W. (2004). The propensity score with continuous treatments. *Applied Bayesian modeling and causal inference from incomplete-data perspectives*, *226164*, 73–84.

Jacob, D. (2021). Cate meets ml: Conditional average treatment effect and machine learning. *Digital Finance*, *3*(2), 99–148.

Jean, N., Burke, M., Xie, M., Davis, W. M., Lobell, D. B., & Ermon, S. (2016). Combining satellite imagery and machine learning to predict poverty. *Science*, *353*(6301), 790–794.

Jedwab, R., & Storeygard, A. (2022). The average and heterogeneous effects of transportation investments: Evidence from sub-saharan africa 1960–2010. *Journal of the European Economic Association*, *20*(1), 1–38.

Kakoulaki, G., & Moner-Girona, M. (2020). *Electricity grid africa* [Dataset]. http://data.europa.eu/89h/624c6e71-3b9c-4f48-8c67-645911798d41. European Commission, Joint Research Centre (JRC).

Kmoch, A., Matsibora, O., Vasilyev, I., & Uuemaa, E. (2022). Applied open-source discrete global grid systems. *AGILE: GIScience Series*, *3*, 41.

Krantz, S. (2023). osmclass: Classify open street map features [Computer software manual]. Retrieved from https://CRAN.R-project.org/package=osmclass (R package version 0.1.3)

Kummu, M., Taka, M., & Guillaume, J. H. (2018). Gridded global datasets for gross domestic product and human development index over 1990–2015. *Scientific data*, *5*(1), 1–15.

Lee, K., & Braithwaite, J. (2022). High-resolution poverty maps in sub-saharan africa. *World Development*, *159*, 106028.

Lee, K., Miguel, E., & Wolfram, C. (2020, February). Does household electrification supercharge economic development? *Journal of Economic Perspectives*, *34*(1), 122-44. Retrieved from https://www.aeaweb.org/articles?id=10.1257/jep.34.1.122 doi: 10.1257/jep.34.1.122

Lundberg, S. M., Erion, G., Chen, H., DeGrave, A., Prutkin, J. M., Nair, B., ... Lee, S.-I. (2020). From local explanations to global understanding with explainable ai for trees. *Nature machine intelligence*, *2*(1), 56–67.

Lundberg, S. M., & Lee, S.-I. (2017). A unified approach to interpreting model predictions. *Advances in neural information processing systems*, *30*.

Maina, J., Ouma, P. O., Macharia, P. M., Alegana, V. A., Mitto, B., Fall, I. S., ... Okiro, E. A. (2019). A spatial database of health facilities managed by the public health sector in sub saharan africa. *Scientific data*, *6*(1), 134.

Moneke, N. (2020). *Infrastructure and structural transformation: evidence from ethiopia* (Unpublished doctoral dissertation). London School of Economics and Political Science.

MSI. (2019). *World port index 2015* (Tech. Rep.). Retrieved from https://msi.nga.mil/Publications/WPI

Nelson, A. (2022, 10). *Travel time to cities and ports in the year 2015* (Tech. Rep.). Retrieved from https://figshare.com/articles/dataset/Travel_time_to_cities_and_ports_in_the_year_2015/7638134 doi: 10.6084/m9.figshare.7638134.v4

Nelson, A., Weiss, D. J., van Etten, J., Cattaneo, A., McMenomy, T. S., & Koo, J. (2019). A suite of global accessibility indicators. *Scientific data*, *6*(1), 1–9.

Nie, X., & Wager, S. (2021). Quasi-oracle estimation of heterogeneous treatment effects. *Biometrika*, *108*(2), 299–319.

Nordhaus, W., Azam, Q., Corderi, D., Hood, K., Victor, N. M., Mohammed, M., ... Weiss, J. (2006). The g-econ database on gridded output: methods and data. *Yale University, New Haven*, *6*, 11.

Peng, C., & Chen, W. (2021). Roads to development? Examining the Zambian context using AI-Sat.

Robins, J. M., Rotnitzky, A., & Zhao, L. P. (1994). Estimation of regression coefficients when some regressors are not always observed. *Journal of the American statistical Association*, *89*(427), 846–866.

Robinson, P. M. (1988). Root-n-consistent semiparametric regression. *Econometrica*, 931–954.

Román, M. O., Wang, Z., Sun, Q., Kalb, V., Miller, S. D., Molthan, A., ... others (2018). Nasa's black marble nighttime lights product suite. *Remote Sensing of Environment*, *210*, 113–143.

Sahr, K. (2022). User documentation for discrete global grid generation software. *Southern Oregon Univ., Ashland, OR, USA, Tech. Rep. Dggrid version*, *7.5*.

Sahr, K., White, D., & Kimerling, A. J. (2003). Geodesic discrete global grid systems. *Cartography and Geographic Information Science*, *30*(2), 121–134.

Stekhoven, D. J., & Bühlmann, P. (2012). Missforest: non-parametric missing value imputation for mixed-type data. *Bioinformatics*, *28*(1), 112–118.

Storeygard, A. (2016). Farther on down the road: transport costs, trade and urban growth in sub-saharan africa. *The Review of economic studies*, *83*(3), 1263–1295.

Tibshirani, J., Athey, S., Sverdrup, E., & Wager, S. (2023). grf: Generalized random forests [Computer software manual]. Retrieved from https://CRAN.R-project.org/package=grf (R package version 2.3.0)

Van der Laan, M. J., Polley, E. C., & Hubbard, A. E. (2007). Super learner. *Statistical applications in genetics and molecular biology*, *6*(1).

Weiss, D. J., Nelson, A., Gibson, H., Temperley, W., Peedell, S., Lieber, A., ... others (2018). A global map of travel time to cities to assess inequalities in accessibility in 2015. *Nature*, *553*(7688), 333–336.

Appendix

Constructing the Africa Infrastructure Database

The basis for the database is the Open Street Map (OSM) of Africa from April 2024, downloaded from Geofabrik.de. OSM has three basic data structures (nodes, ways, and relations) labeled through tags. A tag consists of a key and a value. Under the free tagging system, an object can have unlimited tags. However, the community agrees on certain key-value combinations for the most commonly used tags, which act as informal standards. In particular, the OSM Feature Documentation lists 29 primary tags, such as amenity, building, highway, water, landuse, shop, craft, etc. These primary tags are used with specified values to classify certain features, for example, amenity = school, shop = bakery, or building = hotel, and often accompanied by supplementary tags providing more precise information about a feature, e.g., name, description, denomination, etc.

There are three main obstacles to reconciling this tagging system with the economic significance of map features: (1) a feature can be classified according to multiple primary tags, e.g., amenity = school, building = education, landuse = education or amenity = hospital, healthcare = laboratory, emergency = yes; (2) sometimes classifications based on primary tags can conflict, e.g., for a religious school amenity = school and religion = christian, or for a hotel with restaurant building = hotel and amenity = restaurant; (3) the proximity of the object to the economic activity concerned may not be very clear, e.g., amenity = school and landuse = education both signify the primary use of an object for educational purposes, but the 'school' tag is a lot more specific. The tagging system of OSM is also subject to changes, and due to the crowdsourced nature of the map, some features are not classified according to current standards.

Constructing a functional classification of OSM is thus more an art than a science. One needs to devise a system of economic categories and lay out all tags according to which an economic category is to be assigned and the order in which these tags and categories are to be matched. This needs to be informed by both the OSM tagging standards and empirical accounts of current mapping practice. Once a classification scheme has been specified and applied to the map, features assigned to multiple categories need to be investigated, and the classification needs to be iteratively refined to minimize overlap and misclassification.

Following this process, I have developed a classification scheme to classify point and polygon (closed ways) map features into 33 economic categories based on 33 (mostly primary) tags and 341 values to be matched, including matching on any value for specific tags like 'sport' or 'power.' Within each category, tags providing precise information about the nature of the feature are matched first, and more general tags like 'building' or 'landuse' are matched last. The classification excludes natural features like mountains or lakes, natural or administrative boundaries, and minor features with little economic significance, such as traffic signs or flag poles. Minor infrastructure related to power, telecommunications, and military purposes is, however, included.

The *osmclass* R package developed for this purpose helps apply such classifications - defined as nested lists of categories, tags, and values - to OSM PBF files imported as spatial data frames. It includes the classifications used in this paper. Table A1 summarizes the classification and features extracted from the Africa OSM of April 2024, sorted by the number of features on the map.[18]

[18] This is not the order in which categories were matched, which was chosen to minimize misclassification in Africa. A detailed view of the classification is provided in the R package at https://github.com/SebKrantz/osmclass/blob/main/R/classifications.R.

Table A1: Classification of Africa OSM Point and Polygon Features: April 2024

Category	NTags	NVals	Tags and Number of Matched Values	N
residential	3	11	building (8), building:use (2), landuse (1)	6,382,886
power	4	4	power (all), utility (1), building (1), tower:type (1)	1,672,204
farming	4	19	place (1), man_made (1), building (9), landuse (8)	1,252,658
construction	2	2	building (1), landuse (1)	566,912
transport	12	49	amenity (21), highway (9), railway (all), aerialway (all), waterway (6), aeroway (all), public_transport (all), bridge (all), junction (all), office (2), man_made (2), building (3)	453,510
shopping	4	9	amenity (2), shop (2), building (4), landuse (1)	358,407
education	3	7	amenity (3), building (3), landuse (1)	328,016
sports	3	13	leisure (7), sport (all), building (5)	177,134
facilities	2	19	amenity (18), building (1)	161,083
religion	6	21	amenity (6), building (11), office (1), landuse (1), religion (all), denomination (all)	118,861
food	1	7	amenity (7)	115,087
health	3	11	amenity (9), healthcare (all), building (1)	106,353
utilities_other	5	18	man_made (12), water (1), office (1), building (3), landuse (1)	95,801
commerical	2	2	building (1), landuse (1)	90,549
industrial	4	7	industrial (all), man_made (2), building (1), landuse (3)	84,928
recreation	4	20	amenity (5), leisure (13), landuse (1), building (1)	79,447
historic	1	1	historic (1)	75,332
accommodation	2	8	tourism (7), building (1)	67,054
craft	1	1	craft (all)	59,246
tourism	3	4	tourism (1), shop (1), office (2)	47,617
financial	2	11	amenity (6), office (5)	46,040
institutional	3	7	office (5), building (1), landuse (1)	42,775
public_service	2	12	amenity (10), building (2)	36,658
mining	2	5	man_made (4), landuse (1)	29,711
communications	7	17	amenity (2), telecom (all), communication (all), utility (1), man_made (6), office (1), tower:type (5)	28,740
storage	3	6	man_made (2), building (3), landuse (1)	28,308
office_other	2	2	office (all), building (1)	26,158
waste	4	8	amenity (5), water (1), man_made (1), landuse (1)	21,313
education_alt	3	9	amenity (6), office (2), building (1)	13,852
military	3	5	military (all), building (3), landuse (1)	12,696
entertainment	2	17	amenity (13), leisure (4)	6,028
emergency	1	1	emergency (1)	4,622
creativity	3	8	amenity (2), leisure (1), office (5)	2,142
SUM	33	341		12,592,128

Table A2 shows a similar classification of line-based features. Residential roads are excluded as they are irrelevant to trade and strongly overlap with residential buildings recorded on the map. Smaller natural water features such as streams, wadis, and ponds are also excluded.

Table A2: Classification of Africa OSM Line Features: April 2024

Category	NTags	NVals	Tags and Number of Matched Values	N	Length (Km)
road	1	10	highway (10)	763,912	1,621,144
waterway	3	12	waterway (8), water (1), man_made (3)	359,756	1,507,112
power	1	1	power (all)	120,052	422,504
railway	1	1	railway (all)	84,707	128,408
aeroway	1	1	aeroway (all)	27,360	11,019
pipeline	1	1	man_made (1)	9,453	55,394
storage	1	2	man_made (2)	8,551	389
ferry	1	1	route (1)	2,412	48,259
aerialway	1	1	aerialway (all)	171	175
telecom	2	2	telecom (all), communication (all)	87	28,682
SUM	11	32		1,376,805	3,834,579

Harmonized Classification

I then combine the point/polygon data from OSM with the 824 thousand POIs from the Overture Places layer to create a uniform classification. This involves creating 47 detailed categories and matching features to them based on OSM tags or primary POI categories in Overture maps, of which there are more than 1000. To simplify the dataset again for most analytical use cases and ensure that each category has sufficient features, I combined some of the 47 categories, yielding a simplified classification of 26 categories. The other POI data, e.g., from All The Places, is more limited and easier to classify (e.g., mostly shops, restaurants, and hotels clearly tagged) and can seamlessly be assigned to the 47 categories.

Deduplication

Having classified POIs from 11 different sources (Table 1) into 47 categories, it remains to sort out duplicates across sources. The order of precedence is to favour curated data (such as Global Integrated Power Tracker or health facilities by Maina et al. (2019)) above OSM, which in turn takes precedence over Overture places (which various online appraisals found less accurate). POIs are then deduplicated within each category and 10m square. This resolution is motivated by considering a dense shopping mall where stores may be only 10m apart. POIs are resolved to grid cells by dividing their coordinates by the degree-equivalent of 10m at the equator [10/(40075017/360) $\approx$ 9e-5], subtracting the modulus of this division from the coordinates and using them to group and deduplicate features. To ensure equal distance representation across Africa, longitudes are multiplied beforehand by $cos(lat \times \pi/180)$, where lat is the latitude. After a deduplication round, the coordinates are incremented by 1m degree-equivalent ($\approx$ 9e-6), and the process is repeated. A sequence of such 1m nudges to the lon and lat coordinates is used to 'shift the grid' across space in a structured way until no more duplicates can be found. Since which POIs are first compared depends on the initial position of the 'grid,' there is some path dependence in this process. However, the clear hierarchy across sources ensures that curated datasets are generally fully retained.

Table A3 summarizes the finally classified and deduplicated POI data, including the corresponding number of POIs and the share of OSM and OSM polygons (tagged buildings).

Linestring (network) data is mainly taken from OSM, which is a reliable data source for roads, waterways, and railways. However, its coverage of power lines is limited to major lines in most regions. To increase granularity, I add Africa electricity grid maps from the EU's Joint Research Center (Kakoulaki & Moner-Girona, 2020) and the World Bank, which more than doubles the total length of power lines observed from 423 thousand km in OSM to 967 thousand km (Table 2) following harmonization. To combine/harmonize the linestrings, I compute a geometric union between all three data sources. This obscures definitions of individual power lines from different datasets and breaks up the linestrings into smaller segments, but for the purposes of this research, only the total length of lines per cell matters. Table 2 summarizes the final lines dataset.

Table A3: Africa Infrastructure Database: Places Dataset by Category

detailed (47)	simplified (26)	count	perc	polygons	poly_perc	osm	osm_perc	src_cat
residential	residential	6,276,302	41.42	6,256,643	99.69	6,267,969	99.87	12
communications_network	communications	1,914,448	12.64	502	0.03	20,092	1.05	31
communications_other	communications	14,245	0.09	826	5.80	8,239	57.84	31
power	power	1,654,373	10.92	1,711	0.10	1,651,175	99.81	92
farming	farming	1,228,969	8.11	1,219,018	99.19	1,223,781	99.58	28
construction	construction	585,168	3.86	565,752	96.68	574,167	98.12	90
transport_other	transport	303,186	2.00	21,166	6.98	293,233	96.72	188
automotive	transport	164,845	1.09	61,571	37.35	118,311	71.77	84
education_essential	education	392,361	2.59	216,007	55.05	326,848	83.30	27
education_other	education	27,943	0.18	2,520	9.02	10,811	38.69	36
shopping_essential	shopping	227,820	1.50	43,393	19.05	173,233	76.04	42
shopping_other	shopping	176,718	1.17	5,459	3.09	106,535	60.29	1,239
wholesale	shopping	9,994	0.07	5,094	50.97	6,185	61.89	18
facilities	public_service_utility	173,669	1.15	50,344	28.99	170,252	98.03	37
utilities_other	public_service_utility	109,465	0.72	18,261	16.68	108,419	99.04	48
public_service	public_service_utility	58,369	0.39	18,571	31.82	40,192	68.86	32
health_essential	health	247,386	1.63	33,318	13.47	95,917	38.77	233
health_specialized	health	8,295	0.05	38	0.46	538	6.49	51
health_other	health	5,722	0.04	125	2.18	1,037	18.12	68
sport	sport	181,758	1.20	123,156	67.76	158,453	87.18	242
industrial	mining_industrial	138,407	0.91	62,032	44.82	121,246	87.60	156
mining	mining_industrial	30,209	0.20	22,378	74.08	29,824	98.73	10
SEZ	mining_industrial	387	0.00	0	0.00	0	0.00	6
religion	religion	161,716	1.07	59,682	36.91	116,015	71.74	84
food	food	160,645	1.06	7,602	4.73	74,966	46.67	141
financial	financial	151,493	1.00	3,289	2.17	42,018	27.74	37
accommodation	accommodation	123,248	0.81	19,853	16.11	61,228	49.68	34
parks_and_nature	tourism_recreation	66,925	0.44	43,918	65.62	57,798	86.36	32
tours_and_sightseeing	tourism_recreation	40,796	0.27	1,698	4.16	26,200	64.22	42
museums	tourism_recreation	5,096	0.03	812	15.93	1,805	35.42	28
beaches_and_resorts	tourism_recreation	4,856	0.03	171	3.52	312	6.43	8
outdoor_activities	tourism_recreation	3,110	0.02	157	5.05	1,033	33.22	53
commercial	commercial	109,580	0.72	97,251	88.75	108,351	98.88	11
historic	historic	100,738	0.66	27,458	27.26	72,683	72.15	94
beauty	beauty	65,711	0.43	769	1.17	27,305	41.55	29
professional_services	services	30,948	0.20	413	1.33	2,427	7.84	65
home_services	services	27,575	0.18	391	1.42	5,466	19.82	78
business_services	services	6,168	0.04	56	0.91	382	6.19	31
institutional	institutional	62,313	0.41	9,974	16.01	44,450	71.33	65
drinking	entertainment	35,314	0.23	2,256	6.39	23,858	67.56	18
performing_arts	entertainment	11,584	0.08	1,415	12.22	2,785	24.04	19
nightlife	entertainment	7,865	0.05	302	3.84	2,011	25.57	14
gaming	entertainment	1,425	0.01	65	4.56	250	17.54	13
storage	storage	28,077	0.19	22,761	81.07	27,757	98.86	17
military	military_emergency	13,104	0.09	9,953	75.95	12,441	94.94	41
emergency	military_emergency	3,348	0.02	75	2.24	3,200	95.58	39
port	port	244	0.00	0	0.00	0	0.00	9
total	total	15,151,918	100.00	9,038,206	59.65	12,221,198	80.66	35

Notes: Table summarizes places of interest (POIs) data collected from different sources (Table 1), classified into 47 economic categories and deduplicated by category and location (as described above). Column 'count' records the number of POIs, 'perc' the percentage in total POIs, 'polygons' the number of tagged OSM polygons (buildings) interpreted as POIs, 'poly_perc' the percentage of POIs that are polygons, 'osm' the number of POIs taken from OSM, 'osm_perc' the feaction of POIs from OSM, and 'src_cat' the number of primary categories (across sources) mapping to a specific detailed category (e.g., there are 1,239 different kinds of small/specialized shops mapping to the 'shopping_other' category).

Descriptive Statistics

Table A4: Dataset of Spatial Predictors (Simplified Categories) over 96km2 Grid, N = 160,499

#	Variable	Ndist	Mean	SD	Min	25%	50%	75%	Max
POIs: simple counts combined across detailed categories									
1	accommodation	224	0.8	9.8	0.0	0.0	0.0	0.0	1399.0
2	automotive	307	1.0	17.7	0.0	0.0	0.0	0.0	2114.0
3	beauty	207	0.4	10.3	0.0	0.0	0.0	0.0	1382.0
4	commercial	205	0.7	34.7	0.0	0.0	0.0	0.0	8264.0
5	construction	536	3.6	86.6	0.0	0.0	0.0	0.0	13209.0
6	farming	770	7.7	49.8	0.0	0.0	0.0	1.0	2581.0
7	financial	276	0.9	18.1	0.0	0.0	0.0	0.0	2208.0
8	food	316	1.0	19.0	0.0	0.0	0.0	0.0	1696.0
9	historic	183	0.6	15.6	0.0	0.0	0.0	0.0	5580.0
10	institutional	169	0.4	6.6	0.0	0.0	0.0	0.0	794.0
11	port	4	0.0	0.0	0.0	0.0	0.0	0.0	3.0
12	power	2435	115.9	319.9	0.0	0.0	0.0	20.0	14536.0
13	religion	248	1.0	11.0	0.0	0.0	0.0	0.0	1079.0
14	residential	1739	39.1	488.8	0.0	0.0	2.0	10.0	65378.0
15	sport	280	1.1	31.9	0.0	0.0	0.0	0.0	5112.0
16	storage	133	0.2	5.9	0.0	0.0	0.0	0.0	765.0
17	transport_other	383	1.9	32.3	0.0	0.0	0.0	0.0	2999.0
18	communications	1194	14.9	198.7	0.0	0.0	0.0	0.0	22867.0
19	education	363	2.6	20.9	0.0	0.0	0.0	0.0	2414.0
20	health	332	1.9	22.9	0.0	0.0	0.0	1.0	3521.0
21	entertainment	420	1.7	32.4	0.0	0.0	0.0	0.0	3944.0
22	services	197	0.4	9.4	0.0	0.0	0.0	0.0	1573.0
23	shopping	698	5.5	126.8	0.0	0.0	0.0	0.0	21543.0
24	public_service_utility	140	0.4	5.7	0.0	0.0	0.0	0.0	952.0
25	mining_industrial	272	1.2	11.5	0.0	0.0	0.0	0.0	1027.0
26	military_emergency	75	0.1	1.7	0.0	0.0	0.0	0.0	249.0
27	tourism_recreation	288	1.0	15.8	0.0	0.0	0.0	0.0	2441.0
Lines: total length in km in each cell									
28	dam_len	1868	29.5	431.6	0.0	0.0	0.0	0.0	79889.0
29	aeroway_len	2607	66.6	805.7	0.0	0.0	0.0	0.0	68671.0
30	ferry_len	1362	57.4	958.9	0.0	0.0	0.0	0.0	95065.0
31	pipeline_len	4031	281.0	2675.5	0.0	0.0	0.0	0.0	331527.0
32	railway_len	7707	776.7	4975.3	0.0	0.0	0.0	0.0	706405.0
33	roads_paved	18393	2825.1	9028.5	0.0	0.0	0.0	0.0	465351.0
34	roads_unpaved	27757	6361.4	10741.4	0.0	0.0	0.0	10768.0	625255.0
35	waterway_len	36356	23069.8	150937.0	0.0	0.0	0.0	13141.5	11753756.0
Raster Layers: sum of population and mean of travel time and internet speed (bytes/s) in each cell									
36	internet_speed	53324	20800.5	22664.3	151.0	6209.0	12031.0	27115.0	278876.0
37	pop_gpw4_ages_0_14	14147	2323.1	9063.3	0.0	192.0	716.0	2013.0	729958.0
38	pop_gpw4_ages_15_49	15038	2786.9	14553.7	0.0	207.0	726.0	2071.0	1503562.0
39	ttime_city_50k	3380	281.8	457.2	0.0	76.0	156.0	312.0	9303.0
40	ttime_city_1m	4333	610.5	631.5	0.0	245.0	451.0	779.0	9868.0
41	ttime_port_any	4723	811.5	758.8	0.0	316.0	602.0	1054.0	10065.0
42	ttime_port_ml	5229	1093.5	909.3	1.0	453.0	849.0	1472.0	10216.0

Figure A1: Histogram of Wealth/Activity Measures in 96km^2 Grid, Avg. Obs.: 101,417

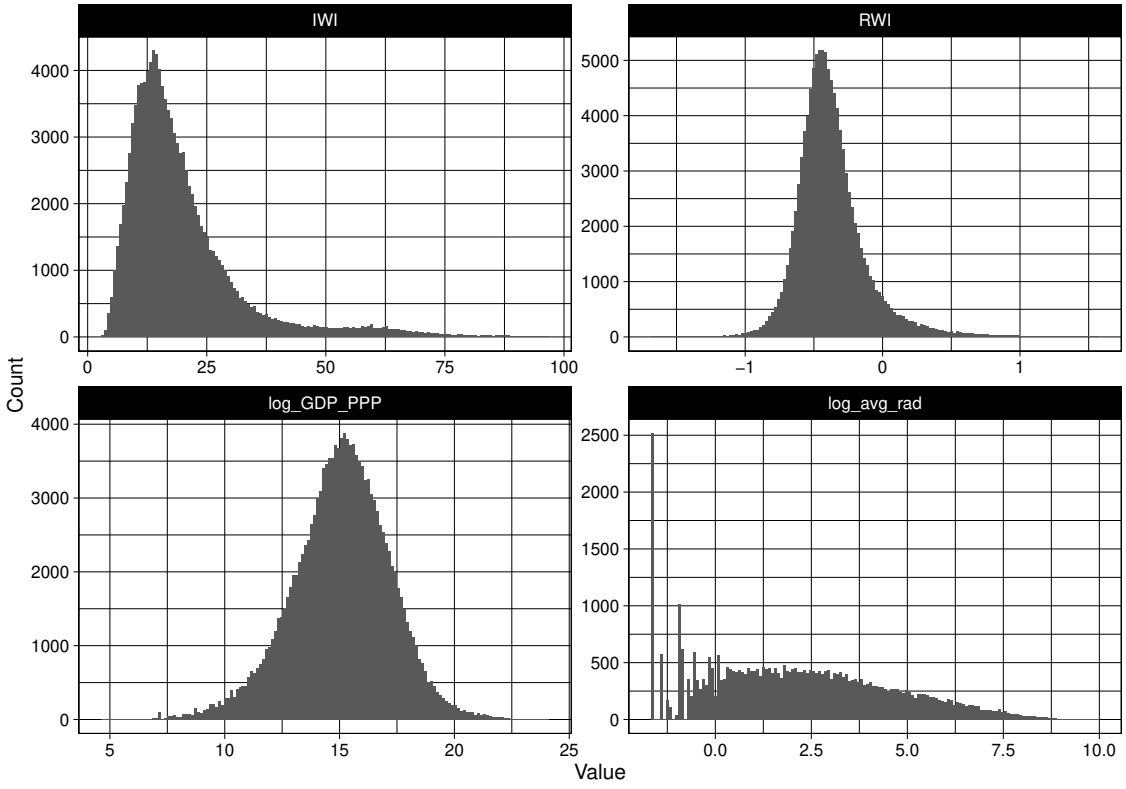

Table A5: Pearson's Correlations of Wealth/Activity Measures in 96km^2 Grid

		log_GDP_PPP	log_avg_rad	IWI	RWI
Pooled	log_GDP_PPP	1 (126123)			
Across	log_avg_rad	.453* (33293)	1 (36656)		
Countries	IWI	.397* (98948)	.576* (25608)	1 (105924)	
	RWI	.449* (95295)	.577* (31858)	.550* (88101)	1 (101456)
Scaled	log_GDP_PPP	1 (126123)			
and	log_avg_rad	.436* (33293)	1 (36656)		
Centered	IWI	.363* (98948)	.578* (25608)	1 (105924)	
by Country	RWI	.349* (95295)	.560* (31858)	.533* (88101)	1 (101456)

Notes: N. obs in parentheses, a '*' denotes significance at the 5% level.

Table A6: Detailed Category Combination Weights (β_{jp}) for 3 Categories

communications	communications_network	communications_other	telecom_len
IWI	1.00	5.70	0.24
RWI	1.00	13.65	0.10
GDP_PPP	1.00	8.86	0.02
avg_rad	1.00	18.65	0.03
Average	**1.00**	**11.72**	**0.098**
mining_industrial	industrial	mining	SEZ
IWI	1.00	3.43	89.13
RWI	1.00	0.93	66.93
GDP_PPP	1.00	0.00	52.49
avg_rad	1.00	0.86	23.97
Average	**1.00**	**1.31**	**58.13**
shopping	shopping_essential	shopping_other	wholesale
IWI	1.00	1.46	15.41
RWI	1.00	1.46	14.73
GDP_PPP	1.00	3.82	52.37
avg_rad	1.00	2.57	18.71
Average	**1.00**	**2.33**	**25.31**

Notes: The weights are normalized, then averaged across outcomes.

Table A7: Correlations of Total Infrastructure with Wealth/Activity and Population

	IWI	RWI	GDP_PPP	avg_rad	pop_gpw4	pop_wpop
Cell-level, N = 88,961 populated cells (>10 *persons/km*^{2})						
Total PP Feature Count	0.302	0.401	0.481	0.484	0.546	0.562
Total PP Features ERFPC	0.249	0.351	0.586	0.590	0.603	0.617
Total Line Length	0.519	0.578	0.477	0.623	0.491	0.515
Total Line Length EW	0.558	0.588	0.482	0.640	0.490	0.515
Country-level, N = 55						
Total PP Feature Count	-0.009	-0.263	0.538	-0.055	0.800	0.799
Total PP Features ERFPC	-0.010	-0.265	0.535	-0.057	0.799	0.799
Total Line Length	0.412	-0.040	0.730	0.265	0.719	0.721
Total Line Length EW	0.530	0.049	0.769	0.332	0.671	0.667

ERFPC = excluding residential buildings, farmland, power and construction
EW = excluding waterways

Figure A2: Clustered Correlations of Variables

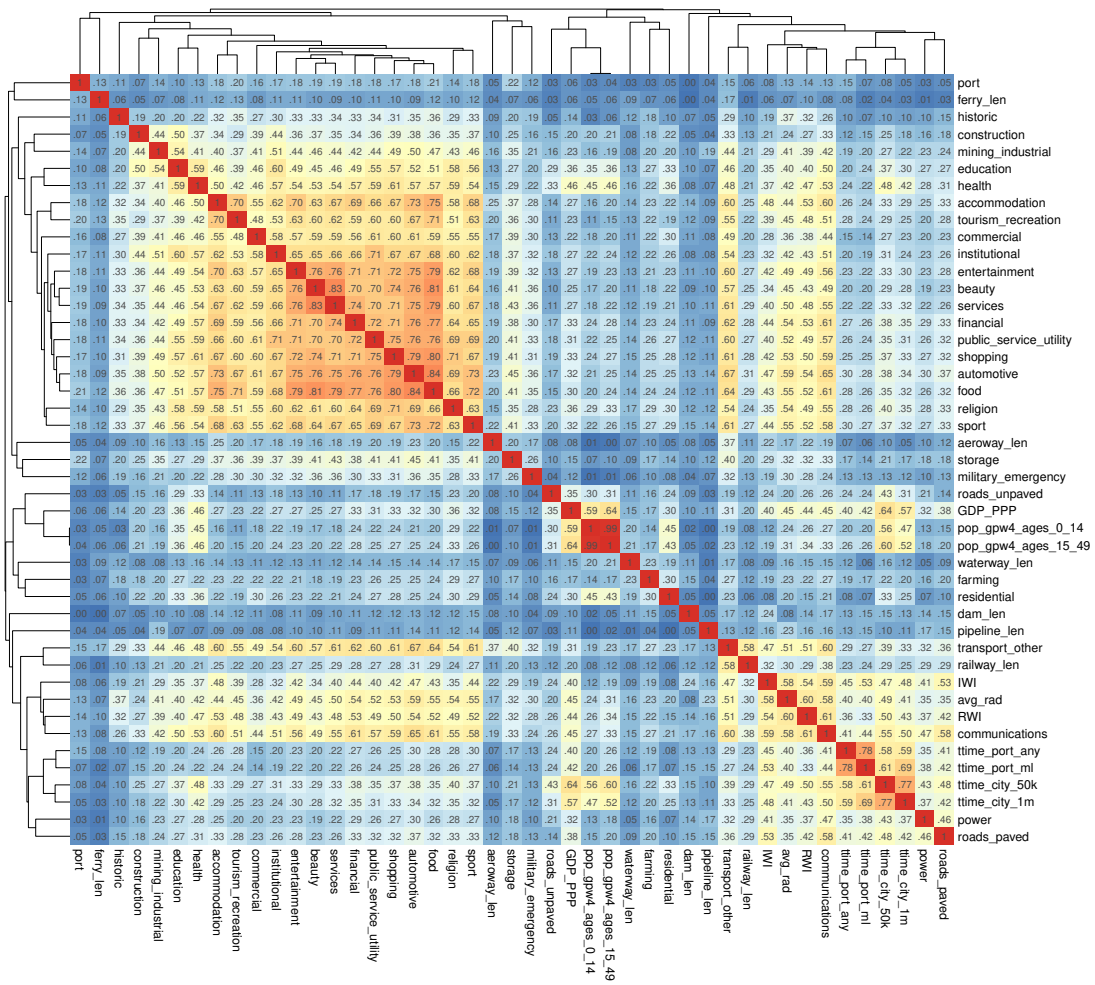

Figure A3: Index of Spatial Efficiency

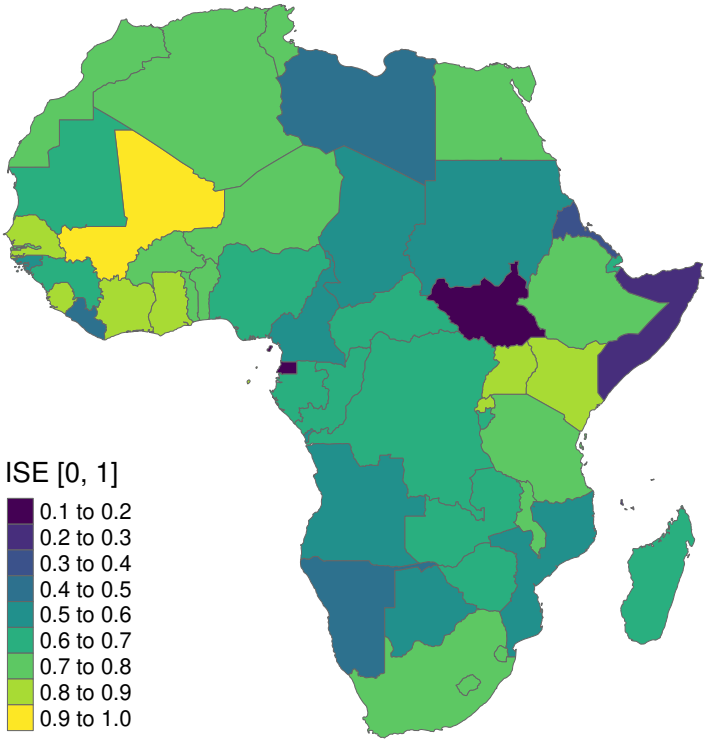

Figure A4: Empirical CDF's of Residuals from ML Models Predicting the Log of Nightlights 2022

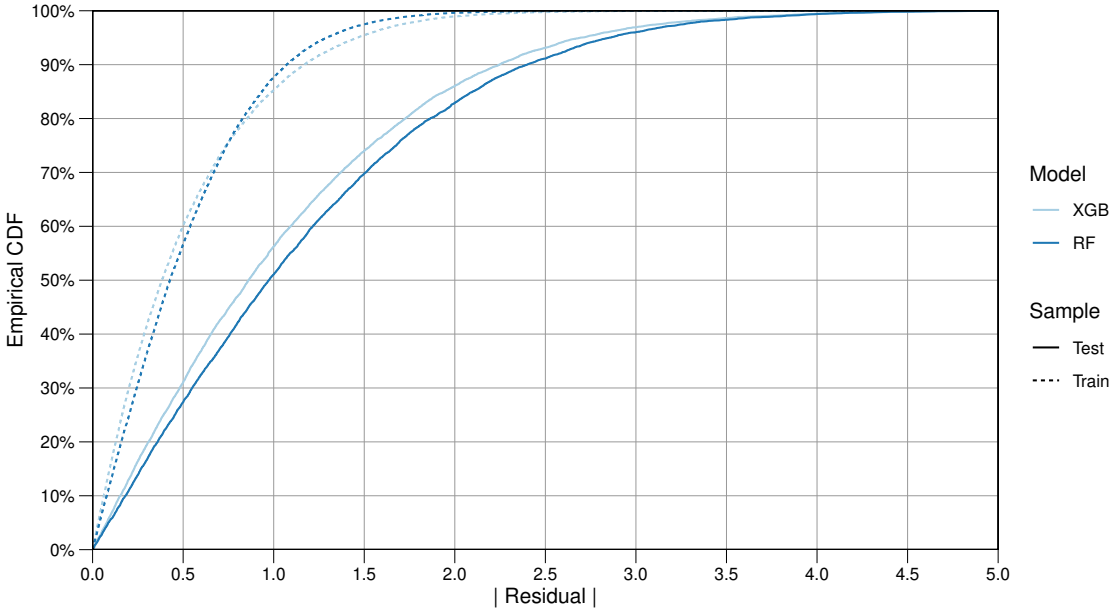

Notes: Dataset includes 42 predictors, excluding spillover variables. The training set has 28,976 observations, the test set 9,655. The training set R^2 is 91.8% for XGB and 92.7% for RF. The test set R^2 is 68.4% for XGB and 63.6% for RF.

SHAP Values for Other Outcomes

Figure A5: SHAP Variable Importance: Log Nightlights 2022

With Population and Travel Time

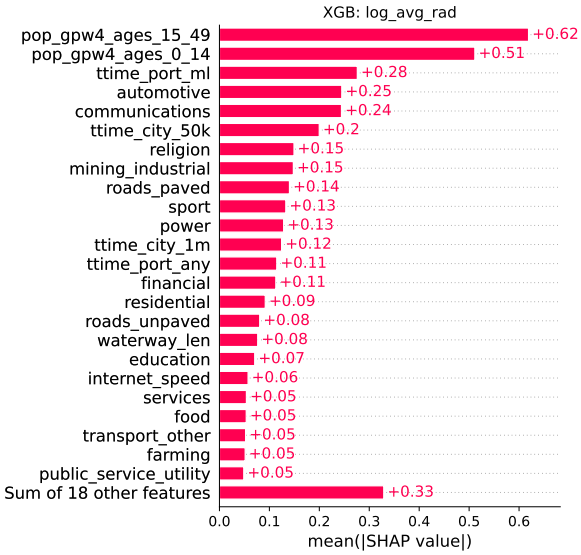

No Population and Travel Time

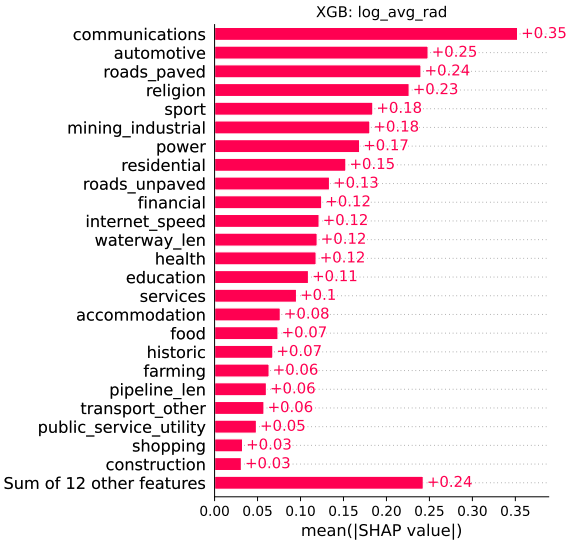

Figure A6: SHAP Effect Distribution: Log Nightlights 2022

With Population and Travel Time

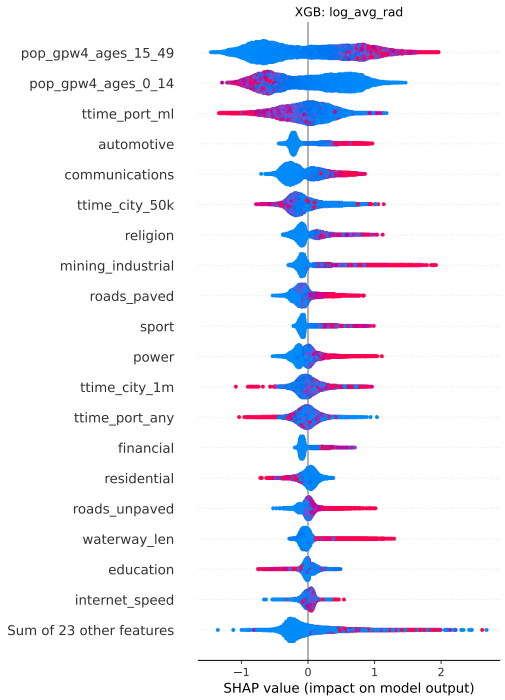

No Population and Travel Time

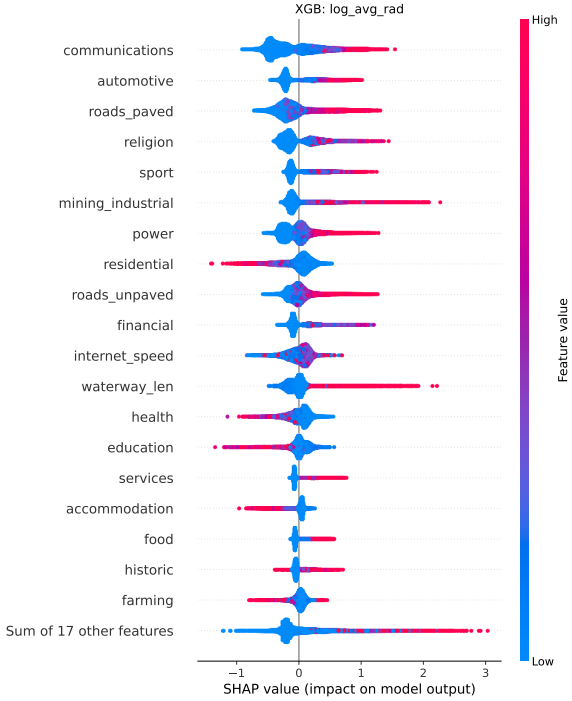

SHAP Values from Feature Counts

Figure A7: SHAP Variable Importance: Simple Feature Counts

IWI, no POPTT

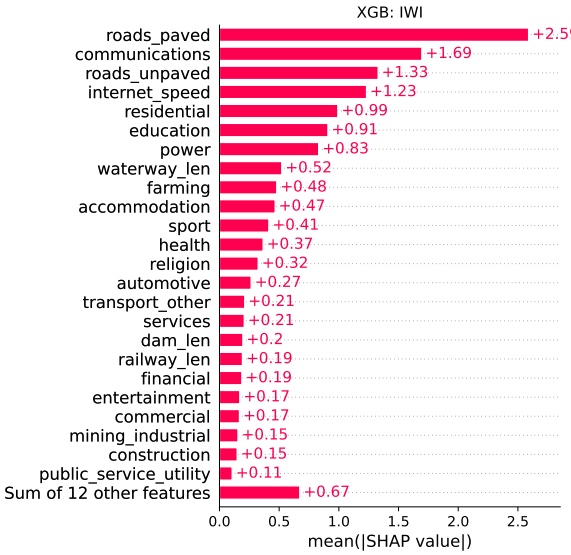

Log Nightlights, no POPTT

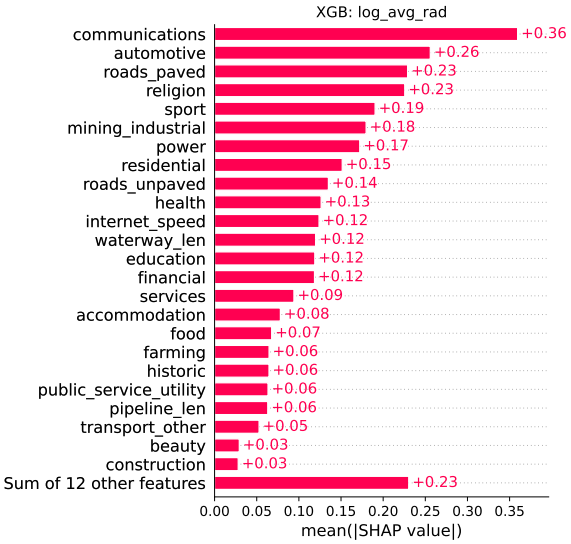

Figure A8: SHAP Effect Distribution: Simple Feature Counts

IWI, no POPTT

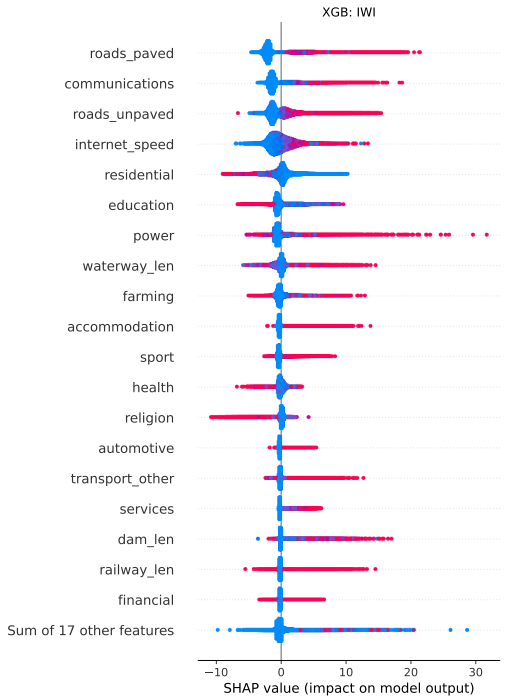

Log Nightlights, no POPTT

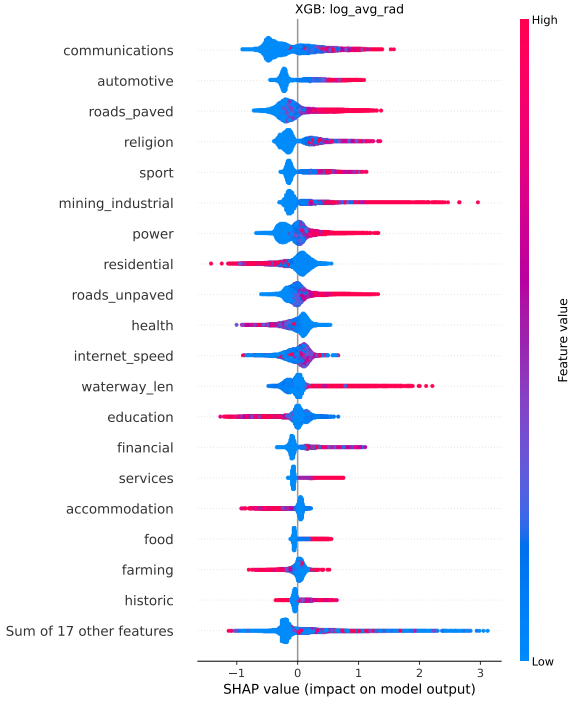

SHAP Values Scatter (ALE) Plots

Figure A9: IWI: SHAP Values and Feature Levels - Top 12 Predictors

With Population and Travel Time

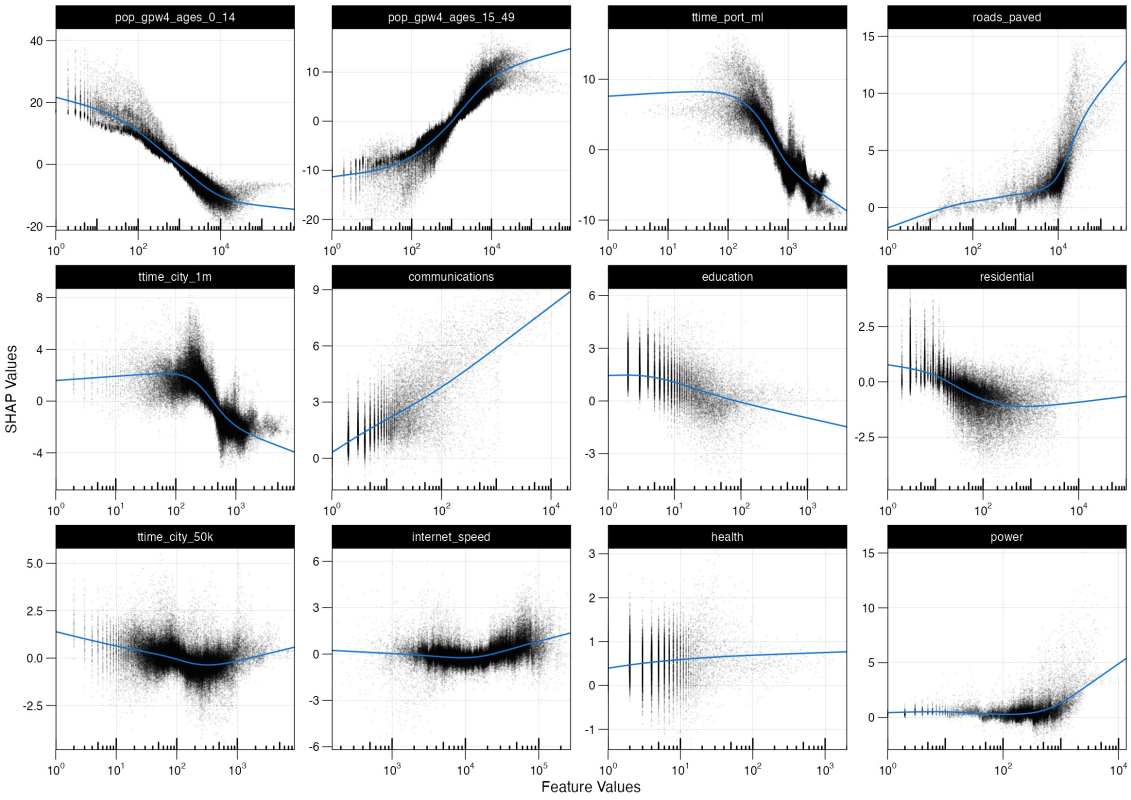

No Population and Travel Time

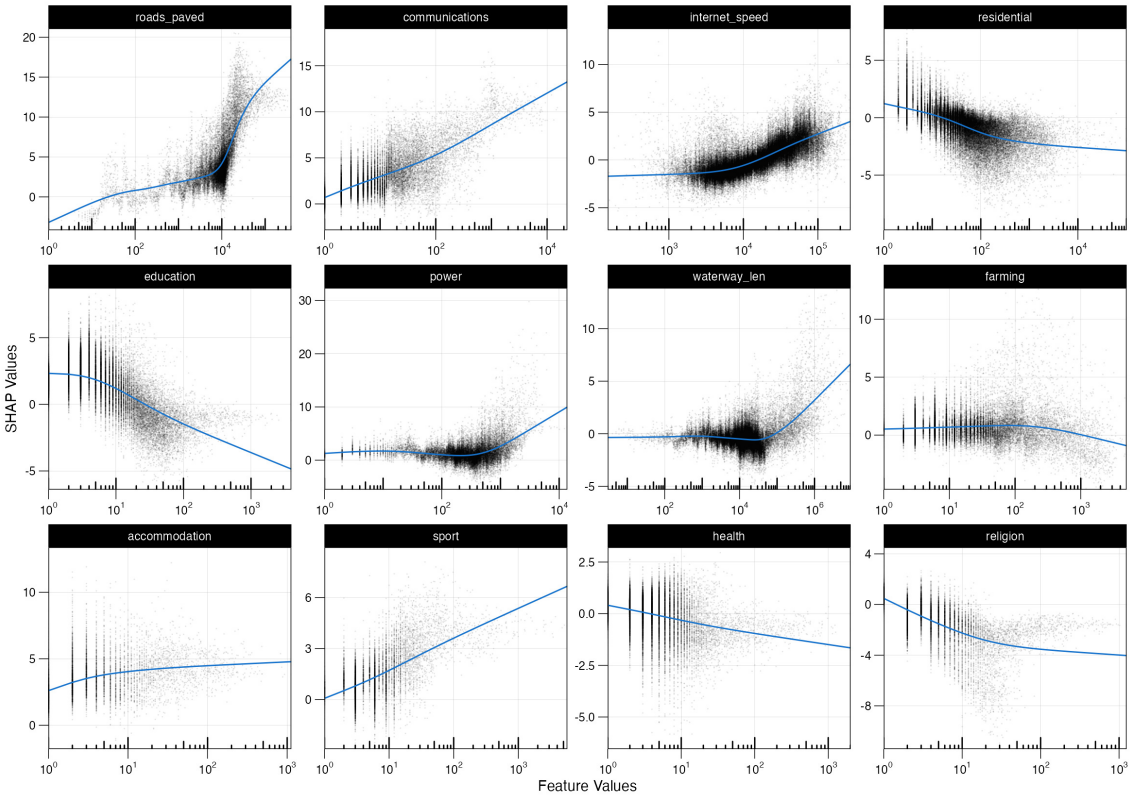

Figure A10: Log Nightlights 2022: SHAP Values and Feature Levels - Top 12 Predictors

With Population and Travel Time

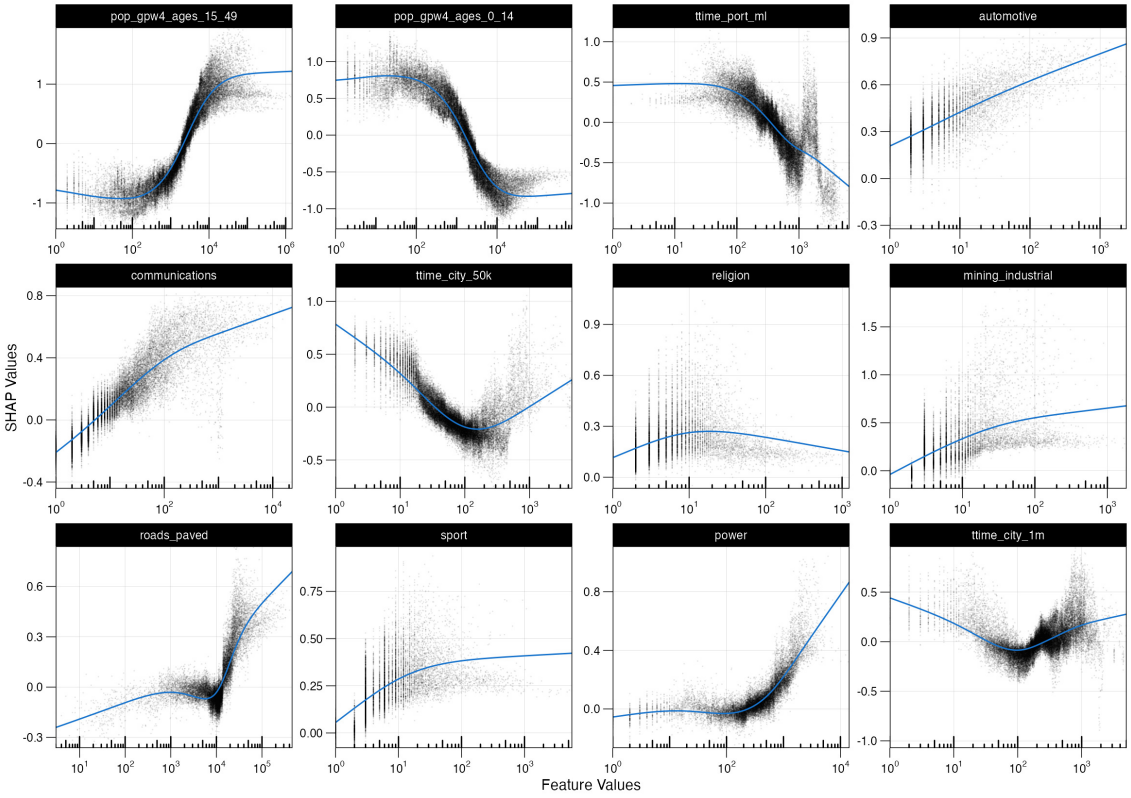

No Population and Travel Time

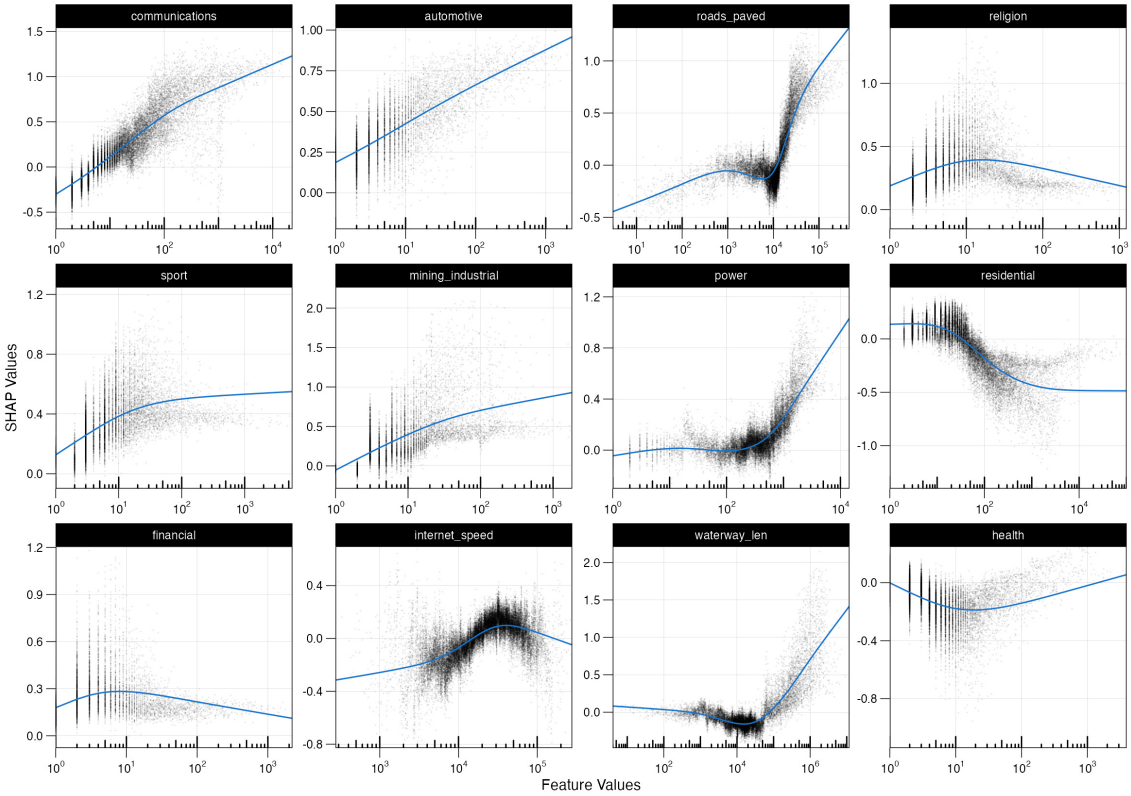

Robustness Checks and Additional Results

Figure A11: CAPE Estimates for Power and Health using Only OSM Data (February 2024 Version)

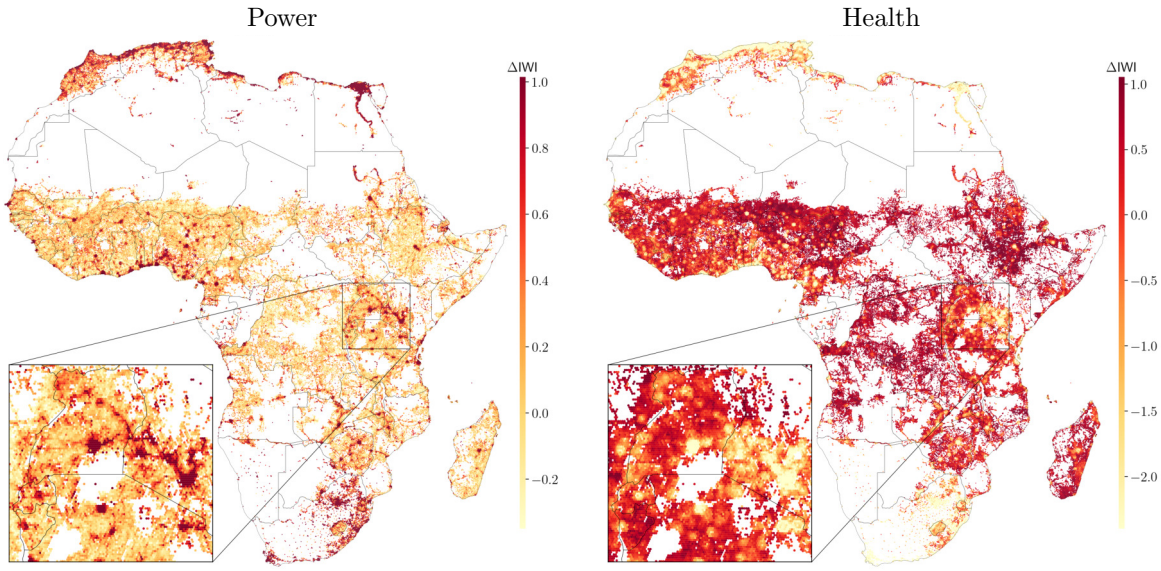

Table A8: ML Debiased Infrastructure and Favouritism: Simple Feature Counts

	Colonial Railroads		Political Favouritism				Ethnic Favouritism			
	Ln Kilometers		Ln Years in Power		Ever in Power		Discriminated		Excl. from Gov.	
feature	Raw	Ctrl	Raw	Ctrl	Raw	Ctrl	Raw	Ctrl	Raw	Ctrl
Raw Infrastructure Data, in Natural Logs										
roads_paved	.517***	.29***	.521***	.02	1.506***	.355	-.164	.225	-.674***	-.061
power	.374***	.287***	.417***	.066	1.024***	.224	.571**	.304	-.186	.338*
education	.097***	.041***	.149***	-.02	.369***	-.005	.052	.038	-.29***	.001
health	.076***	.029***	.122***	-.048**	.324***	-.076	.048	-.05	-.128***	.037
communications	.212***	.115***	.236***	-.013	.622***	.078	.106	.118	-.229***	.133
public_service_utility	.037***	.02***	.063***	-.016	.161***	-.018	.01	.006	-.018	.037*
automotive	.062***	.036***	.08***	-.023	.203***	-.031	.045	.054	-.021	.065**
transport_other	.142***	.102***	.114***	-.021	.292***	-.013	.06	.071	-.031	.027
financial	.057***	.025***	.067***	-.049***	.169***	-.091**	.066**	.031	-.002	.009
services	.039***	.015***	.045***	-.034***	.104***	-.074***	.017	.03*	-.003	.028*
ttime_city_1m	-.162***	-.088***	-.189***	.051*	-.477***	.076	.098	.108	.316***	.066
ttime_port_any	-.121***	-.069***	-.21***	-.017	-.585***	-.104*	-.003	-.004	.366***	-.128***
residential	.032**	.052***	.167***	-.075	.444***	-.129	-.085	-.007	-.257**	.019
accommodation	.074***	.036***	.081***	-.013	.24***	.019	.07*	.07*	-.025	.008
Debiased Data via Ensemble ML Models										
roads_paved	.015	.012	-.031	-.067	.025	-.063	-.034	.191	.006	-.186
power	0	.003	.023	.028	.021	.024	.205**	.186	.048	.051
education	0	-.003	-.014	-.011	-.048	-.031	-.011	.002	0	-.007
health	-.005*	-.007**	-.005	-.007	-.005	-.014	-.014	-.046*	-.005	-.021
communications	-.007*	-.007	-.001	.016	-.005	.043	.018	-.011	-.032	-.039
public_service_utility	-.003*	-.001	.005	.006	.012	.015	-.003	-.009	.006	.022*
automotive	-.002	0	-.002	0	-.021	-.013	.018*	.019	-.005	.002
transport_other	.003	.003	-.004	-.001	-.02	-.012	.042***	.017	.021*	-.005
financial	-.002	-.001	-.012*	-.016**	-.024	-.034*	.018*	.02	.002	-.011
services	.001	-.002*	0	0	.001	.003	.002	.008	.001	.008
ttime_city_1m	-.005	-.002	.002	.002	-.025	-.024	.011	.015	.012	.046
ttime_port_any	-.014***	-.006*	-.033**	-.015	-.125***	-.081**	.008	.046	.034	-.003
residential	-.002	-.002	-.011	-.044	-.053	-.108	-.039	-.035	-.027	-.008
accommodation	.005***	.004*	0	0	.008	.007	.007	.027	-.003	-.01
Observations	5346	5346	5346	5346	5346	5346	385	385	385	385
Country FE	No	Yes	No	Yes	No	Yes	No	Yes	No	Yes
Geographic Controls	No	Yes	No	Yes	No	Yes	No	Yes	No	Yes
Simulation Controls	No	Yes	No	Yes	No	Yes	No	Yes	No	Yes

*Signif. Codes: ***: 0.01, **: 0.05, *: 0.1; based on cluster-robust standard-errors*
Notes: See Graff (2024) Tables 1 and 2 for further details about the variables and controls.

Table A9: ML Debiased Infrastructure and Favouritism: Quantile Feature Counts

	Colonial Railroads		Political Favouritism				Ethnic Favouritism			
	Ln Kilometers		Ln Years in Power		Ever in Power		Discriminated		Excl. from Gov.	
feature	Raw	Ctrl	Raw	Ctrl	Raw	Ctrl	Raw	Ctrl	Raw	Ctrl
Raw Infrastructure Data, in Natural Logs										
roads_paved	.517***	.29***	.521***	.02	1.506***	.355	-.164	.185	-.674***	-.067
power	.373***	.286***	.416***	.065	1.022***	.222	.571**	.273	-.186	.31*
education	.111***	.046***	.186***	-.012	.465***	.025	.047	.014	-.341***	.034
health	.079***	.031***	.137***	-.047*	.375***	-.063	.04	-.083	-.147***	.023
communications	.212***	.115***	.237***	-.012	.624***	.078	.106	.072	-.229***	.086
public_service_utility	.045***	.026***	.079***	-.011	.213***	.01	.037	.005	-.026	.029
automotive	.069***	.04***	.093***	-.022	.238***	-.022	.062*	.069*	-.02	.07**
transport_other	.146***	.105***	.119***	-.02	.306***	-.009	.075	.074	-.027	.048
financial	.058***	.026***	.067***	-.049***	.171***	-.091**	.064**	.028	-.005	.007
services	.039***	.015***	.045***	-.035***	.103***	-.075***	.017	.027	-.004	.024
ttime_city_1m	-.162***	-.088***	-.189***	.051*	-.477***	.076	.098	.116	.316***	.089
ttime_port_any	-.121***	-.069***	-.21***	-.017	-.585***	-.104*	-.003	-.002	.366***	-.124***
residential	.01	.049***	.153**	-.102	.413**	-.195	-.094	-.058	-.176	.021
accommodation	.076***	.037***	.088***	-.01	.261***	.031	.07*	.06	-.03	.012
mining_industrial	.073***	.045***	.096***	-.022	.219***	-.054	-.077	.009	-.151***	.17***
tourism_recreation	.044***	.027***	.086***	-.012	.241***	.009	0	.022	-.031	.014
construction	.056***	.027***	.114***	-.012	.286***	-.004	-.056	.085	-.359***	.107
Debiased Data via Ensemble ML Models										
roads_paved	.018	.015	-.025	-.06	.027	-.059	-.057	.161	.002	-.159
power	-.005	-.002	.041	.043	.076	.07	.246***	.202	.073	.087
education	.001	-.003	-.019	-.018	-.068	-.057	-.026	-.029	-.009	-.024
health	-.006*	-.006*	-.012	-.015	-.02	-.033	-.019	-.068**	.001	-.019
communications	-.01***	-.009**	-.004	.013	-.016	.03	.035	.012	-.033	-.053*
public_service_utility	-.003	-.001	.011	.012	.035*	.04*	.007	-.001	-.004	.002
automotive	-.003	-.001	.001	.004	-.016	-.008	.026**	.028*	-.001	.003
transport_other	.003	.003	-.004	0	-.023	-.015	.052***	.021	.029**	.006
financial	-.002	-.001	-.009	-.014**	-.02	-.03*	.02**	.02	.003	-.009
services	0	-.002*	-.001	0	-.002	.001	-.002	.004	0	.007
ttime_city_1m	-.006**	-.004	-.002	-.003	-.033	-.034	.007	.002	.009	.053*
ttime_port_any	-.015***	-.006*	-.033**	-.017	-.127***	-.082**	-.002	.048	.032	.001
residential	-.003	-.001	-.021	-.058	-.068	-.134	-.034	-.091	-.016	-.062
accommodation	.005**	.004	.002	.004	.014	.017	.004	.022	-.004	-.004
mining_industrial	-.003	-.002	.003	.004	-.023	-.023	-.045*	-.04	.01	.031
tourism_recreation	-.004*	-.001	0	-.002	.005	-.005	-.018	-.009	-.011	-.022
construction	-.006	-.003	-.005	.006	-.023	.001	.044	.117*	-.007	.126**
Observations	5346	5346	5346	5346	5346	5346	385	385	385	385
Country FE	No	Yes	No	Yes	No	Yes	No	Yes	No	Yes
Geographic Controls	No	Yes	No	Yes	No	Yes	No	Yes	No	Yes
Simulation Controls	No	Yes	No	Yes	No	Yes	No	Yes	No	Yes

*Signif. Codes: ***: 0.01, **: 0.05, *: 0.1; based on cluster-robust standard-errors*

Notes: See Graff (2024) Tables 1 and 2 for further details about the variables and controls.

Table A10: Median CAPE: DHS IWI vs. IWI Prediction by Lee & Braithwaite (2022)

	Simple Counts		Quantile Counts	
Feature	DHS	L&B	DHS	L&B
roads_paved	0.248	0.231	0.179	0.225
power	0.197	0.068	0.221	0.071
education	0.009	0.509	-0.032	0.347
health	0.932	0.724	1.033	0.661
communications	0.798	0.655	0.571	0.624
public_service_utility	0.770	0.214	0.149	0.381
automotive	0.615	0.580	0.437	0.468
transport_other	0.593	0.300	0.686	0.296
financial	3.054	0.992	2.302	0.891
services	1.766	0.412	0.651	0.262
ttime_city_1m	-1.285	-0.566	-1.323	-0.521
ttime_port_any	-0.965	-0.215	-1.003	-0.229
residential	-0.068	-0.047	0.007	-0.025
accommodation	1.507	0.802	1.356	0.654
mining_industrial	0.841	0.509	0.497	0.544
tourism_recreation	-0.061	0.149	-0.185	0.198
construction	0.246	0.153	0.093	0.180
Median Abs. Coef.	0.770	0.412	0.497	0.347
Corr. Spearman	0.865		0.809	
Corr. Pearson	0.857		0.902	

Abbreviations: DHS = IWI estimate from Demographic and Health Survey; L&B = Predicted IWI estimate by Lee & Braithwaite (2022).

Notes: the DHS-based IWI estimate is computed from all DHS surveys conducted in SSA since 2010. It is averaged across $96km^2$ hexagonal grid cells just like the IWI estimate of Lee & Braithwaite (2022). Grid cells with less than 5 households or less than 10 people per km^2 population density are excluded. This yields 17,396 cells with DHS-based IWI estimates used for training, versus 89,048 cells available with the predicted IWI by Lee & Braithwaite (2022). After the ensemble CAPE model is trained, a CAPE prediction is made for 103,922 cells which have a population density above 10 persons/km^2 and any POI feature. The median of these CAPE estimates is reported in this table.

Table A11: Average Partial Effect: DHS IWI vs. IWI Prediction by Lee & Braithwaite (2022)

	Simple Counts		Quantile Counts	
Feature	DHS	L&B	DHS	L&B
roads_paved	0.202	0.218	0.173	0.216
power	0.087	0.068	0.114	0.068
education	0.031	0.563	-0.073	0.436
health	0.585	0.803	0.645	0.772
communications	1.037	0.689	1.031	0.689
public_service_utility	0.842	0.327	0.470	0.331
automotive	1.482	0.873	0.952	0.444
transport_other	0.382	0.332	0.324	0.305
financial	1.857	0.626	1.641	0.543
services	1.911	1.380	4.506	0.748
ttime_city_1m	-1.158	-0.513	-1.174	-0.502
ttime_port_any	-1.014	-0.293	-0.937	-0.295
residential	-0.097	-0.068	-0.101	-0.052
accommodation	1.518	0.807	1.073	0.771
mining_industrial	0.740	0.541	0.508	0.460
tourism_recreation	0.137	0.184	0.094	0.309
construction	0.211	0.161	0.154	0.186
Median Abs. Coef.	0.740	0.513	0.508	0.436
Corr. Spearman	0.863		0.870	
Corr. Pearson	0.895		0.874	

Abbreviations: DHS = IWI estimate from Demographic and Health Survey; L&B = Predicted IWI estimate by Lee & Braithwaite (2022).

Notes: the DHS-based IWI estimate is computed from all DHS surveys conducted in SSA since 2010. It is averaged across $96km^2$ hexagonal grid cells just like the IWI estimate of Lee & Braithwaite (2022). Grid cells with less than 5 households or less than 10 people per km^2 population density are excluded. This yields 17,396 cells with DHS-based IWI estimates used for training, versus 89,048 cells available with the predicted IWI by Lee & Braithwaite (2022). After the ensemble CAPE model is trained, a CAPE prediction is made for 103,922 cells which have a population density above 10 persons/km^2 and any POI feature. The APE is obtained through augmented inverse probability weighting following Eq. 10, and thus only considers cells where outcome data is available. Differences in the estimates are thus expected because with L&B much more cells are available for APE calculation.

Table A12: CAPE Correlations: DHS IWI and IWI Prediction by Lee & Braithwaite (2022)

Feature	Simple Counts	Quantile Counts
roads_paved	0.593	0.119
power	0.157	0.040
education	0.317	0.024
health	0.013	-0.038
communications	0.271	-0.171
public_service_utility	0.100	0.386
automotive	0.108	0.114
transport_other	0.126	0.001
financial	0.287	0.362
services	0.000	-0.006
ttime_city_1m	0.038	-0.022
ttime_port_any	-0.118	-0.025
residential	-0.000	0.383
accommodation	0.246	0.013
mining_industrial	0.422	0.271
tourism_recreation	0.076	0.000
construction	0.488	-0.213
Median Corr.	0.126	0.0128
Median Abs. Corr.	0.126	0.040

Notes: the DHS-based IWI estimate is computed from all DHS surveys conducted in SSA since 2010. It is averaged across $96km^2$ hexagonal grid cells just like the IWI estimate of Lee & Braithwaite (2022). Grid cells with less than 5 households or less than 10 people per km^2 population density are excluded. This yields 17,396 cells with DHS-based IWI estimates used for training, versus 89,048 cells available with the predicted IWI by Lee & Braithwaite (2022). After the ensemble CAPE model is trained, a CAPE prediction is made for 103,922 cells which have a population density above 10 persons/km^2 and any POI feature. Pearson's correlation of these CAPE estimates is reported in this table.

Table A13: CAPE Correlations: DHS IWI and IWI Prediction by Lee & Braithwaite (2022): Previous Estimates without Separate Spillover Variables (One Variable Per Infrastructure)

	Count	Count + SS	Tag Weights	Weights + SS
roads_paved	0.213	0.305	0.245	0.246
power	-0.337	0.249	-0.001	0.078
education	0.550	0.379	0.632	-0.338
health	0.319	0.280	0.251	0.708
communications	0.559	0.271	0.399	0.305
public_service_utility	0.292	0.542	0.802	0.267
automotive	0.301	-0.070	0.575	0.161
transport_other	-0.083	0.329	-0.031	0.181
financial	0.253	0.128	0.402	0.303
services	0.231	0.003	0.025	-0.313
ttime_city_1m	0.325	0.353	0.288	0.419
ttime_port_any	0.500	0.257	0.508	0.375
residential	0.556	0.135	0.454	-0.009
accommodation	0.305	0.481	0.325	0.260
industrial	0.132	0.196	0.727	0.510
tourism_recreation	0.158	0.069	0.374	0.373
construction	0.296	-0.153	0.037	-0.000
Median Corr.	0.294	0.244	0.284	0.195
Median Abs. Corr.	0.298	0.244	0.299	0.232

Abbreviations: SS = Spatial Spillovers.

Figure A12: DML CAPE Kernel Density Estimates for DHS-Based IWI

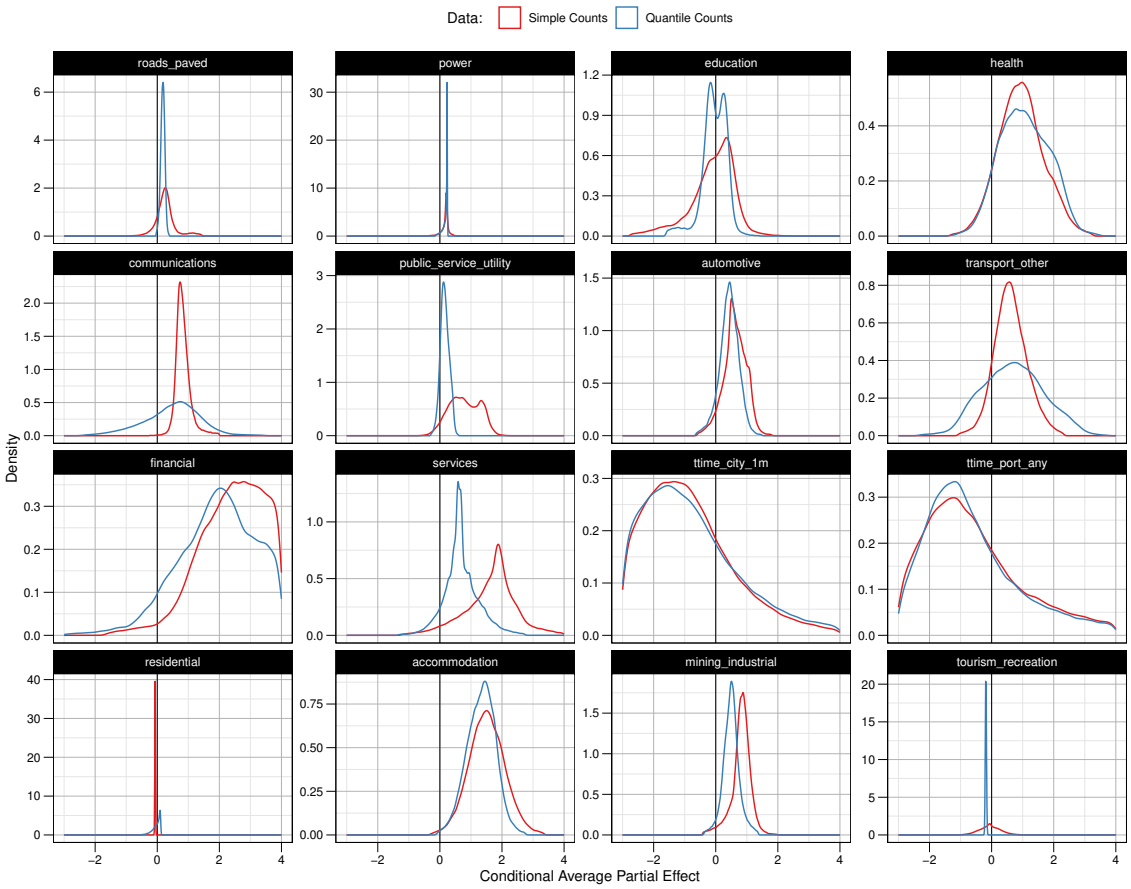

Figure A13: Top 25 Correlates of DHS-Based IWI CAPE Estimates: Average Across Datasets

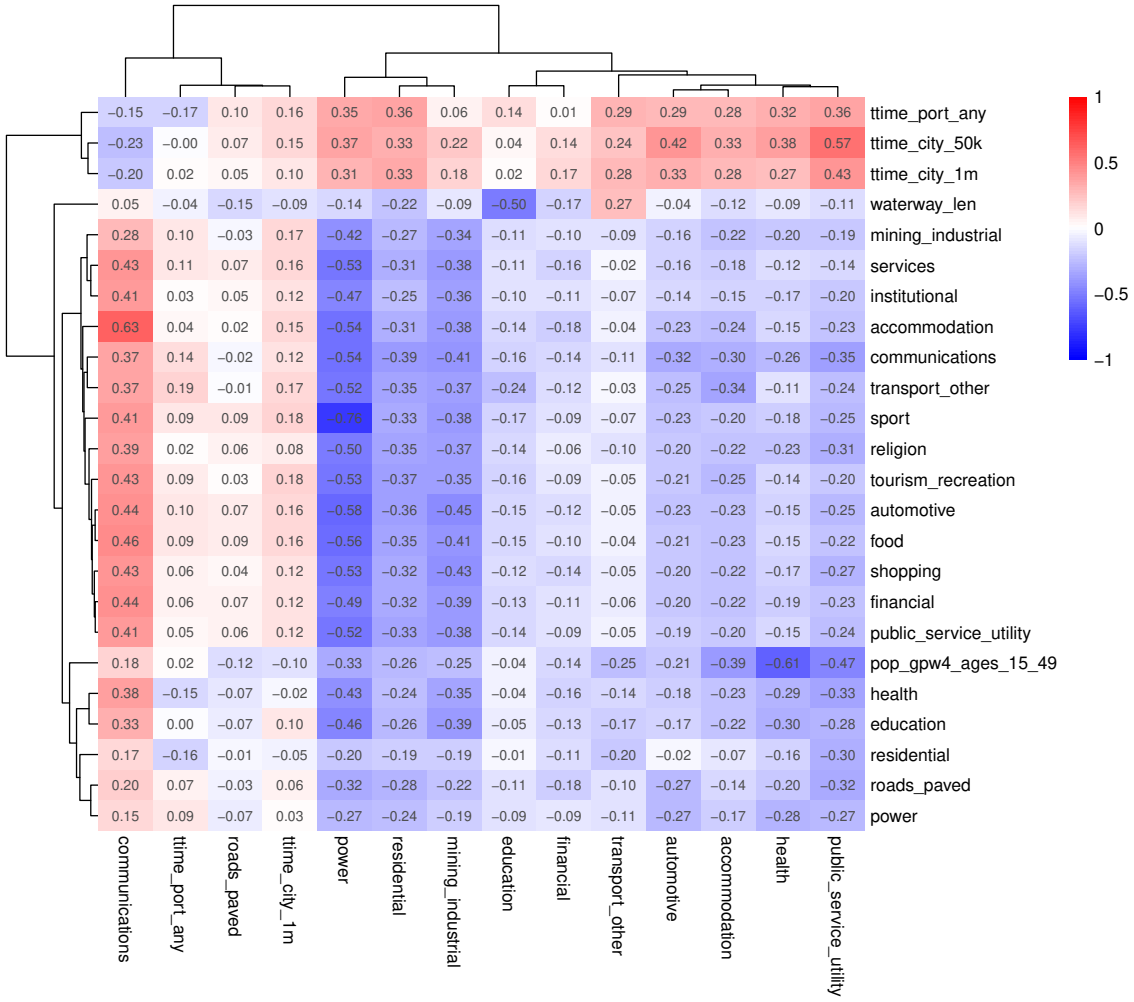

Table A14: Average Partial Effects on Log Nightlights 2022

	Simple Counts				Quantile Counts			
Feature	ATE	High	Low	Diff.	ATE	High	Low	Diff.
roads_paved	**0.0198*** **	0.0328***	0.00682**	0.026***	**0.0193*** **	0.0351***	0.00358	0.0315***
power	**0.0235*** **	0.0436***	0.00338	0.0402***	**0.0247*** **	0.0445***	0.00497	0.0395***
education	**0.0825*** **	0.144***	0.0209	0.123***	**0.0532*** **	0.104***	0.00198	0.102***
health	**0.107*** **	0.252***	-0.0382**	0.29***	**0.101*** **	0.243***	-0.0405**	0.284***
communications	**0.17*** **	0.212***	0.128***	0.0847***	**0.168*** **	0.226***	0.111***	0.115***
public_service_utility	**0.112*** **	0.214***	0.00991	0.204***	**0.106*** **	0.21***	0.00209	0.208***
automotive	**0.247*** **	0.313***	0.181***	0.132**	**0.201*** **	0.272***	0.131***	0.141***
transport_other	**0.107*** **	0.144***	0.0696***	0.0744**	**0.111*** **	0.157***	0.0646***	0.0928***
financial	**0.246*** **	0.414***	0.0787***	0.336***	**0.231*** **	0.451***	0.0109	0.441***
services	**0.184** **	0.277**	0.0908	0.186	**0.133** **	0.214**	0.0527	0.161
ttime_city_1m	**-0.0285**	0.0928***	-0.15***	0.243***	**-0.0119**	0.129***	-0.152***	0.281***
ttime_port_any	**-0.0795*** **	0.0781***	-0.237***	0.315***	**-0.0764*** **	0.0507**	-0.204***	0.254***
residential	**0.0105***	0.0346***	-0.0137	0.0483***	**0.016*** **	0.0444***	-0.0124	0.0568***
accommodation	**0.1*** **	0.197***	0.0035	0.194***	**0.0877*** **	0.206***	-0.0302	0.236***
mining_industrial	**0.235*** **	0.372***	0.097***	0.275***	**0.185*** **	0.282***	0.0878***	0.195***
tourism_recreation	**0.0139**	0.0769**	-0.0491*	0.126***	**-0.000934**	0.0523	-0.0542*	0.107**
construction	**0.0505*** **	0.0921***	0.00898	0.0831***	**0.0515*** **	0.093***	0.0101	0.0829***

*Signif. Codes: ***: 0.01, **: 0.05, *: 0.1*

Notes: Table shows doubly-robust APE estimates of the log feature intensity (simple counts or quantile counts in each cell, see Section 2.4) on the log of NASA nightlights 2022 (Román et al., 2018). The "High" and "Low" estimates report the APE above and below the median CAPE estimate. The "Diff." column indicates their difference to test for heterogeneity. All terms are tested using a two-sided t-test with standard errors derived from the doubly robust scores following Athey & Wager (2019).

Figure A14: DML CAPE Kernel Density Estimates for Log Nightlights 2022

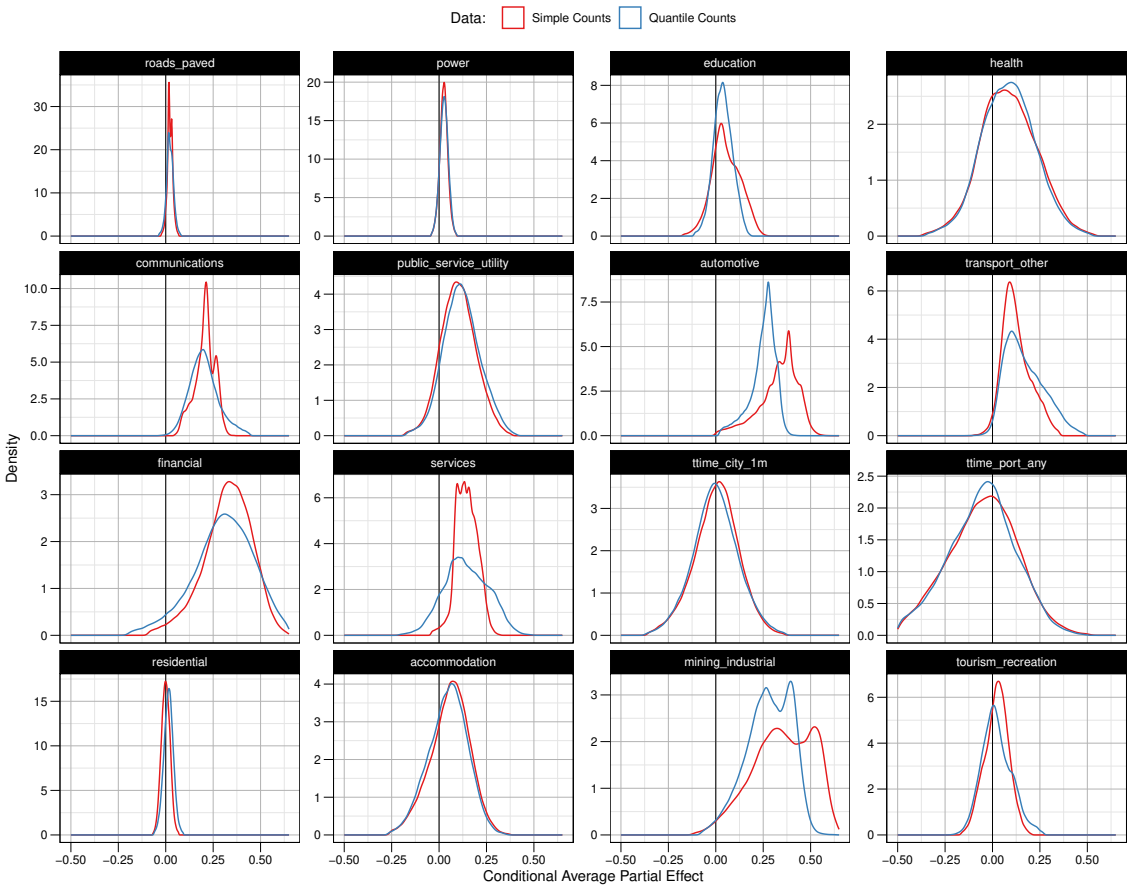

Figure A15: Top Correlates of Nightlights CAPE Estimates: Average Across Datasets

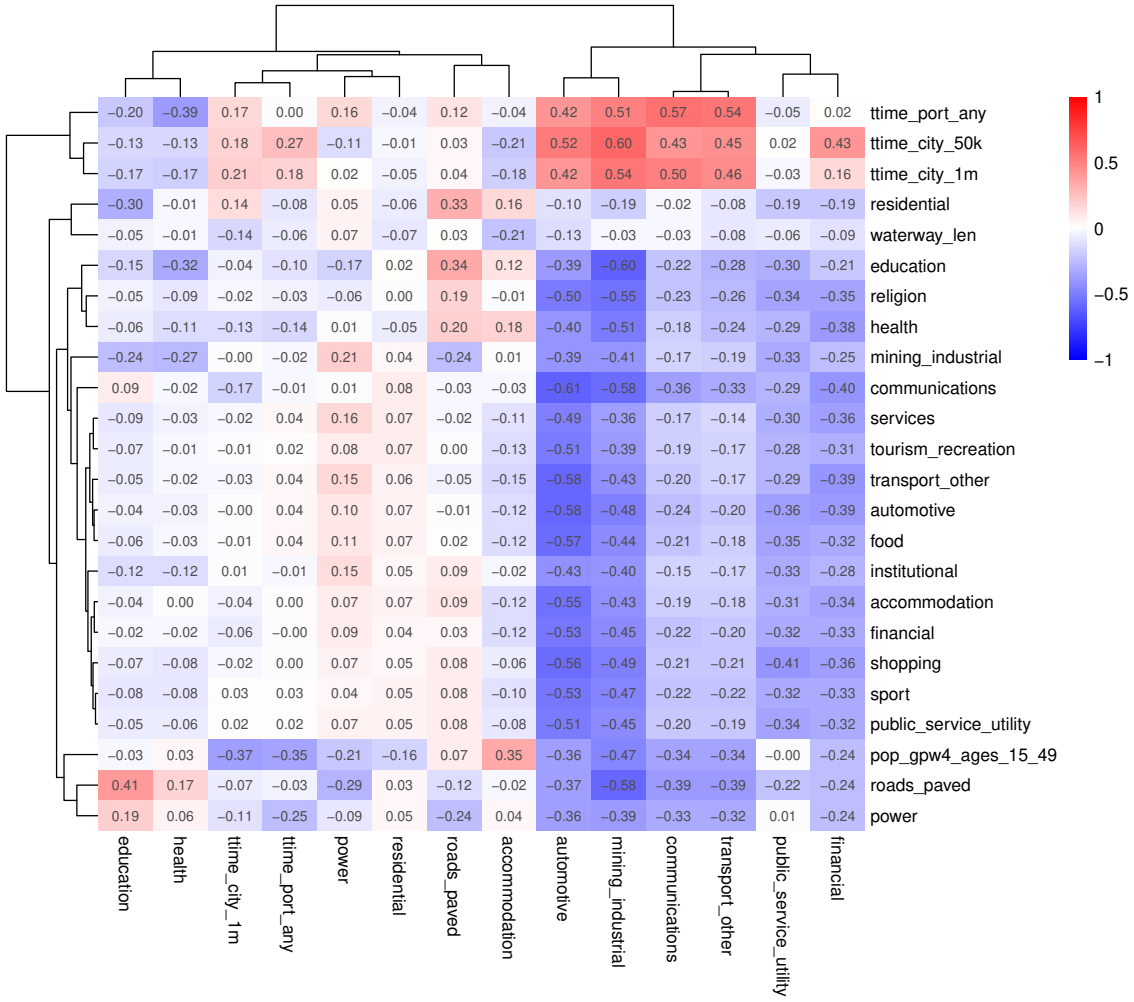

Figure A16: Counterfactual Predictions for Log of Nightlights

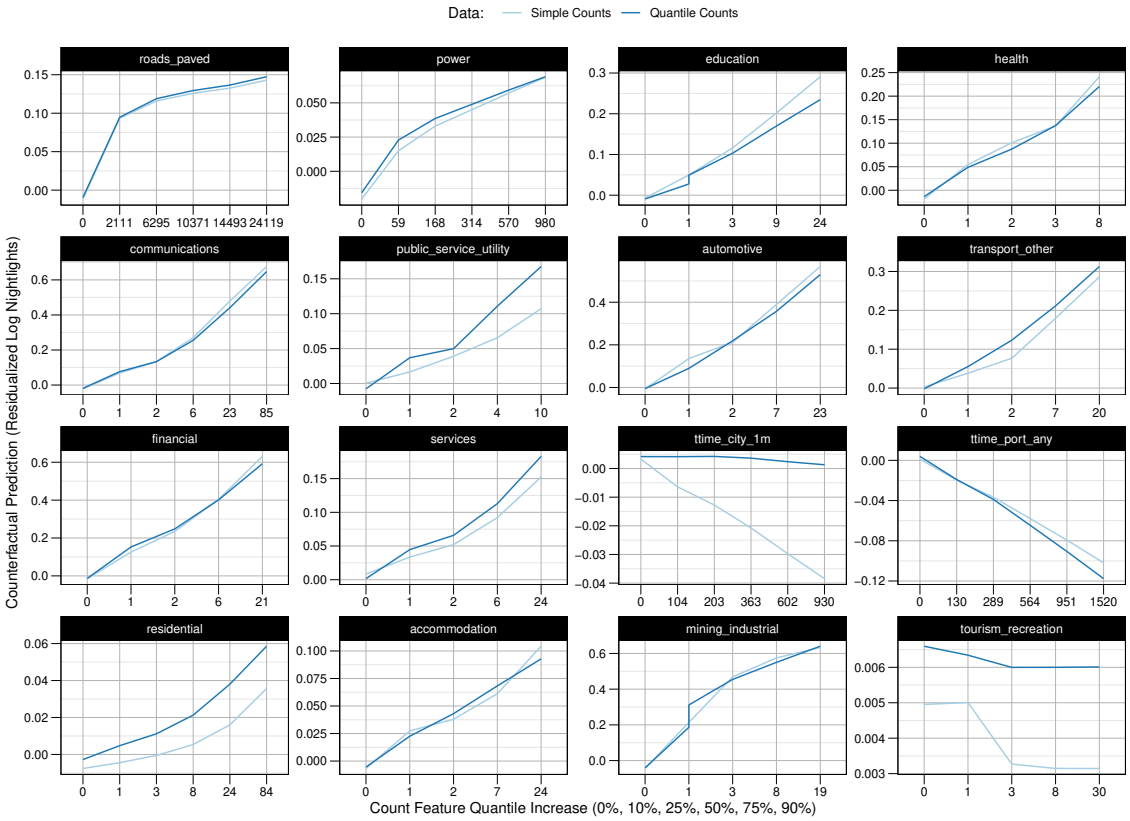

Figure A17: Counterfactual Predictions for IWI: Average Total Wealth Effects per Cell

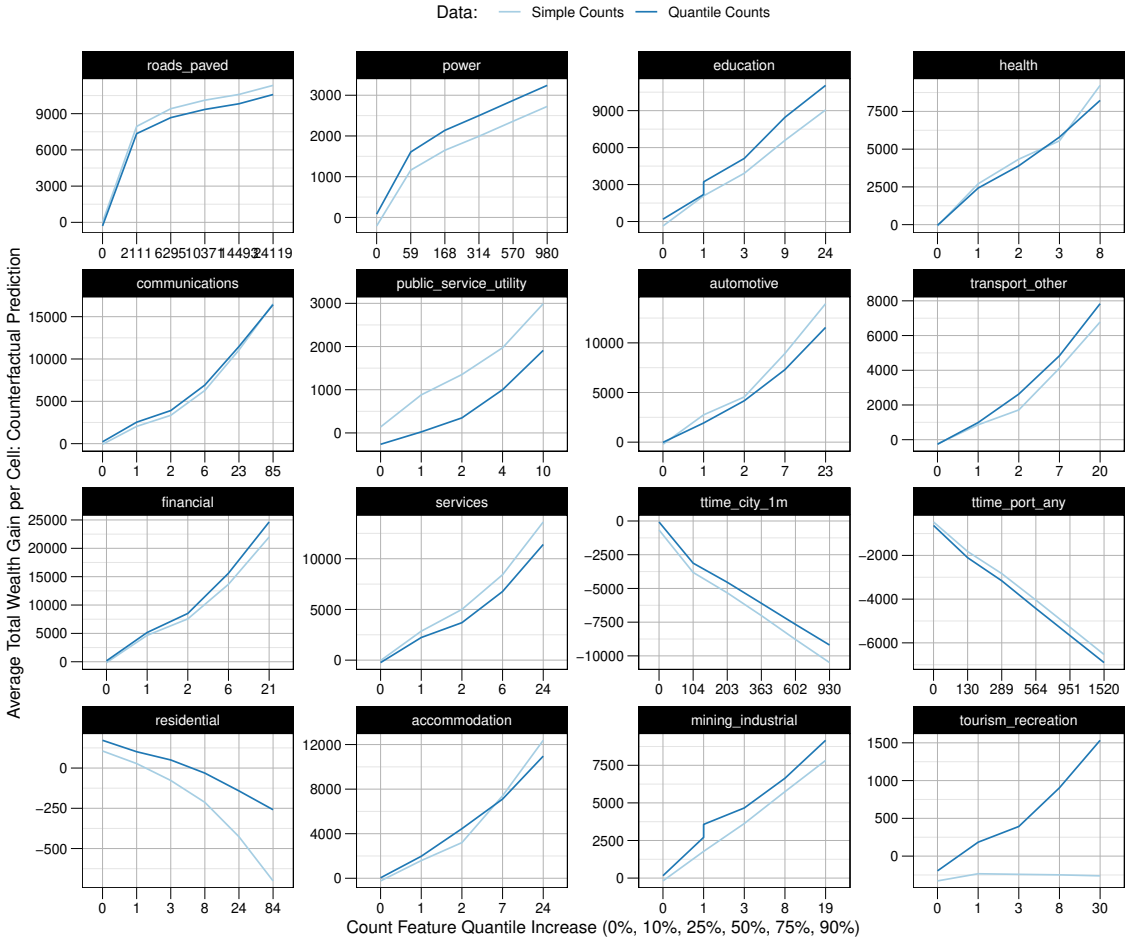

Figure A18: Counterfactual Predictions for DHS-Based IWI

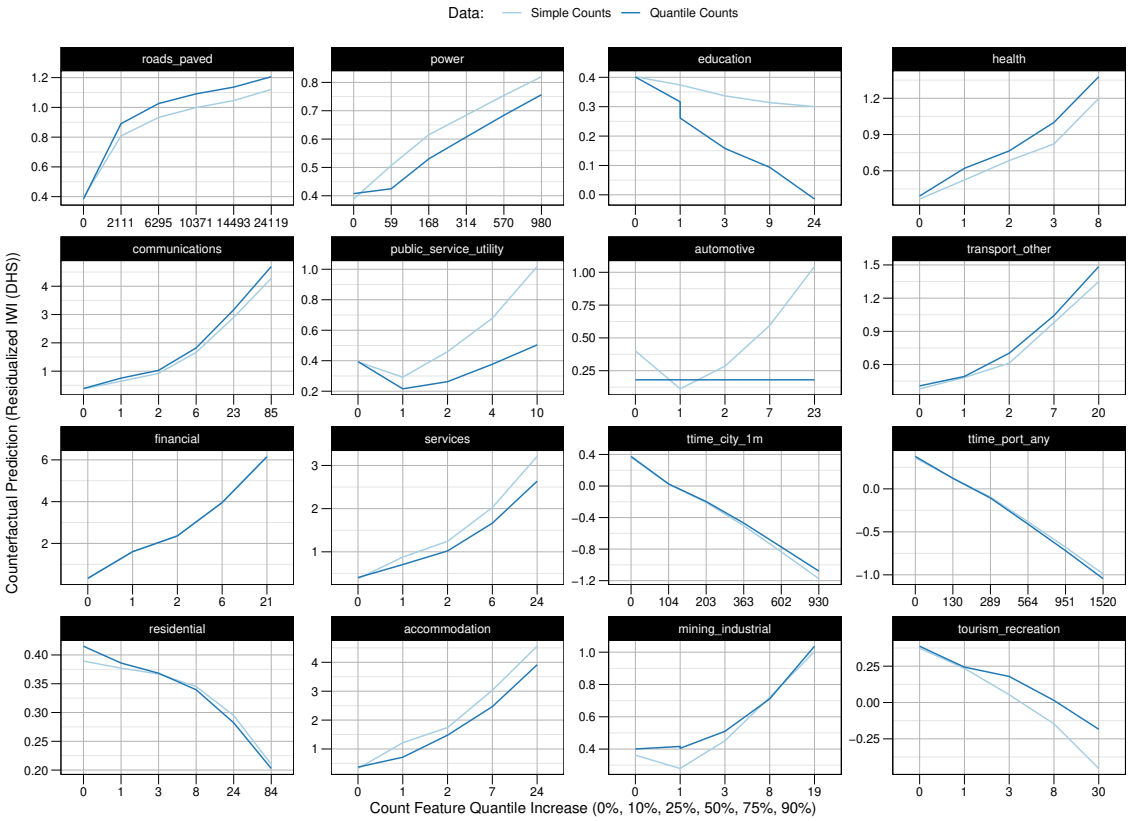

Table A15: Median 50% Counterfactual Prediction: DHS IWI vs. IWI by Lee & Braithwaite (2022)

	Simple Counts		Quantile Counts	
Feature	DHS	L&B	DHS	L&B
roads_paved	1.087	1.622	1.165	1.470
power	0.762	0.302	0.694	0.354
education	0.405	0.662	0.242	0.802
health	0.739	0.776	0.821	0.713
communications	1.710	0.996	1.871	1.112
public_service_utility	0.534	0.131	0.330	-0.007
automotive	0.363	0.583	0.176	0.512
transport_other	0.674	0.171	0.773	0.291
financial	2.368	1.000	2.377	1.112
services	1.285	0.609	1.068	0.435
ttime_city_1m	-0.505	-0.481	-0.469	-0.442
ttime_port_any	-0.365	-0.351	-0.386	-0.371
residential	0.398	-0.068	0.406	-0.044
accommodation	1.762	0.371	1.517	0.533
mining_industrial	0.506	0.477	0.575	0.595
tourism_recreation	0.108	-0.058	0.232	0.012
Median Abs. Coef.	0.604	0.479	0.635	0.477
Corr. Spearman	0.715		0.724	
Corr. Pearson	0.700		0.715	

Abbreviations: DHS = IWI estimate from Demographic and Health Survey; L&B = Predicted IWI estimate by Lee & Braithwaite (2022).

Notes: the DHS-based IWI estimate is computed from all DHS surveys conducted in SSA since 2010. It is averaged across $96km^2$ hexagonal grid cells just like the IWI estimate of Lee & Braithwaite (2022). Grid cells with less than 5 households or less than 10 people per km^2 population density are excluded. This yields 17,396 cells with DHS-based IWI estimates used for training, versus 89,048 cells available with the predicted IWI by Lee & Braithwaite (2022). Counterfactual predictions are made for 103,922 cells which have a population density above 10 persons/km^2 and any POI feature. The median of the 50% increase counterfactual prediction is reported in this table.

Table A16: Correlations of Counterfactual Predictions: DHS IWI and IWI by Lee & Braithwaite (2022)

Feature	Simple Counts	Quantile Counts
roads_paved	-0.045	-0.115
power	-0.019	0.136
education	0.069	0.349
health	0.272	0.219
communications	0.281	0.410
public_service_utility	0.299	0.029
automotive	-0.016	0.323
transport_other	0.109	0.006
financial	0.385	0.505
services	0.177	0.058
ttime_city_1m	0.345	0.540
ttime_port_any	0.127	0.118
residential	0.304	0.271
accommodation	0.298	0.364
mining_industrial	0.145	0.208
tourism_recreation	0.062	0.091
Median Abs. Corr.	0.161	0.214
Median Abs. Corr.	0.161	0.214

Notes: the DHS-based IWI estimate is computed from all DHS surveys conducted in SSA since 2010. It is averaged across $96km^2$ hexagonal grid cells just like the IWI estimate of Lee & Braithwaite (2022). Grid cells with less than 5 households or less than 10 people per km^2 population density are excluded. This yields 17,396 cells with DHS-based IWI estimates used for training, versus 89,048 cells available with the predicted IWI by Lee & Braithwaite (2022). Counterfactual predictions are made for 103,922 cells which have a population density above 10 persons/km^2 and any POI feature. The average Pearson's correlation of these counterfactual predictions across the two IWI estimates is reported in this table.

Table A17: Correlations of Counterfactual Predictions: DHS IWI and IWI by Lee & Braithwaite (2022): Previous Estimates without Separate Spillover Variables (One Variable Per Infrastructure)

	Count	Count + SS	Tag Weights	Weights + SS
roads_paved	0.396	0.743	0.471	0.610
power	0.313	0.141	0.166	0.195
education	0.054	0.297	0.238	0.378
health	0.147	0.091	0.152	0.336
communications	0.184	0.282	0.264	0.345
public_service_utility	0.237	0.166	0.193	0.321
automotive	0.129	0.502	0.215	0.497
transport_other	0.267	0.165	0.218	0.240
financial	0.269	0.057	0.376	0.244
services	0.206	0.302	0.325	0.368
ttime_city_1m	0.216	0.131	0.257	0.125
ttime_port_any	0.226	0.036	0.240	0.108
residential	-0.060	0.057	-0.032	0.081
accommodation	0.233	0.574	0.363	0.651
industrial	0.147	0.218	0.146	0.170
tourism_recreation	0.239	0.161	0.308	0.302
Median Corr.	0.216	0.163	0.248	0.298
Median Abs. Corr.	0.216	0.163	0.248	0.298

Abbreviations: SS = Spatial Spillovers.

Figure A19: Spatial 50% CFPRs (Geometric Mean) × WorldPop 2020 Population

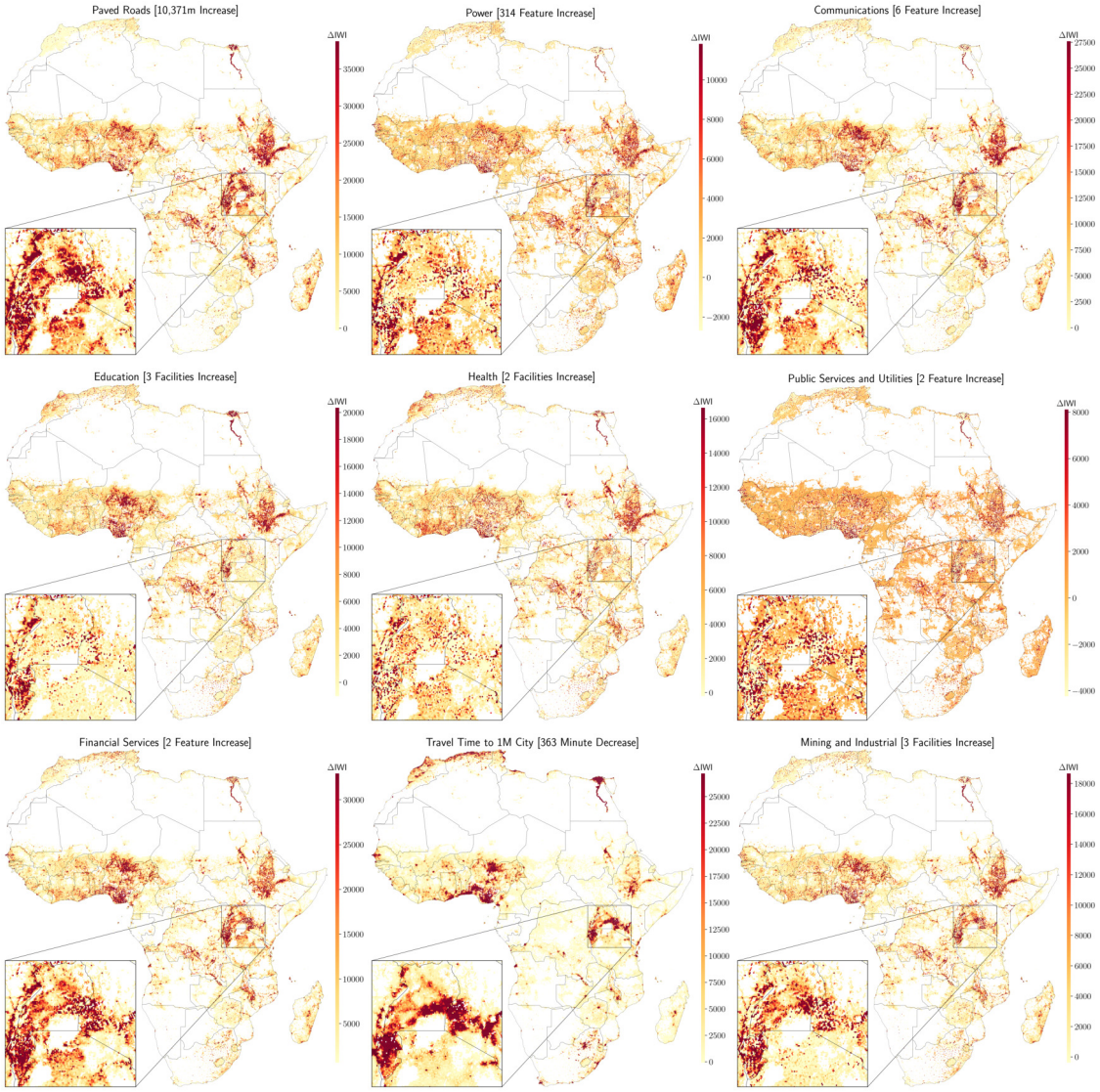

Notes: Figure shows 50% counterfactual predictions of the International Wealth Index (IWI) [0, 100] by Lee & Braithwaite (2022), i.e, the predicted wealth increase (Eq. 12) from an increase in each cell amounting to the median of the non-negative feature density, summarized in Table 7, multiplied with the WorldPop 2020 population measure. It is thus an estimate of the partial effect of the investment in a cell on total welfare.